Faculty of Aerospace Engineering

Attitude modeling of the DelftaCopter

a system identification approach

J.F. Meulenbeld

December 10, 2018

TU Delft Delft University of Technology

Challenge the future

Attitude Modeling of the DelftaCopter

by

Joost Meulenbeld

for obtaining the degree of Master of Science in Aerospace Engineering
at the Delft University of Technology,
to be defended publicly on Monday December 10, 2018 at 13:30.

Student number:	4103548	
Project duration:	September 1, 2017 – December 10, 2018	
Thesis committee:	dr. G.C.H.E. de Croon,	TU Delft, Chair
	ir. C. de Wagter,	TU Delft, Daily supervisor
	dr. A. Menicucci,	TU Delft
	dr. ir. M. Karasek,	TU Delft

An electronic version of this thesis is available at `http://repository.tudelft.nl/`.

TU Delft

DELFT UNIVERSITY OF TECHNOLOGY

DEPARTMENT OF CONTROL AND SIMULATION

The undersigned hereby certify that they have read and recommend to the Faculty of Aerospace Engineering for acceptance a thesis entitled **"Attitude modeling of the DelftaCopter"** by **J.F. Meulenbeld** in partial fulfillment of the requirements for the degree of **Master of Science**.

Dated: December 10, 2018

Readers:

dr. G.C.H.E. de Croon

ir. C. de Wagter

dr. A. Menicucci

dr. ir. M. Karasek

Abstract

Previous years have seen a rise in the use of Unmanned Aerial Vehicles (UAVs). Reaching a large endurance and range while being able to perform Vertical Take-Off and Landing (VTOL) landings allows a broad range of applications. For this purpose the DelftaCopter (DC) was developed, a tilt-body tailsitter UAV. It hovers using a single helicopter rotor for lift and transitions to forward flight by pitching its body down by 90°. In this forward flight state, wings generate the lift, while the helicopter rotor now provides thrust. The single rotor is more efficient than using multiple smaller rotors and helicopter swashplate is used for attitude and speed control.

The heavy single helicopter rotor introduces significant gyroscopic moments, as is the case for all helicopters. In contrast with normal helicopters, the DC has a heavy fuselage putting the attitude dynamics between a helicopter and aircraft. In previous research, a controller based on a model incorporating the rotor as a rotating cylinder was implemented. This controller was unable to counteract the gyroscopic pitch-roll coupling, leading to the question of this thesis: how should the DC be modeled to allow control design.

In this thesis, the previous model is called the Cylinder Dynamics (CD) model, and is compared with another model from literature. The latter model, in this thesis called the Tip-Path Plane (TPP) model, includes the flapping dynamics through the tip-path plane dynamics and is also a linear state-space model. In flight tests, chirps were used to cover a broad frequency range. Fitting both the CD and TPP models on this flight test data, it is shown that the CD model lacks accuracy in the high-frequency area, while the TPP is able to accurately model these dynamics. This shows that the flapping dynamics are important to the attitude dynamics of the DC. An Linear Quadratic Regulator (LQR) controller was implemented based on the fitted TPP model, and shows adequate tracking performance, further validating the applicability of the model to the DC.

For forward flight, extensions to the hover models are proposed. The extension including the elevator and aerodynamic damping is shown to simulate key dynamics of the DC in forward flight with reasonable accuracy. The parameters and eigenfrequencies of this model are not significantly different from the hover model. Therefore it can be concluded that the gyroscopic effect plays an important role in forward flight attitude dynamics. Another extension which estimates of angle of attack and sideslip using high-pass filtered rotational rates, yields better accuracy, but significantly changes the model parameters also present in the hover model. More research with angle of attack and sideslip vanes could validate this modeling approach.

It was also found that for a new version of the DC with a smaller, more quickly rotating rotor, the modeling done before resulted in much worse fits. It was shown that the CD and TPP model response is much more comparable for this version. Control performance also suffers due to this lower accuracy model fit. Further research is required to understand why this is the case.

"In theory, theory and practice are the same.
In practice, they are not.
-Benjamin Brewster"

- Joost Meulenbeld

Preface

The road from start to end of this thesis research was not easy for me. Getting the responsibility for my own research project proved difficult, but rewarding. I look back on an interesting project with a very cool Unmanned Aerial Vehicle. The possibility to join the Outback Challenge in September 2018 was also awesome and I learned a lot from working closely with the team there. I am proud to say that I could contribute to the exciting research done at the MAVLab.

I would like to thank my thesis supervisor, Christophe de Wagter. I learned a lot from his structured project approach and have come to appreciate his thoughtfulness and enthusiasm. Any motivational dip was quickly subdued after a meeting with Christophe. And, I will never forget his bravery shown as pilot of the DelftaCopter being in the same Cyberzoo during flight.

Also, I want to thank the DelftaCopter team. Bart Remes, Christophe de Wagter, Dennis van Wijngaarden, Erik van der Horst, Freek van Tienen and Kevin van Hecke helped greatly with the flight testing required for my research. I genuinely enjoyed my time in Australia with you.

Bart Slinger and Willem Melching were of great help due to the fruitful discussions regarding control theory we had, for which I want to extend my thanks.

Furthermore, thanks to Sonja Lukkenaer and Willem Meulenbeld for proof-reading my paper. I also want to thank my family in general for the moral and financial support, without which everything would have been much harder.

And last but not least, thanks to my college Apollo, the single constant during my entire studies in Delft. The friendship and borrels that we shared made studying in Delft that much more interesting and worthwile.

Joost Meulenbeld

Contents

List of Acroynyms

CD Cylinder Dynamics.

COM Center of Mass.

DC DelftaCopter.

DC2 DelftaCopter 2.

DC3 DelftaCopter 3.

EKF Extended Kalman Filter.

HTOL Horizontal Take-Off and Landing.

INDI Incremental Non-linear Dynamic Inversion.

LQR Linear Quadratic Regulator.

MPC Model-Predictive Control.

NDI Non-linear Dynamic Inversion.

NRMSE Normalized Root Mean Squared Error.

PID Proportional, Integral and Derivative Controller.

RPM Rotations Per Minute.

TPP Tip-Path Plane.

UAV Unmanned Aerial Vehicle.

VTOL Vertical Take-Off and Landing.

List of Symbols

Symbol	Unit	Description
a	[rad]	Flapping angle when blade is at negative x-axis
b	[rad]	Flapping angle when blade is at positive y-axis
c	[m]	Chord length
C_l	[−]	2D lift coefficient
$\underline{D}$	$\left[\mathrm{kg\,m\,s^{-1}}\right]$	Angular momentum vector
h	[m]	Distance between rotor and Center of Mass
I_b	$\left[\mathrm{kg\,m^2}\right]$	Body inertia (subscript details around which axis)
I_r	$\left[\mathrm{kg\,m^2}\right]$	Rotor inertia around its rotation axis
k_β	$\left[\mathrm{N\,m\,rad^{-1}}\right]$	Apparent spring stiffness
L	[N]	Lift force
n	[−]	Number of blades on the rotor
p	$\left[\mathrm{rad\,s^{-1}}\right]$	Roll rate
q	$\left[\mathrm{rad\,s^{-1}}\right]$	Pitch rate
Q	-	Linear Quadratic Regulator state cost matrix
R	[m]	Radius of the rotor blade
R	-	Linear Quadratic Regulator input cost matrix
S	$\left[\mathrm{m^2}\right]$	Wing/rotor surface area
T	[N]	Thrust
V	$\left[\mathrm{m\,s^{-1}}\right]$	Velocity
V_∞	$\left[\mathrm{m\,s^{-1}}\right]$	Airspeed
α	[rad]	Angle of attack
β	[rad]	Angle of sideslip
δ_{elev}	[−]	Control input on elevator
δ_x	[−]	Control input on x-axis
δ_y	[−]	Control input on y-axis
θ	[rad]	Pitch angle
ρ	$\left[\mathrm{kg\,m^{-3}}\right]$	Air density
Ψ	[rad]	Angle of the rotor in its rotation, 0 when at the right wing
$\underline{\omega}$	$\left[\mathrm{rad\,s^{-1}}\right]$	Angular velocity vector
Ω	$\left[\mathrm{rad\,s^{-1}}\right]$	Rotational rate of the rotor

List of Figures

List of Tables

Chapter 1

Introduction

The DelftaCopter (DC) is an Unmanned Aerial Vehicle (UAV) that is designed for both flexible landing requirements and efficient forward flight, shown in fig. 1.1a. It achieves this by combining Vertical Take-Off and Landing (VTOL) capability through a standard helicopter rotor-head, with large wings. During VTOL state, the UAV hovers using the rotor-head, while the entire UAV pitches down around 90° to a forward flight state, as shown in fig. 1.1b. In this forward flight state the wings generate the required lift and thrust is efficiently generated by the single helicopter rotor. This translates directly in an enlarged range of this so-called tilt-body UAV compared to normal VTOL UAVs without horizontal flight mode. The combination of VTOL and a large range is exactly what was needed for the 2016 Outback Challenge[1]. The new rules of the outback challenge again specify that landing in a cluttered environment is one of the challenges, as per the rules[2], such that a VTOL UAV seems to be the required solution.

(a) DC in the cyberzoo, the experiment room for testing UAVs at the TU Delft

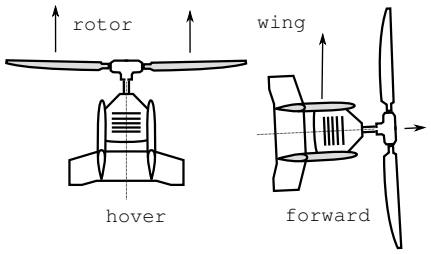

(b) In the air, the UAV transitions by rotating 90° downwards and flies using its wings as main lift source. Image courtesy of de Wagter et al.[3]

Figure 1.1: DelftaCopter photo and schematic presentation of the transition

The single rotor that generates the required hover thrust is a relatively heavy system that rotates at a high rate, which means there is a significant amount of gyroscopic effect. This effect leads to a coupling between the pitch and roll rotations of the vehicle in hover mode and roll and yaw rotations in forward flight. While this coupling is expected in single-rotor system comparable to a helicopter, the fact that the fuselage has a high inertia makes the vehicle dynamics different from ordinary helicopters. Multicopters usually have their rotors counter-rotating to eliminate the gyroscopic effect, which will be further discussed in section 2.1. This leads the DC to be "in between" a helicopter and a multicopter regarding the amount of gyroscopic effect, which is an area that is not well studied.

According to earlier research on the DC[3], the effect of the fuselage inertia on the coupling is very prominent. The controller that was implemented to compensate for this coupling did not function without

an extra tuning parameter, and it was not completely understood why. This problem is present both in hover mode and horizontal flight. Finding better models for this UAV will improve the understanding of its attitude dynamics. This leads to the possibility of improving the control of the platform. This is even more true in forward flight mode, for which no research has been done before.

On an applied level, many companies are developing UAVs or UAV applications. Some of them, for example Atmos UAV[1] are also developing a UAV that is comparable to the DC: they combine VTOL and horizontal flight by tilting the entire UAV. The difference is that these systems use multiple rotors for providing thrust, which in theory is less efficient than using a single rotor. The one comparable UAV that also has a single rotor is developed by Aerovel[2]. It is a combustion-engine driven UAV that can hover and tilt to forward flight, using wings and a V-tail to generate lift and stabilize. But since it is a commercial product, little is known about the modeling and control of this UAV.

1.1 Research objective

Better attitude control of the DC can lead to a widening of the use-cases of the platform. Before the controller can be improved, more should be known about the DC's attitude dynamics. As explained above, the hover mode dynamics still have questions unanswered. The forward flight attitude dynamics have not been researched yet. Therefore, the goal of this thesis was formulated at the start as follows:

> The research objective is to make the DelftaCopter flyable in hover and horizontal flight mode by modeling its dynamic behavior and implementing a controller compensating unwanted motions.

1.2 Research questions

At the start of this thesis project, research questions were formulated to aid choosing areas of research to focus on. These research questions thus help solve the research objective. The wobble in hover mode has been solved, but more research is needed to completely understand why the current solution works[1]. In order to find out about the mechanics behind the solution, a good mathematical model of the DC dynamics needs to be found, and for this several aspects of the dynamics may or may not be important.

Forward flight modeling is one of the main goals of the research. Since the gyroscopic effect plays such a large role in the dynamics of the DC, its effect on forward flight attitude control must be researched. Is it detrimental to flight performance or can it actually be used? Since cyclic pitch makes the lift distribution of the blade in rotation more uneven, efficiency is lowered. Flying the aircraft with as least cyclic pitch as possible may thus be good for performance. In the end, the following research questions were answered:

1. Which physical phenomena should be modeled to sufficiently model the DC dynamics?
   (a) What is the influence of the gyroscopic effect on the dynamics?
   (b) Do the rotor blade flapping dynamics have a significant effect on the system dynamics?
   (c) Does aerodynamic damping of the rotor have a significant effect on the dynamics?
2. What combination of cyclic pitch and aerodynamic control surface inputs can control the DC in horizontal flight?
   (a) What is the effect of the elevons on the attitude?
   (b) Is cyclic pitch control of the rotor required for attitude control in forward flight?

These research questions were answered by combining theory with experimentation. It is clear that the problems raised by previous research were due to the physical system responding different than expected. In this research, the focus lied first on a better model for hover. It was suspected that the gyroscopic effect still has a large influence in forward flight, so the hover model should help understanding the forward flight.

[1] http://www.atmos.com/
[2] http://aerovel.com/

1.3 Structure of this thesis

The rest of this thesis contains the results oft he research performed to answer these research questions. The structure is as follows.

A literature review of modeling and control of small UAVs comparable to the DC is given in chapter 2.

In the following chapter, chapter 3, a theoretical, simplified model of a helicopter is derived, assuming a rigid rotor. This model is then used to draw some general conclusions regarding the gyroscopic effect that plays a large role in helicopter dynamics.

Chapter 4 contains an introduction to the research paper published in the IMAV2018 conference. This paper contains a concise overview of the bulk of this thesis' research. It describes the used models, compares how well they can be fitted on flight data recorded on the DC, shows a working controller and explains concisely an extension proposed to the hover model to allow forward flight modeling.

In chapter 5, a more elaborate overview of the different extensions developed and tested is given.

Up till this point, all research has been performed on the DelftaCopter 2 (DC2). This UAV was partially rebuilt to include a different rotor and rotor blades for efficiency reasons. This new setup is called the DelftaCopter 3 (DC3). Due to timing, some research was still to be completed at this point in time, but it was found that the new setup proved difficult for the modeling approach used for the DelftaCopter 2 (DC2). Chapters 6 and 7 detail the problems encountered in modeling and control respectively of this updated version.

Finally, in chapter 8 this thesis is wrapped up and a conclusion is drawn.

Chapter 2

Literature review

In this chapter, a summary of the literature review is given. First, a comparison of different VTOL UAVs with forward flight capability is given. Then the modeling is detailed of first the single rotor dynamics and then the aerodynamics, and finally the control of the tilt-body is elaborated upon.

2.1 Comparison of Vertical Take-Off and Landing concepts

To understand DC's behavior, research on comparable UAVs is compared for its value to the present research. To find comparable UAVs, the DC first needs to be characterized.

In the original paper on the DC[1], it is described to have a helicopter rotor-head with both cyclic and collective pitch control of the blades. The blades are stiff and no real flapping hinge is present, but the blades are mounted using rubber rings that are modelled as a torsional spring system. Furthermore they can rotate in the lead-lag direction albeit with quite some friction. To compensate the yawing moment in hover mode due to the single rotor, two tail-rotors are added at the end of the wings. One other important characteristic is the fact that the fuselage underneath the rotor has a high inertia compared to normal (small-scale) helicopters: the wing span is relatively high and antennae are put at the wing tips, leading to better reception at the cost of a larger rotational inertia. This makes it different from normal helicopters that usually have a body with low rotational inertia.

With this in mind, research on aerial systems is summarized to help explain the flight behavior of comparable systems. In fig. 2.1 a broad classification of UAVs is given. This classification is adapted from [4], keeping in mind the requirement that the UAV shall both allow VTOL and a forward flight that covers a large distance (around 100 km including wind) and therefore contains a sub-classification for the most promising classes of UAVs for this purpose. In this classification the Horizontal Take-Off and Landing (HTOL) class is not sufficient due to the requirements of the outback challenge. In literature, the class containing VTOL UAVs that use wings for fast forward flight are also called "convertible".

In [5], a qualitative comparison is made between different concepts for propulsion in VTOL UAVs. This can be summarized as follows:

- Helicopter: a single rotor provides all required lift and a rotor-head with servos and a swashplate are required for control, as well as a tail rotor. Since it does not use wings for horizontal flight, its efficiency at flying large distances or at high speeds is lower than that of a fixed-wing aircraft.
- Multi-rotor: since these UAVs have multiple rotors, they can be controlled by using differential thrust rather than cyclic and collective pitch control. Having counter-rotating rotors removes the need for a tail rotor since the moment generated by the multiple rotors is canceled. No servos or heavy rotor-head are needed in this approach, leading to lower mechanical complexity than a helicopter, possibly at the expense of more weight due to the fact that multiple rotors (usually more than four) are required. Also, the range is still lower than of fixed-wing aircraft, and the smaller radius blades are theoretically less efficient than the single blade of a helicopter.

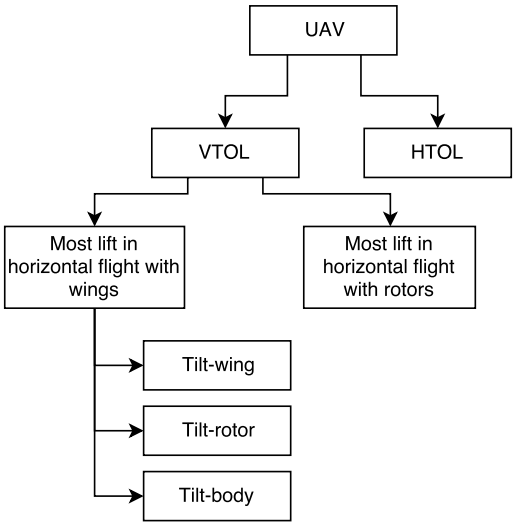

Figure 2.1: Classification of UAVs for the Outback Challenge. The DC is part of the Tilt-Body class. Adapted from [4].

- Tilt-rotor: a normal horizontal flying aircraft is appended with rotors that can be rotated from a vertical orientation for hover mode, to a horizontal orientation for forward flight. Since the rotor-rotating servo's don't rotate the wing, the servo's and rotation construction can be lighter than in the tilt-wing concept. Also, rotors may be switched off during horizontal flight, increasing efficiency if the horizontal flight rotor is designed for a higher velocity regime[6]. Disadvantages are:
  - In vertical climb, there is a high frontal area since the wings are mounted horizontally. This leads to high drag and as such increases the hover power during ascent.[6]
  - For high rotor tilts, the wake of the rotor cannot smoothly follow an airfoil due to high incidence angle between wake and wing. During transition this leads to a higher flight velocity required before the airflow attaches to the wing.
  - Either 3 or more rotors are required or 2 rotors with cyclic and collective pitch control. For every rotor a servo which rotates the rotor is required. This increases mass and complexity of the design compared to tilt-body. All in all this concept has been researched a lot[5]. Examples include one designed by van der Mey[7], while Ducard describes another example that is implemented in a commercial solution[8].[1]
- Tilt-wing: in this concept, the rotors are rigidly attached to the wings and the entire wing assemblies are rotated. Control can be comparable to tilt-rotor aircraft while the tilting assembly is probably heavier since the wings themselves are also tilted. During hovering ascent, the disadvantage of the big frontal area is not present since the wing is rotated vertically.[6] As stated above, the weight of a mechanism that tilts the entire wing may be heavier than the tilt-rotor. Examples include [9, 10].
- Tilt-body: the entire aircraft is tilted and therefore no rotor tilting servos are required, which saves weight and lowers complexity. However, any used rotor in hover will be perpendicular to the airflow in horizontal flight as well, so there's no opportunity to improve efficiency by switching off 1 or multiple rotors and fly with the propulsion of just one or two rotors designed for efficient forward flight. Another disadvantage is that while descending quickly, the vertical wind velocity may lead to a reversed flow over control surfaces, which leads first to a low actuator effectiveness, and when descending even faster, a switching sign of the control derivative. This disadvantage is partially solved by having blown actuators in the wake of the propeller.[11] The required actuators for attitude control can be supplied with the following options:
  - Four rotors which then do not require further aerodynamic control surfaces, such as the Atmos UAV[2], Quadshot[12] and VertiKUL [13]. Control and actuator complexity is the lowest for this concept since it can be controlled like a (heavy) quadcopter, and no significant gyroscopic effect is present since the rotors are counter-rotating. Since no aerodynamic control surfaces are used, control reversal during fast descent is not a problem.

[1] http://www.wingcopter.com/
[2] http://www.atmosuav.com/

- Two rotors with aerodynamic control surfaces, such as the MAVIon[14] or Cyclone[11] which have two separate rotors or the Vertigo[15] which has a two rotors in a coaxial rotation mounting. The aerodynamics control surfaces can also work while in hover mode if they are in the propeller slipstream, but they may be subject to control reversal when descending: then the flow over the airfoil is inverted and the effectiveness is reversed[11]. Since only 2 motors and 2 servos are required, this is probably the lightest solution.
- A single rotor with or without aerodynamic control surfaces, of which only two exist at the present moment: the DC [1] and the Flexrotor by a commercial company[3]. Using a single rotor rather than multiple smaller ones is more efficient, and if the rotor is fitted with a collective pitch control mechanism, the rotor can be set at a high incidence angle during forward flight for high efficiency. The helicopter rotor-head gives a high control authority during hover mode, but it is relatively heavy since it uses a heavy wing, the three servos required for cyclic and collective pitch control and two tail rotors to counteract yaw moments. Another disadvantage is the gyroscopic effect that is very present and leads to problems in control of the DC[1, 3].

2.2 Modeling of single-rotor UAV

One of the key ingredients to the model will be the gyroscopic effect, which describes the dynamics of a rotating object. The gyroscopic effect leads to a coupling between roll and pitch, which was found to be a problem for the DC[1]. In [3] the modeling and control was further developed, yielding further research questions which are discussed in section 1.1.

Helicopters are controlled by changing the pitch angle of the blade using a swashplate. This pitch angle is described by both the collective pitch, which controls the amount of thrust, and the cyclic pitch, which changes the pitch angle over the rotation of the blade. The cyclic pitch makes the blade have a higher pitch angle in some places of the rotation than in other, thus generating a non-uniform lift distribution over the rotation. This allows a moment to be generated. However, the maximum lift is not directly equal to the place where the pitch angle is maximum, due to the fact that the blade can flap up and down. This property is affected by the gyroscopic effect. In helicopters the gyroscopic effect is mitigated by applying the maximum lift 90° out of phase with the direction that the pilot wants to go. It will be described in chapter 3 that this is logical for normal helicopters, but also not sufficient in the case of the DC due to the high inertia of its wings.

2.2.1 Flapping dynamics versus rotating disk

In literature, modeling of the gyroscopic effect is done in two ways. The first method is modeling the flapping dynamics of the rotor, such as done in the standard textbook Bramwell's helicopter dynamics[16], which is an approach generally used for human-scale helicopters. The flapping dynamics model describes how the rotor's blade flaps up and down, which is mainly caused by the cyclic pitch, which changes the amount of lift the blade makes over a rotation. Due to difference in lift of the blade, the blade tends to go up and down over this rotation. Due to the relatively low stiffness of the blades, the flapping angle follows the cyclic pitch angle[16] and thus the cyclic pitch differential doesn't directly create a moment on the fuselage. This flapping moment is transferred to the fuselage due to the alignment of the rotor blades in flapped state or through a torsional hinge, the latter of which is the approach taken for the DC model[3]. In [17], a comprehensive model of a small helicopter including flapping dynamics is given, including validation which showed good correspondence between simulation and flight data. The helicopter has a horizontal stabilizer bar, so it will have to be adapted for use in the DC, but its equations are relatively simple, albeit non-linear.

A relatively simple representation of a small-scale helicopter has been derived by Mettler[18]. In this work, higher-than-first-order vibrations and rotations of the blades are neglected and the flapping dynamics can then be fully described by the plane in which the tip of the rotor travels, called the Tip-Path Plane (TPP). The plane that the rotor moves in is represented as a two-state first-order system influenced by the cyclic pitch commands and rotational rates of the fuselage. The thrust vector is assumed perpendicular to the rotor TPP, inducing control moments on the fuselage since the plane tilts with respect to the body frame.

[3] `http://aerovel.com/`

In the research, the model was simplified as much as possible, using system identification techniques to identify which parameters of the model are important and which aren't. If in this model the Bell-Hiller stabilizer bar dynamics are removed and the yaw damper is also removed out of the system, a 10-state linear state-space results, which has been fitted to good accuracy for hover mode. Since it is a linear model, it is unable to capture both hover and forward flight mode as the linearization applies to a single equilibrium position of the rotorcraft. System identification and results are well described in the book, so this will be a valuable asset to the present research. In the present thesis, the flapping dynamics model as derived by Mettler will be called the TPP model.

Another method is to model the rotor as a rotating disk with representative inertia. According to Kondak[19], small UAV rotors can be modeled as spinning disks with no flapping dynamics included, due to the fact that the rotor has high relative inertia, rotational velocity, and stiffness. This may be logical, since for an infinitely stiff rotor the TPP stays fixed to the fuselage body frame and any control moments are just created by assuming the cyclic pitch yields more lift on one side of the fuselage than on the opposite. Note that this approach does include gyroscopic effect since dynamic moments of the spinning disk are still transferred to the fuselage.

No criterion is given, however, as to when the spinning disk model can be used as opposed to the flapping rotor model. In an overview paper on modeling of small helicopter UAVs, Sandino[20] uses a disk as model for the rotor, using Newton-Euler formulation, Lagrange formulation and Kane formulation to achieve roughly the same result. Some other researchers also model the system with a spinning disk, like [8, 21], or [22], where the qualitative magnitude of the gyroscopic effect is shown.

In conclusion, there is quite some material available that describes two main ways of modeling a helicopter. No definitive answer is found as to which way is applicable to which system, which means that the proper way will have to be figured out for the DC specifically.

2.2.2 Lead-lag dynamics

None of the research found on the modeling of small helicopter UAVs incorporates the lead-lag dynamics of the rotor. The lead-lag dynamics are in-plane rotations of the rotor blades, caused by both the Coriolis moments due to flapping, and aerodynamic drag. According to Bramwell[16, Sec. 1.8], the motion due to aerodynamic drag causes a damped out simple vibration, but the lead-lag motion due to the flapping dynamics yields a steady undamped vibration which lags the flapping angle by 90°. The lead-lag angle could be calculated from the flapping dynamics, if the friction of the lead-lag hinge can be estimated. In Mettler[18, Sec. 2.2], it is stated that for the lead-lag motion of the blades leads to very small forces on the hub compared to the flapping motion, and can be ignored.

2.2.3 Aerodynamic damping of blade

Aerodynamic damping of the blade is caused by the fact that the blade moves up and down during its rotation. In the reference frame of the blade, a downward motion leads to an increase in the angle of attack of that blade, which then leads to an increase in the lift generated by the blade. Moving upwards has the exact opposite effect, leading to a decrease in the lift generated by the blade. This force opposite to the movement leads to a damping effect. The implementation of this damping in the model of a helicopter is different between the flapping dynamics model and rotating disk model, since in the rotating disk model the blade itself does not flap with respect to the body. It is then just the pitch and roll rates of the helicopter itself that induce an angle of attack.

In Bramwell's[16], the aerodynamic forces on the blade are incorporated in the flapping dynamics, assuming that the lift of the blade is linearly depending on the angle of attack. Since the blade flaps up and and with respect to the body, the extent of this flapping is determined partly by the aerodynamic characteristics[16, Sec. 1.6]. In Mettler's linear model[18], the aerodynamic damping is explicitly used in the formulation of the TPP: it changes its orientation of the plane, thereby also changing the orientation of the lift vector. In this model, the pitch angle leads to an angle of attack, which leads to a aerodynamic force generating the flapping motion, so in this case aerodynamic damping cannot be seen independent of the dynamics of the blade.

In a rigid-disk rotor model, aerodynamic damping may still be important, but it was not found to be used in the research presented using this modeling approach. It may be implemented by assuming linear

aerodynamics (lift coefficient changes linearly with blade angle of attack, an approach taken often in modeling rotor blade aerodynamics[16, 18]) and letting the angle of attack vary with the body angular rates of the fuselage.

2.3 Modeling of aerodynamics

Dorobantu et al[23] used an Extended Kalman Filter (EKF) to estimate the aerodynamic parameters of a small fixed-wing aircraft, the size of which corresponds roughly to the DC. These parameters are part of a linear representation of the dynamics, using states such as angle of attack and pitch rate as relevant parts of the dynamics equations, which is a standard approach. The model yields good predictions of in-flight measurements, and the linear model and estimation technique may be useful for estimating a model of the DC in forward flight.

After identification of an aerodynamic model of the DC in forward flight, the dynamic model that describes the response to control inputs will be adapted to incorporate the aerodynamic moments as well as the rotor moments.

2.4 Control systems of UAVs

Transitioning UAVs have multiple flight states, each with their own characteristics: in hover mode, the UAV is basically a rotorcraft UAV, for which an informative overview paper on control is available[24]. Linear controllers with gains chosen through Linear Quadratic Regulator (LQR) or pole placement are described as well as Proportional, Integral and Derivative Controller (PID) controllers that require elaborate tuning. All yield a relatively simple means to control a UAV compared to non-linear controllers. The disadvantage is that a linear controller is only effective around its operating condition, so multiple controllers need to be tuned for different operating points.

Non-linear controllers such as input-output linearization, also called Non-linear Dynamic Inversion (NDI), and Model-Predictive Control (MPC) don't have this disadvantage. NDI uses a model of the system to invert the system dynamics, and calculate the required actuator deflections to attain a certain (angula) acceleration using the inverted dynamics. MPC solves an optimization problem in real-time, predicting for a certain time window into the future the UAV's state given the control inputs, and then optimizes the control inputs for the time window with a given cost function. This cost function can include accelerations and tracking errors, which makes makes it a flexible approach, at a large computational cost. The non-linear model-based controllers NDI and MPC are better able to deal with the non-linear dynamics of a helicopter and unmodeled dynamics.[24]

An adaptive approach to these model-based controllers lowers the demands on model quality. In that case, the system parameters are estimated during flight, which means that any unmodeled dynamics are compensated for by changing the parameters to best fit the measurements at that state.

Finally, incremental approaches to controllers compensate for unmodeled dynamics by not working on absolute control signals, but signals relative to the current operating point. This is made use of in Incremental Non-linear Dynamic Inversion (INDI), which only requires actuator effectiveness and dynamics to be well known, and requires no other system dynamics parameters to be estimated.[11]

2.4.1 Control of hybrid UAVs

The tilting concepts all have to deal with transition: changing from hover mode to horizontal forward flight mode. During this transition, the wind speed over the wing increases and thus the flight behavior changes drastically, which makes the transition an active research area, i.e. in [9, 11, 25, 26]. Transition can be done using discrete flight phases, where the change from hover mode to transition phase to forward flight mode is a sudden change in controller settings. This is done for example by Kita et al.[25], where a reference pitch trajectory is computed beforehand to minimize altitude loss during transition, and this trajectory is sent to a PID pitch angle controller. Another example is the work by Muraoka et al.[9], where the gains of the helicopter mode controller and fixed-wing controller are changed depending on

the pitch angle during transition. This makes the transition less of a discrete state, and allows any pitch angle between 0 and 90°.

In [26], a single control architecture is described to solve this problem instead of interpolating the gains of hover mode and forward flight mode controllers. The control architecture is based on NDI, which means a model is needed during flight.

A smooth transition with freely selectable pitch angle allows the UAV to be used in harsher wind conditions: if there is a lot of wind, the UAV can still hover in-place by setting a high pitch angle with respect to the vertical. The thrust vector is then tilted in the direction of the wind, compensating the drag caused by the oncoming flow which would blow the UAV away if it was hovering straight up. This leads to a flight between hover mode and horizontal flight.

2.4.2 Control of the DelftaCopter (DC)

However, since the DC is the only scientific research aircraft with tilt-body and single rotor design, papers considering control of comparable aircraft are scarce. In [3], the control of the DC in hover mode is detailed. Compensation for gyroscopic effect is introduced, based on identified system parameters regarding system derivatives in pitch and roll. The identified system contains two states, namely the pitch and roll rate in hover mode. A direct coupling between these two states and pitch and roll accelerations is estimated and this coupling is subtracted from the control signal as a feed-forward correction.

However, the compensation needed tuning through a tuning parameter K_c that determined the amount of compensation used. A tuning parameter of $K_c = 1$ would mean full compensation as predicted using system identification, but finally a value $K_c = 0.5$ was found to be most effective. It remains unclear why this was the case.[3] Furthermore, no research has been presented on the horizontal flight mode, and some challenges are still to be solved. It appears that flying turns in one direction is much more difficult than in another direction, which is probably due, again, to the gyroscopic effect.

Chapter 3

Rigid-rotor model

In this chapter, a simple rigid rotor model is developed. Later in the thesis, the Cylinder Dynamics (CD) model is used that is based on this model. Section 3.6 explains the connection between the rigid-rotor model in this chapter and the Cylinder Dynamics (CD). The rigid rotor model is the simplest representation of the attitude dynamics of the DC incorporating the gyroscopic effect. It ignores any blade flapping, thus assuming a perfectly rigid rotor, and assumes a moment to be applied directly to the body instead of via the cyclic pitch setting of the rotor.

3.1 Model and assumptions

To allow powerful conclusions to be drawn from the model, some simplifications and assumptions are made to lower the complexity. The validity of these assumptions is as of now not known and is the subject of further research. A schematic image of the model is shown in fig. 3.1. The following assumptions are made for modeling the system:

1. The system is modelled as two parts: the body (lower part) of the UAV with representative inertia matrix I_b and a spinning disk above this body with representative inertia matrix I_r. Other than the disk's spinning, the body and rotor do not translate or rotate with respect to each other. The initial orientation is that of vertical hover mode as in fig. 3.1.
2. The DC is hinged in its center of gravity such that translations are not possible. The subject of this derivation is the attitude dynamics, not the translations dynamics.
3. Any moment that causes the model to yaw (rotate around the body z-axis as in fig. 3.1) is directly compensated by the tail rotor. Therefore, the yaw angle and yaw rate are set to zero. Resulting from the derivations, the actual yaw moment required for this to be true can be calculated.
4. The rotational rate of the rotor disk is assumed constant. This is achieved by having an (infinitely fast) engine governor.
5. The mass of the rotor and body are assumed in center of gravity of the entire UAV. The change introduced here only slightly changes the moment of inertia but does not qualitatively influence the dynamics.
6. No lift is generated by the rotor or wing. This means that the only effect on the dynamics is the internal gyroscopic moments and external moments applied to the UAV.
7. The body is symmetrical around the xz- and yz plane such that its inertia matrix is diagonal. The rotor has all of its mass in a single plane. allowing the perpendicular axis theorem to be used.

3.2 Reference frames

Six reference frames are defined to describe the motion in:

- $\underline{E}_E$: The earth-fixed reference frame. z points downwards.

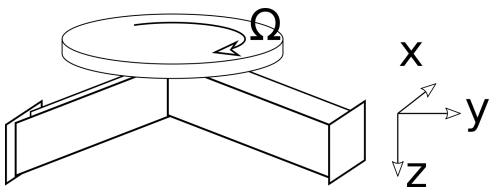

Figure 3.1: Simplified model of the DelftaCopter, the disk represents the rotating mass of the rotor, with its inertia taken as the average of the real inertia over 1 rotation.

- $\underline{E}_b$: The body-fixed reference frame, fixed to the wing of the DC with its center in the CoM of the UAV. z points downwards, y towards the right wing and x forward.
- $\underline{E}_{E_1}$: The frame after rotating $\underline{E}_E$ with the yaw angle.
- $\underline{E}_{E_2}$: The frame after rotating $\underline{E}_{E_1}$ with the pitch angle. Rotating this frame with the roll angle yields the body frame $\underline{E}_b$.
- $\underline{E}_r$: The rotor frame, rotating with the rotor with its center in the rotor (and the CoG of the UAV as discussed in section 3.1). This frame is reached by rotating the body frame along its z-axis by angle Ψ in the positive direction.

3.3 Equations of motion

The equations of motion are derived from a first principle's view of the relevant dynamics. The total angular momentum of the UAV will be derived, and this will be differentiated to yield the required moments for a certain rate of change in angular momentum.

3.3.1 Angular velocity

The angular rate of the body $\underline{\omega}_b$ and rotor $\underline{\omega}_r$ are given below. In here use is made of the fact that the z-axis of the body frame and rotor frame coincide, such that the z-component in the rotor frame is equivalent in the body frame. p and q are the angular rates of the UAV around the x- and y-axis of the body frame, respectively. The assumption $r = 0$ is already implemented.

$$\underline{\omega}_b = (p, q, 0)\,\{\underline{E}_b\} \tag{3.1}$$
$$\underline{\omega}_r = (p, q, 0)\,\{\underline{E}_b\} + (0, 0, \Omega)\,\{\underline{E}_r\} \tag{3.2}$$
$$= (p, q, \Omega)\,\{\underline{E}_b\} \tag{3.3}$$

3.3.2 Moments of inertia

For the angular momentum, the moment of inertia is required of both the rotor and the body. For the inertia of the body no assumptions are made other the symmetry planes. The rotor is assumed to be flat, so its moments of inertia around the x- and y- axes are half that of the one around the z-axis (which is denoted I_r). The moments of inertia are given in the body frame: since the rotor is modelled as a disk its inertia is the same irrespective of its rotation Ψ.

$$[J_b] = \begin{bmatrix} I_{b_x} & 0 & 0 \\ 0 & I_{b_y} & 0 \\ 0 & 0 & I_{b_z} \end{bmatrix} \tag{3.4}$$

$$[J_r] = \begin{bmatrix} \frac{1}{2}I_r & 0 & 0 \\ 0 & \frac{1}{2}I_r & 0 \\ 0 & 0 & I_r \end{bmatrix} \tag{3.5}$$

The value of the moment of inertia of the rotor in the z-axis is the moment of inertia of a slender rod with its mass m distributed evenly along its length $2R$: $I_r = \frac{1}{3}mR^2$.

3.3.3 Angular momentum

The angular momenta of the DC and separate bodies are given below.

$$\underline{D}_b = \underline{\omega}_b \left[J_b\right] \{\underline{E}_b\} \tag{3.6}$$
$$\underline{D}_r = \underline{\omega}_r \left[J_r\right] \{\underline{E}_b\} \tag{3.7}$$
$$\underline{D} = \left[(p,q,0)\left[J_b\right] + (p,q,\Omega)\left[J_r\right]\right] \{\underline{E}_b\} \tag{3.8}$$
$$= \left(p\left[\tfrac{1}{2}I_r + I_{b_x}\right], q\left[\tfrac{1}{2}I_r + I_{b_y}\right], \Omega I_r\right) \{\underline{E}_b\} \tag{3.9}$$

The time derivative of the angular momentum is given next. In here, rotor rotational velocity is assumed constant. The derivative of the angular momentum is equal to the external moment applied to the structure in the body frame, M_{ext}.

$$\dot{\underline{D}} = \underline{M}_{ext} = \left[\dot{\underline{\omega}}_b \left[J_b\right] + \dot{\underline{\omega}}_r \left[J_r\right] + \underline{\omega}_b \times \underline{D}\right] \{\underline{E}_b\} \tag{3.10}$$
$$= \left[(\dot{p},\dot{q},0)\left(\left[J_b\right] + \left[J_r\right]\right) + \underline{D}\left[\omega_X\right]\right] \{\underline{E}_b\} \tag{3.11}$$

Where the rotational operator $[\omega_X]$ is given below (for $r = 0$).

$$\left[\omega_X\right] = \begin{bmatrix} 0 & 0 & -q \\ 0 & 0 & p \\ q & -p & 0 \end{bmatrix} \tag{3.12}$$

Performing all the matrix multiplications yields the following final expression of the angular momentum derivative.

$$\underline{M}_{ext} = \begin{Bmatrix} \dot{p}\left[I_{bx} + \frac{1}{2}I_r\right] + q\Omega I_r \\ \dot{q}\left[I_{b_y} + \frac{1}{2}I_r\right] - p\Omega I_r \\ -qp\left[\frac{1}{2}I_r + I_{b_x}\right] + pq\left[\frac{1}{2}I_r + I_{b_y}\right] \end{Bmatrix}^T \{\underline{E}_b\} \tag{3.13}$$
$$= \begin{Bmatrix} \dot{p}\left[I_{b_x} + \frac{1}{2}I_r\right] + q\Omega I_r \\ \dot{q}\left[I_{b_y} + \frac{1}{2}I_r\right] - p\Omega I_r \\ pq\left[-I_{b_x} + I_{b_y}\right] \end{Bmatrix}^T \{\underline{E}_b\} \tag{3.14}$$

If the applied external moment about the z-axis is equal to the third component in this vector, the yaw rate r and angle ψ will be equal to zero and the original assumption is satisfied.

3.3.4 State-space system

Equation (3.14) can be written in state-space form to facilitate easy simulation, where the output equations consists of an identity C-matrix and zero D-matrix:

$$\begin{Bmatrix} \dot{p} \\ \dot{q} \end{Bmatrix} = \begin{bmatrix} 0 & -\frac{\Omega I_r}{I_{b_x}+\frac{1}{2}I_r} \\ \frac{\Omega I_r}{I_{b_y}+\frac{1}{2}I_r} & 0 \end{bmatrix} \begin{Bmatrix} p \\ q \end{Bmatrix} + \begin{bmatrix} \frac{1}{I_{b_x}+\frac{1}{2}I_r} & 0 \\ 0 & \frac{1}{I_{b_y}+\frac{1}{2}I_r} \end{bmatrix} \begin{Bmatrix} M_x \\ M_y \end{Bmatrix} \tag{3.15}$$

The diagonal of the A-matrix currently only has zeros on it, but this would be the place to implement (aerodynamic) damping as described in section 3.4.

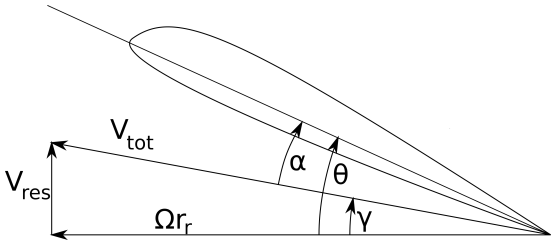

Figure 3.2: Movements of the rotor blade in the incoming flow. V_{res} is the resulting incoming flow, including induced rotor flow and pitch and roll movements of the fuselage. r_r is the radial position of this portion of the blade from the center of the rotor.

3.4 Aerodynamic Damping

As described in section 2.2.3, aerodynamic damping is usually not derived analytically when a rigid rotor is assumed. Aerodynamic damping of roll and pitch motions due to the rotor can be implemented by deriving the extra angle of attack on the blade due to the rolling and pitching motion. To this end, the lift coefficient of the blade will be linearized: $C_l = C_{l_\alpha}\alpha$. Since this relation is linear, the extra moment around x and y axes of the fuselage can be calculated simply using the extra angle of attack added by the effect of the angular motions of th UAV. The physical situation is given in fig. 3.2

From this image, the angle of attack as a function of roll and pitch angles can be derived. Take note that, seen from the top, the DC blade rotates in the clockwise direction. Ψ is then the angle of the rotor as measured from the positive x-axis as shown in fig. 3.1.

$$V_{res} = V_i - pr_r \cos\Psi - qr_r \sin\Psi \tag{3.16}$$

$$\alpha = \theta - \arctan\frac{V_{res}}{\Omega r_r} \tag{3.17}$$

When disregarding the blade pitch angle θ and assuming small angles, eq. (3.17) shows a simple relation for the extra angle of attack due to pitching and rolling. This angle is denoted α_{pq}:

$$\alpha_{pq} = \frac{1}{\Omega}\left(p\cos\Psi + q\sin\Psi\right) \tag{3.18}$$

Now integrating the lift generated by this extra angle of attack over the length of the blade yields the moment of the blade as a function of the angle over its rotation Ψ. Chord length c is assumed constant over the blade radius. Use is also made of lift formula $L = \frac{1}{2}\rho V^2 C_L S$ and the air velocity of a piece of blade is approximately $V_{blade} \approx \Omega r_r$.

$$dL = \tfrac{1}{2}\rho(\Omega r_r)^2 \alpha_{pq} C_{l_\alpha} c dr_r \tag{3.19}$$

$$= \tfrac{1}{2}\rho\Omega r_r^2 C_{l_\alpha} c\left(p\cos\Psi + q\sin\Psi\right) dr_r \tag{3.20}$$

$$M = \int_0^R r_r dL \tag{3.21}$$

$$= \tfrac{1}{8}\rho\Omega R^4 C_{l_\alpha} c\left(p\cos\Psi + q\sin\Psi\right) \tag{3.22}$$

The moments in x and y direction can be calculated by multiplying the moment by $\cos\Psi$ and $\sin\Psi$ respectively and averaging over a single rotation (2π). Making use of trigonometric integration rules, this reduces to the following equation. In this equation, the number of blades on the rotor n is incorporated. A minus is now introduced since the previous moment was calculated blade-up, but it should be blade-down for these two moments.

$$M_x = -p\tfrac{1}{16}\rho\Omega R^4 C_{l_\alpha} cn \tag{3.23}$$

$$M_y = -q\tfrac{1}{16}\rho\Omega R^4 C_{l_\alpha} cn \tag{3.24}$$

These moments will not be used further in this chapter. They do, however, provide a source of aerodynamic damping that is included in the CD model used later in the thesis.

3.5 Conclusions from Equations of Motion

From the first two components in the vector of eq. (3.14), the pitch and roll dynamics can be simulated when given moments as control input. The system behavior can then be studied to better understand the differences in output response for different parameters. Firstly, the response to a constant moment will be shown. Afterwards, the required moment to get a pure roll or pitch rotation will be calculated.

3.5.1 Constant moment along single axis

In order to see the effect the gyroscopic effect has on the attitude dynamics, a constant moment is applied to the fuselage in simulation, as given in eq. (3.15). The parameters used for this model are comparable to the DC in the first case, but later a comparison will be made with a human-scale helicopter. Both sets of parameters are given in table 3.1. Since this simulation is used to get a qualitative understanding of the involved dynamics, the exact figures are not important, but relative time-scales between different parameter sets may be interesting.

Table 3.1: Simulation model parameters for the rigid rotor model. The rotor inertia $I_r = \frac{1}{12}mD^2$ is that of a thin rod with its mass and diameter as given in the table. The fuselage is modeled as a box with dimensions as given in the table. The data from the DC are measured, while for the human scale equivalent parameters the data on the Sikorsky S-61 is estimated using parameters found on a website[1].

	DC equivalent	Human scale equivalent
Rotations Per Minute (RPM)	1650	203
Rotor diameter	1 m	18.9 m
Rotor mass	0.11 kg	474.5 kg
Body mass	3.9 kg	6886 kg
Body length x	0.2 m	7 m
Body length y	2 m	3 m
Body length z	0.3 m	3 m

The response is shown in fig. 3.3. From the plots the cross-coupling between pitch and roll is very clearly visible. A pure roll moment (left column in the figure) generates some roll motion but actually has a bigger effect on the pitch rate. Furthermore, looking at the actual angles, it is seen that a roll moment induces an increase in the pitch angle over time, while the roll moment stays relatively constant. The opposite direction shows similar behavior: a pitch moment generates a roll rate, but even then the pitch rate oscillations are more intense. This is due to the fact that the pitch inertia of the body is much lower than the roll inertia, since the wings are aligned along the y-direction. Furthermore, a pure pitch moment over time yields an oscillating pitch angle, but a roll angle that is increasing over time.

It can thus be concluded that the cross-coupling is very severe, not symmetric (pitch-to-roll coupling is less than vice versa), and control of the helicopter has to be done 90° off the direction that the drone is intended to go. While an applied roll moment generates a pretty clean pitch angle increase, an applied pitch moment yields a steadily increasing roll angle while showing pitch oscillations that are quite severe.

3.5.2 Moments required for pure roll dynamics

To better understand what is required to control this helicopter, an idealized feedback system is created: instead of applying a moment purely in one axis, the moment to be applied to calculated every time-step to exactly counter the cross-coupling between the axis. An extra constraint is applied to the maximum amount of moment that can be applied (i.e. maximum control deflection of the cyclic pitch), such that the total moment applied is equal to the amount of moment applied in the previous simulation. The remaining moment is calculated using Pythagorean's theorem: $M_x^2 + M_y^2 = 0.1^2$, corresponding to a change of point of maximum lift over the rotation of the rotor. This shows what is required to perform i.e. a pure roll angle change.

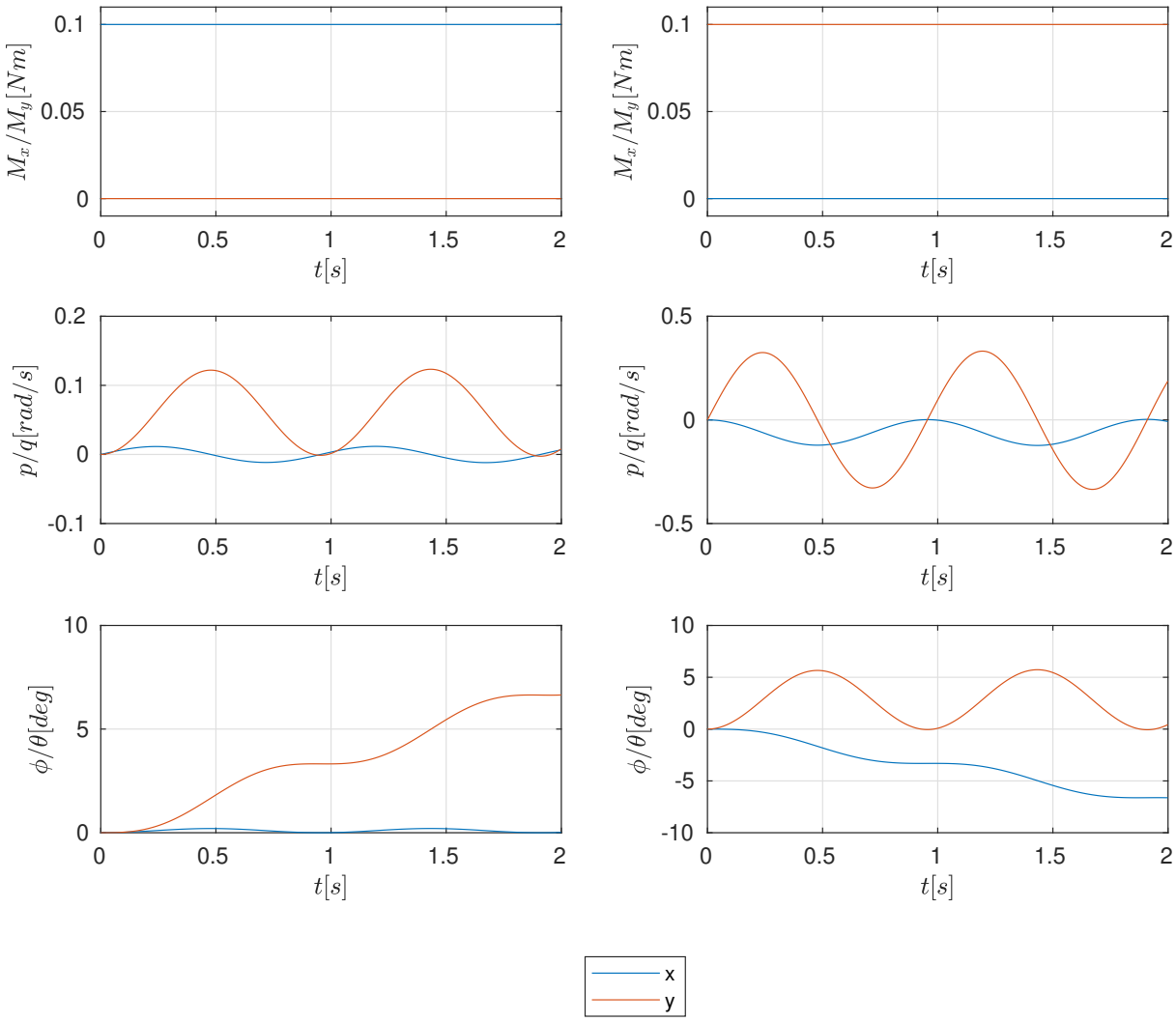

Figure 3.3: A constant moment is applied to the DC, modelled as a box as fuselage and rotating cylinder as rotor. In the left column, a moment is applied to the roll-axis, in the right column, a moment is applied to the pitch-axis. The motion cross-coupling is clearly visible in this system, as well as the fact that the cross-coupling is very non-symmetric: a roll motion generates a sharp pitch moment but a pitch moment has less influence on the roll dynamics. Also, it is clear that to achieve a roll rate, a pitch moment has to be produced and vice versa.

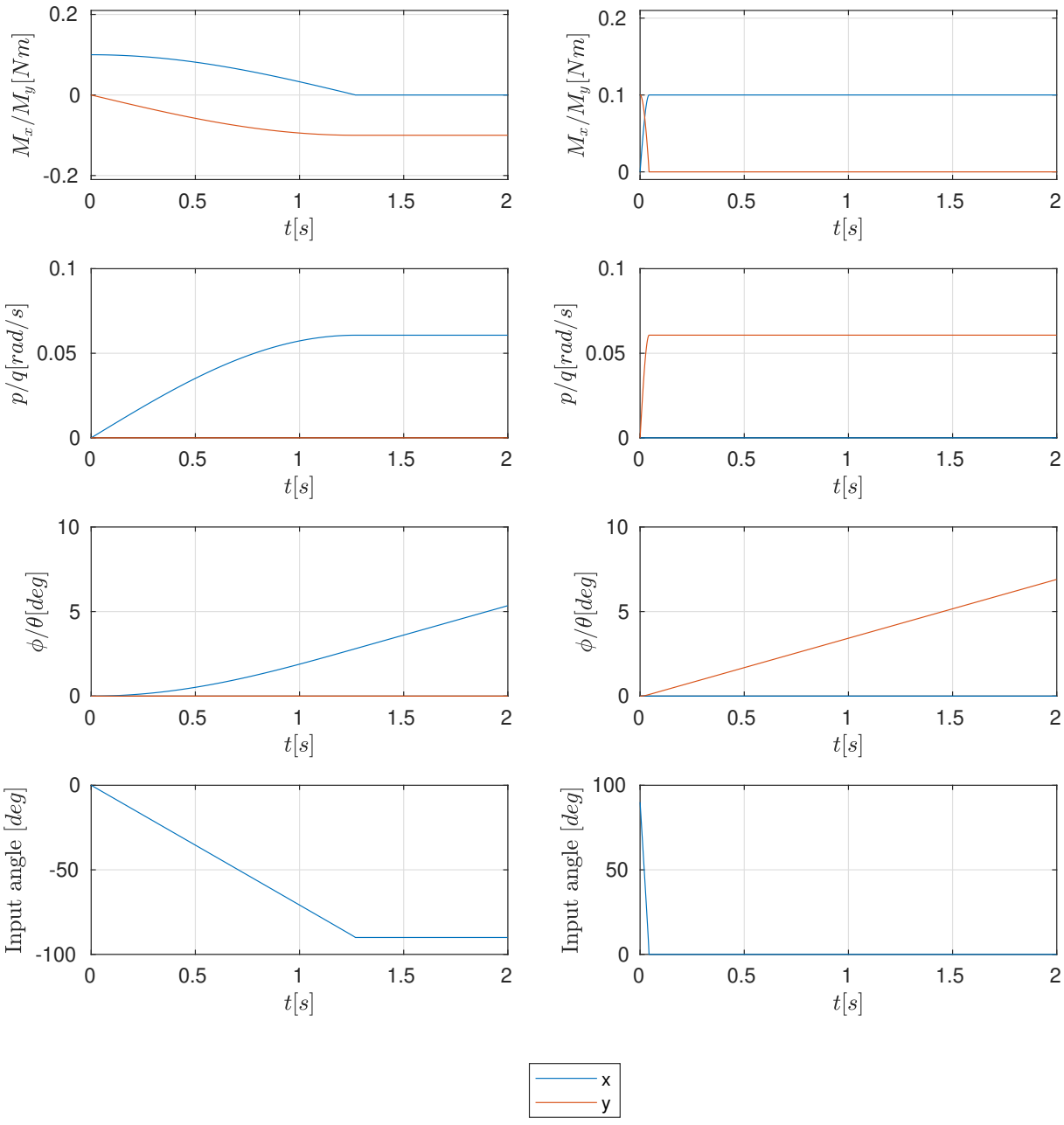

Figure 3.4: The rigid rotor model of the DC is used to find what control moments are needed to get a pure roll and pitch movement. The left column has pure roll movement and the right column has pure pitch movement. The input angle shows the angle of the moment applied ($\arctan 2(M_y, M_x)$).

The simulation results are presented in fig. 3.4. From the graphs there are clearly two time-scales. During roll rotation, the inertia is very high, which leads to a slow increase in roll rate. Therefore, the moment to counteract the gyroscopic effect on the pitch-axes increases very gradually during the first second. Thus, the input angle changes linearly from 0 to 90° offset: after 1.2 s, all the available control moment is applied in the pitch direction to counteract the gyroscopic effect. In the right column, the same simulation is performed but for a pitch rotation. In this case, the maximum pitch rate is quickly reached, and at that point all control moment is used on the roll direction to counteract the gyroscopic effect. This behavior is probably so fast that it can be ignored, i.e. simply applying a constant moment in the roll direction will yield a pitch movement and very little cross-coupling will be observed.

Comparing this response to the constant moment response presented in fig. 3.3, shows that a pure pitch response is quite easy to achieve by simply applying a roll moment. There will still be some roll oscillations but they are negligible. Obtaining a roll rate is more difficult and requires good coordination of the moments applied to the input axes.

When a human-scale helicopter is simulated in the same way, it is clear that the cross-coupling between pitch and roll requires the control angle to switch much quicker to 90°. This is due to the fact that the gyroscopic effect is faster in this case, and the fuselage is less elongated.

3.6 Cylinder Dynamics as Rigid-rotor model

In the rest of the thesis, a model similar to the rigid rotor model is used. This model is called the Cylinder Dynamics (CD) model. When using the CD model for system identification, the A and B matrices will both be simply full $2x2$ matrices, yielding eight parameters to be identified. The parameters in the A matrix can be thought of as the aerodynamic damping on the diagonal and gyroscopic effect on the cross-diagonal. The two zeros in the B matrix as given in eq. (3.15) will also be set to an identifiable constant, since the control signal will pass through a mixer which distributes the pitch and roll moment over the swashplate servos. This way, the distribution itself including any phase lag in the control moment application due to blade flapping will be incorporated in the B matrix.

3.7 Conclusion

A simplified rigid-rotor model was developed from first principles. It was shown that a human-scale helicopter's dynamics are close to that of a pure gyroscope such that a pitch rate can be achieved by applying a roll moment and vice versa. The DC, however, has a much heavier fuselage. Therefore, the transient response is much slower and simply applying a pitch moment will lead to a lot of wobble on both the axes.

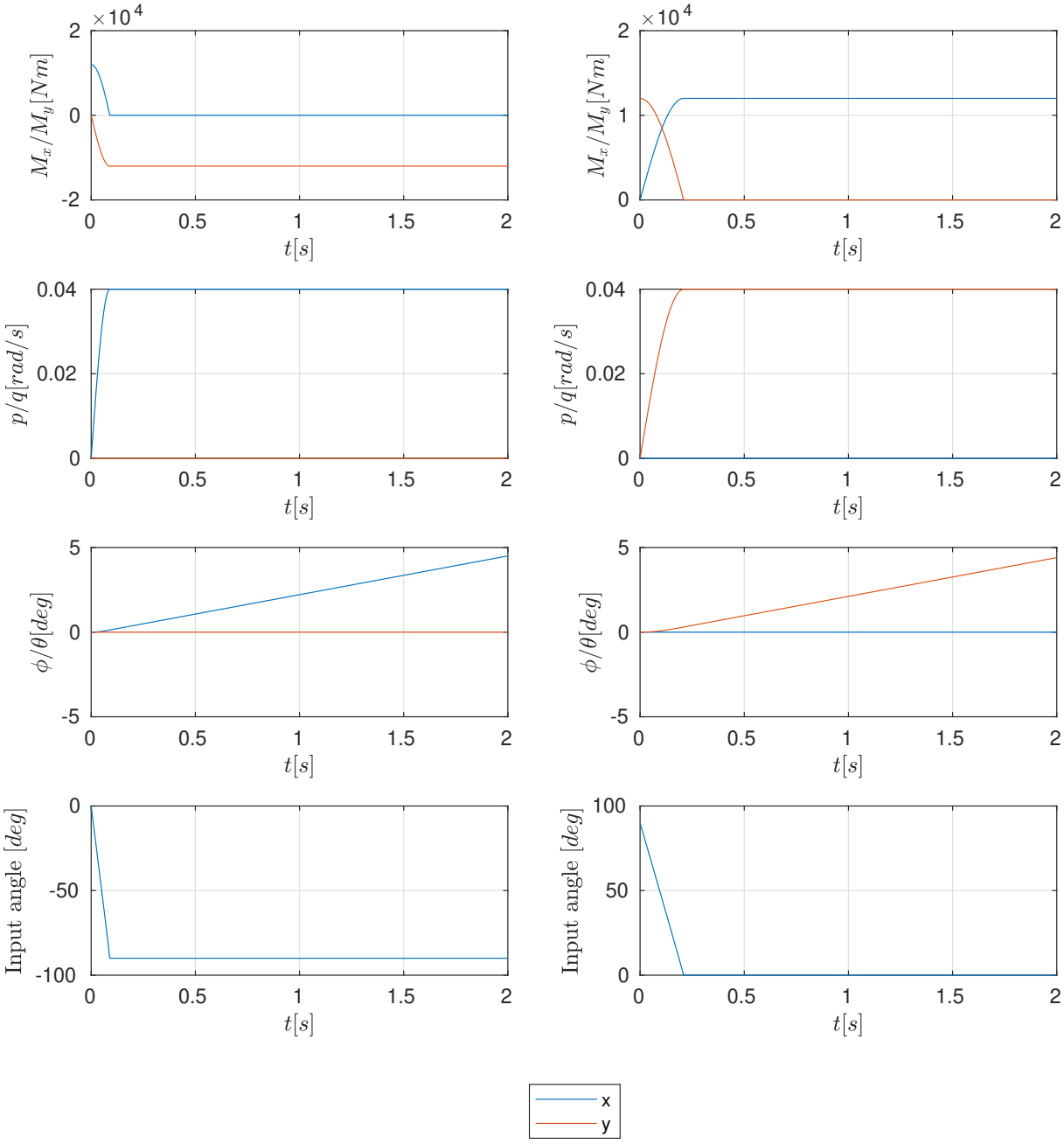

Figure 3.5: The rigid rotor model of a Sikorsky S-61 (parameters in table 3.1) is used to find what control moments are needed to get a pure roll and pitch movement. The left column has pure roll movement and the right column has pure pitch movement. The input angle shows the angle of the moment applied ($\arctan 2(M_y, M_x)$). It is clear that the angle switches much faster to 90° than in the DC parameter set in the pure roll case.

Chapter 4

Research paper

The following paper was published in the IMAV2018 conference[27]. It concisely shows most of the results gotten during this research project: it starts with model selection, then compares two models, the Cylinder Dynamics (CD) and Tip-Path Plane (TPP) models, for how well they can replicate in-flight data recorded on the DelftaCopter (DC). Afterwards, a controller based on the best model is implemented and its performance is shown. Finally, a short overview of the proposed extension to the hover model for forward flight is given and its fit on test flight data is shown.

All flight tests, model fitting and control tests described in this paper and chapter 5 were performed using the DelftaCopter 2 (DC2). The research paper shown here functions as a summary of the work performed on this version of the DC. Chapter 5 provides more detail on the forward flight modeling, which is described only concisely in the paper.

Due to external circumstances the DC2 was changed by using a different motor and rotor blades. This new version is called the DelftaCopter 3 (DC3). This version has a smaller rotor rotating at a higher speed. Chapters 6 and 7 details the problems experienced while attempting the same modeling and control techniques to this new setup of the DC.

Modeling DelftaCopter from Flight Test Data

J.F. Meulenbeld*, C. De Wagter†, B.D.W. Remes
Delft University of Technology, Kluyverweg 1, 2629HS Delft, the Netherlands

ABSTRACT

The DelftaCopter, a tilt-body tailsitter UAV, endures large gyroscopic moments due to the single helicopter rotor providing its thrust. In previous research by de Wagter et al.[1] the DelftaCopter's attitude dynamics were modeled using a rigid rotor, as is customary for small helicopter modeling. A controller based on this model was unable to compensate coupling between pitch and roll rate caused by gyroscopic moments.

In this paper, two models are compared for reproducing the attitude dynamics of the DelftaCopter in hover. The Cylinder Dynamics (CD) model, used in the previous research, assumes a rigid rotor. The Tip-Path Plane (TPP) model incorporates flapping motion of the blades and was developed by Mettler[2]. The two models are compared by fitting each model's parameters on flight data using chirps, sine waves with increasing frequency, as system identification maneuvers. The TPP model is shown to be much more accurate in reproducing the high-frequency attitude dynamics. An LQR controller directly based on the TPP model is shown to yield adequate tracking performance. This validates the applicability of this model to the DelftaCopter.

For forward flight, an extension to the TPP hover model is proposed incorporating the aerodynamics of the wings and elevons. It is shown that with the extension, chirps in forward flight can be simulated with reasonable accuracy. This paves the way for a model-based controller in this flight state.

1 INTRODUCTION

While Unmanned Aerial Vehicles (UAVs) have been around for many years, reaching a large endurance and range on small platforms remains a challenge. The Outback Medical Challenge encourages research on UAVs with the capability of long-distance flights and landing in rough terrain. This requires vertical take-off and landing (VTOL). There are multiple concepts for combining long range and VTOL, of which a qualitative comparison is given by Herbst et al.[3] One of the concepts is the tail-sitter or tilt-body hybrid UAV. This concept has its rotors pointed upwards in hover mode, but can tilt downward by $90°$ to transition to forward flight. In forward flight the wings of the UAV provide the required lift for level flight, which is more efficient than using rotors for lift. The transition is shown in Figure 1.

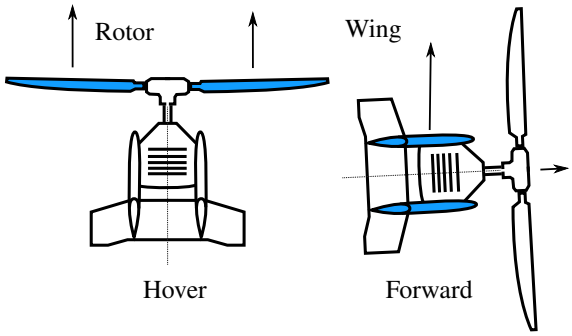

Figure 1: Transition of the DelftaCopter.

Within the class of tilt-body UAVs, the amount of rotors varies. Using four rotors allows to use standard quadcopter control methods in hover, while taking into account aerodynamic forces in forward flight. Examples of this class are the VertiKUL[4] and Quadshot[5]. Two rotor systems have either counter-rotating in-line rotors like the Vertigo[6] or a combination of two rotors that rotate in the same plane, like the MAVIon[7] or Cyclone[8]. Both options use aerodynamic surfaces for control. The single-rotor tilt-body UAV concept is implemented by the DelftaCopter[9] and the Flexrotor, developed by a commercial company[1]. This makes the DelftaCopter a unique platform for researching single-rotor tilt-body UAVs.

The DelftaCopter has been designed and built for the Outback Medical Challenge in 2016 by the DelftaCopter team at TU Delft[9]. In 2018, the new competition again requires a flight of $\approx 60\,\mathrm{km}$ in one hour, landing in rough terrain halfway[10]. This demands a UAV that has a long range and speed, and can do VTOL. The efficiency advantage of a single rotor over four rotors is why this concept was chosen. The DelftaCopter is shown in Figure 2.

Though the single rotor providing thrust and lift is more efficient than a design with multiple rotors, it yields certain control challenges. As for most helicopters, the gyroscopic effect plays an important role in the dynamics of the DelftaCopter. Contrary to most helicopters, the inertia of the fuse-

*joost.meulenbeld@gmail.com
†C.deWagter@tudelft.nl

[1] http://aerovel.com/

Figure 2: DelftaCopter in hover. In forward flight, the entire fuselage pitches down 90° and the rotor provides the thrust as shown in Figure 1.

lage underneath the rotor is quite large compared to the rotor inertia. Often helicopters are controlled with the assumption that an applied roll moment yields a pitch rate and vice versa. This is the case when no bulky fuselage is present under the rotor[11] and the response resembles that of a pure gyroscope. The DelftaCopter has a heavy fuselage due to the long wings and electronics placed at the wing tips for better radio reception. This also makes the inertia much larger in the roll direction than in the pitch direction.

The currently used attitude rate controller was described by De Wagter and Smeur[1]. It uses proportional feedback on the rotational rate error. Additionally, it tries to compensate pitch and roll gyroscopic coupling using identified coupling magnitude $C_{q\dot{p}}$ and $C_{p\dot{q}}$ and another gain K_c. The formulation is given in Equation (1). δ_x is the roll command, δ_y pitch. G is the actuator effectiveness matrix, K_p and K_q are feedback gains, p is roll rate and q is pitch rate, and K_c is a tuning factor.

$$\begin{bmatrix} \delta_x \\ \delta_y \end{bmatrix} = G^{-1} \begin{bmatrix} K_p p_{err} + q C_{q\dot{p}} K_c \\ K_q q_{err} + p C_{p\dot{q}} K_c \end{bmatrix} \quad (1)$$

This controller relies on the model identified using flight data. The model is based on the assumption of a rigid rotor applying gyroscopic moments. The factor $K_c = 0.5$ in Equation (1) yielded the best results with little coupling between pitch and roll, while a value of 1 would be expected to work best if the underlying model is valid.[1] This indicates that the assumed model is incapable of producing all relevant attitude dynamics of the DelftaCopter. This leads to this paper's research question: What is the best model to replicate the attitude dynamics of the DelftaCopter for the purpose of control?

The research question was answered by comparing multiple models for their accuracy. The results are described in this paper as follows. Section 2 describes the models that are compared. To do this comparison, flight tests were performed and the models' parameter identified, as described in Section 4. With the fitted models, a controller was designed and implemented for hover mode, the design and performance of which is shown in Section 5. In Section 6 an extension to the model is proposed to incorporate the effect of the wing aerodynamics during forward flight. Finally, in Section 7 the results are discussed and a conclusion is drawn with respect to the used models for the DelftaCopter.

2 Identification Modeling

For the purpose of modeling the DelftaCopter for control applications, a system identification model is to be chosen. Not all parameters in this model can be found from direct physical measurement, so a grey-box parameter estimation procedure was used that estimates the unknown parameters from flight data. The models used for this are described in this section.

3 Description of Model Types

One of the important differences between the assumptions of different models is how they incorporate the flapping dynamics of the helicopter. The flapping dynamics of a helicopter are well covered in Bramwell's helicopter dynamics[12] as follows. The helicopter pitch and roll attitude are controlled by using the swashplate of the rotor. This device allows to set the variation of the blade pitch angle over the rotation of the rotor using collective (for thrust) and cyclic pitch (for attitude control). The blade pitch angle follows the relation below.

$$\theta = \theta_0 - \delta_x \cos\Psi - \delta_y \sin\Psi \quad (2)$$

In this equation taken from Bramwell's book[12, sec. 1.6.2], θ is the blade pitch angle, Ψ is the in-plane rotation of the blade from the back of the helicopter and θ_0 is the collective pitch angle determining the lift generated by the rotor. δ_x and δ_y are determined by the cyclic pitch setting of the (auto)pilot. This variation of pitch angle over the rotation will generate differences in aerodynamic forces which in turn makes the blade flap up and down. The following categories of models can be distinguished based on how they incorporate the flapping dynamics.

- The first and most elaborate approach is to deal with the flapping blade explicitly, including the flapping angle of every individual blade as a state of the model. This allows theoretical analysis into the response but also requires many physical parameters to be accurately measured. It leads to a model that is very hard to use for control design due to its time-dependence.

- An often applied simplification is to relate attitude dynamics to the Tip-Path Plane (TPP), i.e. the plane in which the tips of the rotor travel. It can be derived directly using the flapping angle equation shown in Equation (2). A mathematical description is derived by Mettler by neglecting high-frequency dynamics of the rotor.[2] The TPP is represented by two angles, a and b,

which indicate the angle between the TPP and the horizontal, in the longitudinal and lateral direction respectively, as shown in Figure 3. The TPP angles change under influence of control inputs, rotations of the fuselage and gyroscopic precession of the rotor. A moment is applied on the fuselage if the a and b angles are not zero, due to the effective spring between the rotor blade and axis and the offset of thrust application point on the rotor and the center of mass of the fuselage.[2, 13] This way, the rotor is a separate body from the fuselage with its own dynamics. This simplification is valid if the rotor rotational frequency ($\approx$ 1650RPM $=$ 27.5 Hz for the DelftaCopter) is much higher than the highest eigenfrequency of the body-TPP coupling dynamics ($\approx$ 5 Hz for the DelftaCopter, as shown later). Then the oscillations of the rotor are damped out by the body dynamics and the forces can be expressed as an average over a rotation of the rotor. Mettler applies this type of model to a small unmanned helicopter, resulting in an accurate model that matches with flight data[2].

- The last simplification is to ignore the flapping dynamics and treat the rotor as a rigid object, with no flapping angle possible. This way, the gyroscopic effect that the rotor produces still affects the fuselage, but the time-dependent coupling between fuselage and rotor are eliminated. This method is used widely for small helicopters[14, 15, 16]. A TPP model can be transformed into a model without flapping dynamics by setting the derivatives of the a and b angles to zero, which is a valid simplification if the flapping dynamics are much faster than the fuselage dynamics[13]. The type of model without flapping dynamics will be called a cylinder dynamics (CD) model, since the gyroscopic effect of the rotor can be included by modeling it as a rigid rotating cylinder.

In this paper, the TPP and CD models are compared for their accuracy to replicate in-flight test data. The formulation for the TPP and CD model will be given below. Both are linear time-invariant models in state-space form, using the equations below.

$$\dot{\bar{x}} = A\bar{x} + B\bar{u} \tag{3}$$

$$\bar{y} = C\bar{x} + D\bar{u} \tag{4}$$

3.1 TPP model description

The Tip-Path plane (TPP) model has been adapted from Mettler's helicopter model, of which only the p, q, a and b states are used[2]. For the TPP model, the state vector is $\bar{x} = (p, q, a, b)^T$ and the input vector is $\bar{u} = (\delta_x, \delta_y)^T$. The state-space A, B and C matrices for the TPP model are given in Equations (5) to (7). The D-matrix consists of only zeros. The model has nine parameters that need to be found from flight testing: L_b and M_a represent the spring constants of the Tip-Path Plane, consisting of both the stiffness of the blade and blade hinge, and the offset between rotor and center of mass of the fuselage. τ_{f_n} is the time constant of the TPP dynamics. A_{b_n} and B_{a_n} are cross-coupling terms that describe how the TPP interchanges the a and b angles over time. The four parameters in the B-matrix give the actuator effectiveness. Since the DelftaCopter may fly with different RPMs, the theoretical dependence of the parameters is made explicit: $\tau_f = \tau_{f_n}/\Omega$, $A_b = A_{b_n}/\Omega^2$ and $B_a = B_{a_n}/\Omega^2$[2, sec. 2.3]. Section 4.3 comments on the validity of this dependence.

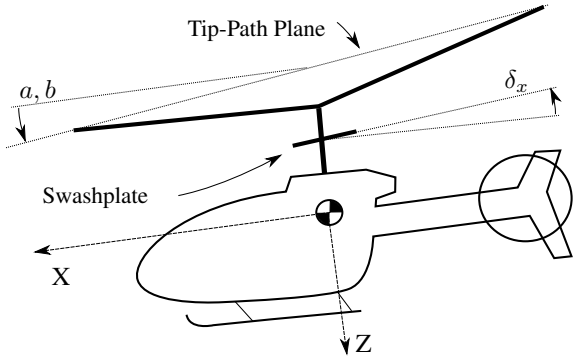

Figure 3: Helicopter Tip-Path plane (TPP) model. The axes shown in this image are as used in the DelftaCopter while it is in hover. The y-axis is chosen using the right-hand rule.

$$A_{TPP} = \begin{bmatrix} 0 & 0 & 0 & \mathrm{L_b} \\ 0 & 0 & \mathrm{M_a} & 0 \\ 0 & -1 & -\frac{\Omega}{\tau_{f_n}} & \frac{\mathrm{A_{b_n}}}{\Omega\,\tau_{f_n}} \\ -1 & 0 & \frac{\mathrm{B_{a_n}}}{\Omega\,\tau_{f_n}} & -\frac{\Omega}{\tau_{f_n}} \end{bmatrix} \tag{5}$$

$$B_{TPP} = \begin{bmatrix} 0 & 0 \\ 0 & 0 \\ \frac{\mathrm{A_{lat}}\,\Omega}{\tau_{f_n}} & \frac{\mathrm{A_{lon}}\,\Omega}{\tau_{f_n}} \\ \frac{\mathrm{B_{lat}}\,\Omega}{\tau_{f_n}} & \frac{\mathrm{B_{lon}}\,\Omega}{\tau_{f_n}} \end{bmatrix} \tag{6}$$

$$C_{TPP} = \begin{bmatrix} 1 & 0 & 0 & 0 \\ 0 & 1 & 0 & 0 \end{bmatrix} \tag{7}$$

3.2 CD model description

The state used in the Cylinder Dynamics (CD) model is $\bar{x} = (p, q)^T$, and the input is the same as for the TPP model. Both the A- and B-matrices consist of four identifiable parameters, as shown in Equations (8) and (9) below. All identifiable variables could be ascribed physical meaning as a steady-state solution of the a and b states in the TPP model, or through gyroscopic moments and aerodynamic damping. The latter option would entail measuring many different parameters including aerodynamic forces, and does not improve usefulness for control design since the final model has the same structure as it has now.

$$A_{cyl} = \begin{bmatrix} L_p & L_q \\ M_p & M_q \end{bmatrix} \quad (8)$$

$$B_{cyl} = \begin{bmatrix} L_{lat} & L_{lon} \\ M_{lat} & M_{lon} \end{bmatrix} \quad (9)$$

3.3 TPP and CD model equivalency

The a and b states of the TPP model can be regarded as the angular accelerations in q and p states respectively, i.e. the a state is directly related to the derivative of q. This means that instead of determining the angular acceleration directly using the control input as in the CD model, the angular acceleration has its own dynamics and is influenced by the control input.

The steady-state solution resulting from $\dot{a} = \dot{b} = 0$ in the TPP models allows substitution of steady-state a and b values in the $\dot{p}$ and $\dot{q}$ equations, which then yields a comparable system to the CD model, with every CD model parameter linked directly to a combination of parameters in the TPP model.[13]

3.4 Conclusion

The CD and TPP models will be fitted purely based on the input-output response. For the TPP model the a and b states are not measured, but result from the measurements of their interactions with the pitch and roll rates and actuators. This means that these states cannot directly be validated from measurements. The TPP model has but one parameter more than the CD model, but more importantly it has two more eigenfrequencies that should allow capturing a broader range of response frequencies.

4 Flight Testing and System Identification

For fitting the model parameters, flight tests were performed in an indoor environment. To make sure that the range of interesting dynamics is covered in every flight test, an automated flight testing procedure was developed. According to Tischler et al., the "chirp" maneuver is able to generate the required frequency content.[17] A chirp is a sine wave with a frequency increasing continuously over time. When a chirp is inserted in a single actuator, the system response shows the coupling between all axes and how this changes with frequency. Tischler also states that to get the best results, the system should be flown open-loop. However, this is not possible with the DelftaCopter due to the dynamics, so the attitude controller is still active during flight tests. To lower the coherence between different axes introduced by the controller, noise is added to every axis independently, as per Tischler's suggestion[17]. The noise is filtered with a first-order low-pass filter with the cut-off at the highest frequency of the chirp. An exponential-time chirp is used to have enough content at the lower frequencies.

The chirp signal is generated and added to the controller signal and the resulting actuator signal is stored with the gyroscope measurements on an SD-card at a frequency of 500 Hz. The chirp settings are given in Table 1. The frequency range starts and ends higher than suggested by Mettler[2]. The lower frequency is limited by the size of the indoor facility in which the tests were performed, while the higher frequency now includes more of the high-frequency dynamics. The eigenfrequencies of the identified model are well within the range of the chirp.

Variable	Value
Start frequency	0.5 Hz
End frequency	10 Hz
Noise fraction	0.2
C_1	4
C_2	$\frac{1}{\exp(C_1)-1}$

Table 1: Settings used for the exponential-time chirp. The noise fraction is the ratio between the amplitude of the chirp and the standard deviation of the white noise that is filtered and added to the chirp signal. C_1 and C_2 are the values used in the exponential-time chirp formulation in the book by Tischler[17].

After flight testing, the data was filtered digitally by an ideal low-pass filter with a cut-off frequency of 15 Hz. This removes vibrations caused by the rotor which rotates at around 27.5 Hz. The input channels were centered around 0 to remove input bias. The resulting data streams were used to fit the parameters in the time domain using the MATLAB system identification toolbox.

4.1 Chirp results

The results for a roll chirp are shown in Figure 6. In this figure, the measured roll and pitch rates are shown for the online measurement, the simulated TPP model and simulated CD model. The pitch rate q is a result of the pitch-roll coupling introduced by the rotor. It is clear that the CD model is able to accurately simulate the response up to a certain frequency, but does not include the eigenfrequency which is excited at around 28.5 s. The TPP model does include this eigenfrequency and is much better at reconstructing the system response. This is due to the fact that the TPP dynamics model has four states, and therefore four eigenfrequencies. The two eigenfrequencies the TPP model has extra compared to the CD model lead to higher frequencies being accurately modeled as well. A pitch chirp is shown in Figure 7. In this chirp, the mismatch between the CD model and measurements is even worse.

4.2 Model fit validation

Figure 4 shows pitch and roll doublets, as flown by a pilot while the attitude controller was active. This flight data was not used for fitting the models and can thus be used as validation for model accuracy. Table 2 shows the eigenfrequencies of both the identified TPP and CD systems. The slower eigenfrequency corresponds to a pitch-roll coupled motion and is present in both models. The faster eigenfrequency is almost

purely pitch and is not present in the CD model. This explains why the pitch response of the CD model is so far off.

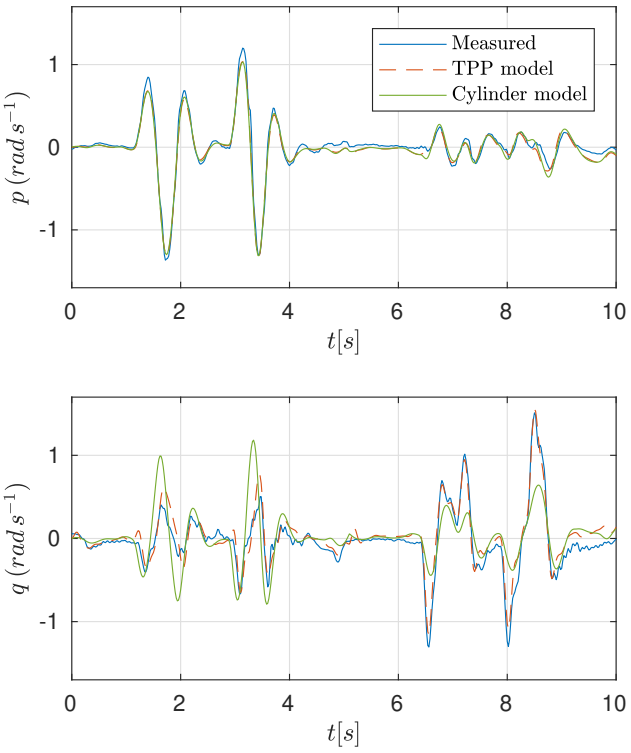

Figure 4: First some roll, then some pitch doublets, flown manually with the attitude controller active. While the roll response is quite accurately modeled by both models, the pitch response is much better in the TPP model. Since the CD model misses the higher eigenfrequency, the fast movements of the pitch are not accurately modeled. This difference is due to the low pitch inertia compared to the roll inertia.

The numerical difference between the measurements and the model output is given in Table 3. The Normalized Root Mean Squared Error (NRMSE) percentage is used as a measure of the goodness of fit, where 100% constitutes a perfect match. The NRMSE percentage is given in Equation (10), where y is the measured signal, $\hat{y}$ is the model output and $\bar{y}$ is the average of the measured signal. The fraction in Equation (10) is thus also equal to the root mean squared error divided by the standard deviation of the measurement.

$$NRMSE = 100\% \left(1 - \frac{||y - \hat{y}||}{||y - \bar{y}||}\right) \tag{10}$$

The fitted parameters are shown in Table 4. The difference in roll and pitch inertia is apparent from the L_b and M_a values, which differ by a factor of 4.8. To validate that the parameters were not overfitted to a particular chirp, the TPP model was fitted to two different sets of chirp data and their fitted parameters were compared. The highest single change in model parameter between the two sets of chirps was 7.7%, but the eigenfrequencies and damping ratios of the systems differ at most 0.9% and 1.8% respectively.

	Pole	Frequency [Hz]	Damping [−]
CD model	1-2	1.54	0.35
TPP model	1-2	1.64	0.39
	3-4	5.04	0.22

Table 2: Comparison of eigenfrequencies of the CD model and flapping dynamics fitted models. The first pole-pair has almost the same eigenfrequency between the two models, which means that in the lower frequencies both models respond comparable. However, the higher eigenfrequency of the flapping dynamics model is not present in the CD model, which explains why high-frequency dynamics are completely damped out in these simulations, as shown in Figure 7.

	Axis	TPP model	CD model
Chirp	p	77.8	77.2
	q	77.3	25.9
Doublets	p	77.6	76.7
	q	64.7	20.0

Table 3: Comparison of NRMSE percentage as given in Equation (10). For both the chirp and doublet value the roll response of both models is similar, but the pitch response matches measurements much better with the TPP model. Still, the pitch response is not perfect, as can also be seen in the doublet time response in Figure 4. The chirp rows show the NRMSE percentage for two pitch and two roll chirps combined while the doublets rows for two pitch and two roll doublets.

4.3 *Parameter RPM dependence*

As stated in Section 2, the dependence of the parameters on RPM has been made explicit in the system identification model. Therefore the remaining identifiable parameters should remain constant for different RPMs. A range of RPMs between 1500 and 1650 was tested, and the parameters, which should stay constant, change up to 185% with many parameters changing tens of percentage points. To analyse how the actual model characteristics have changed, the RPM parameter Ω is changed to 1650 RPM in the A- and B-matrices of the model fitted on the 1500 RPM data. If the theoretical relations are correct, the resulting eigenfrequencies and damping should be equal to the model fitted directly on the 1650 RPM chirp data. In reality, the largest eigenfrequency change was 4%, while the largest damping ratio change is 28%, making the model response substantially different from expected. The model fitted on 1500 RPM yielded NRMSE percentages of 72.4% and 67.1% for roll and pitch axes respectively, when tested on the same chirp signal as used in Table 3. Multiple controllers based on models at different RPMs would proba-

Param	Value	CD	Value
A_b	-1.338	L_p	-2.056
B_a	1.448	M_p	10.536
L_b	147.548	L_q	-7.900
M_a	713.378	M_q	-4.777
τ_f	0.091	L_{lat}	-5.361
A_{lat}	-0.282	M_{lat}	-67.573
A_{lon}	0.296	L_{lon}	9.917
B_{lat}	0.524	M_{lon}	11.136
B_{lon}	-0.050		

Table 4: The fitted values for the TPP and CD models. The variables are those given in Equations (5), (6), (8) and (9), while for the TPP model the variables have been made dependent on the RPM again by using the substitutions $\tau_f = \tau_{f_n}/\Omega$, $A_b = A_{b_n}/\Omega^2$ and $B_a = B_{a_n}/\Omega^2$.

bly be needed to accurately control the DelftaCopter. Further research is thus needed to obtain models that generalize well with different rotor RPMs.

4.4 Conclusion

It is clear that the TPP model is much more accurate than the CD model for the DelftaCopter. The extra complex eigenfrequency pair allows better dynamics resolution at higher frequency. Validation doublets confirm this result.

5 Rate Control in Hover

In order to further test the validity of the model, a rate controller was designed using standard control techniques and tested. Since the a and b angles are not measured, a linear observer was used to estimate these states in real time, of the form as given in Equation (11). $\hat{x}$ is the current state estimate and L is the correction matrix. The A, B and C matrices are as given in Equations (5) to (7).

$$\dot{\hat{x}} = A\hat{x} + B\bar{u} + L(\bar{y}_{measured} - \hat{y}) \tag{11}$$

$$\hat{y} = C\hat{x} + D\bar{u} \tag{12}$$

The L matrix is chosen using pole placement, setting the poles of the observer at $(-50, -50, -51, 51)$. This is small enough to add some damping to the vibrations caused by the rotor on the gyroscope readings.

The controller is designed using the feedback law given in Equation (13), adding the reference attitude rate $\bar{y}_{ref}$ multiplied by the steady-state gain of the controlled system g, which is given in Equation (14).

$$\bar{u} = -K\hat{x} + g\bar{y}_{ref} \tag{13}$$

$$g = (C(-A + BK)^{-1})^{-1} \tag{14}$$

The gain matrix K is chosen using LQR. This technique finds the optimal gain matrix K for the system minimizing a cost function of state and inputs. The cost matrices of the LQR design were chosen such that the a and b state cost is very low at 0.001, since these states are not important to the end goal of stabilizing and controlling the attitude rate. The p and q states were given equal cost, fixed at 1. Controllers were then designed for different costs of the system inputs, yielding controllers that are more or less aggressive depending on the input cost. The lower the cost on the input, the faster the controller steers the system, up to the point where input lag and delay makes the response oscillatory and unstable. The input cost of 5 made the system the fastest without introducing these oscillations. The controlled system response is shown in Figure 5. It can be seen that the roll response is delayed, but the measurement follows the command quite well. The pitch response shows a coupling when larger roll rates are present. The pitch response signal is also larger in magnitude than the commanded rates.

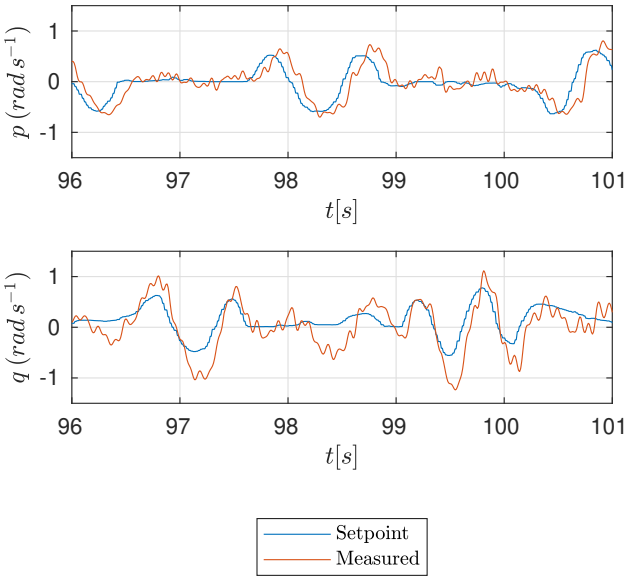

Figure 5: Controller performance during a piloted flight. The pilot directly commands the attitude rate. The roll response is delayed with respect to the command but otherwise has adequate tracking performance. The pitch rate shows coupling with the roll and the response shows larger values than the commands.

The fact that standard control techniques can be used to design a controller for the DelftaCopter, confirms that the TPP model is applicable. While the response is not perfect, the controller is able to stabilize the DelftaCopter without other tuning parameters.

6 Forward Flight Modeling

In forward flight, the DelftaCopter pitches down 90° such that the wings are level with the ground. The airspeed increases and the wings generate the required lift to maintain altitude, while the main rotor head is now providing thrust for the aircraft. This means that the aerodynamic surfaces play a

significant role in the balance of forces and moments of the DelftaCopter. To be able to design a controller for this flight mode, the TPP and CD hover models were extended. During the forward flight mode, the roll angle of the DelftaCopter in hover mode constitutes a yaw angle in the traditional aircraft sense, but is still referred to as roll. Roll rate (yaw rate in standard aircraft reference frames) is still denoted p. In order to come to a linear model, linear aerodynamic moments are assumed. The model is fitted on forward flight data and a conclusion is drawn on how significant the parameters are.

First of all, the DelftaCopter has four movable surfaces that together supply the role of aileron and elevator where every surface deflection is a linear combination of the aileron and elevator commands. The aileron applies moments to the fuselage along the axis of rotation of the rotor, and as such does not induce coupling on the pitch and roll axes. The elevator does induce a moment on the pitch rate and is thus included in the model with parameter M_{elev}. The short-period longitudinal damping due to a pitch rate M_q and lateral side-slip damping due to a roll rate L_p are included. In the CD model, they are lumped into the parameters already present, while in the TPP model these damping parameters are not yet present and are added. The resulting $A_{TPP,FW}$ and $B_{TPP,FW}$ matrices for forward flight are given in Equations (15) and (16). The state vector is the same as for the hover vector while the input vector now is $\bar{u} = (\delta_x, \delta_y, \delta_e)^T$.

$$A_{TPP,FW} = \begin{bmatrix} \mathrm{L_p} & 0 & 0 & \mathrm{L_b} \\ 0 & \mathrm{M_q} & \mathrm{M_a} & 0 \\ 0 & -1 & -\frac{\Omega}{\tau_{f_n}} & \frac{\mathrm{A_{b_n}}}{\Omega \tau_{f_n}} \\ -1 & 0 & \frac{\mathrm{B_{a_n}}}{\Omega \tau_{f_n}} & -\frac{\Omega}{\tau_{f_n}} \end{bmatrix} \tag{15}$$

$$B_{TPP,FW} = \begin{bmatrix} 0 & 0 & 0 \\ 0 & 0 & M_{elev} \\ \frac{\mathrm{A_{lat}}\,\Omega}{\tau_{f_n}} & \frac{\mathrm{A_{lon}}\,\Omega}{\tau_{f_n}} & 0 \\ \frac{\mathrm{B_{lat}}\,\Omega}{\tau_{f_n}} & \frac{\mathrm{B_{lon}}\,\Omega}{\tau_{f_n}} & 0 \end{bmatrix} \tag{16}$$

L_p and M_q represent aerodynamic damping on the roll and pitch rate. As before, the parameters L_b and M_a of the TPP model are the representative spring constants, and their physical meaning is given by Mettler[2, sec. 3.1], with M_a for example given in Equation (17). This relates the TPP angle to the angular acceleration of the fuselage, and contains a rotor stiffness term and a thrust term. The rotor blade spring stiffness k_β is equal to $88\,\mathrm{N\,m\,rad^{-1}}$[1], which is much higher than the thrust contribution at maximum weight $hT \approx hmg \approx 0.15 \cdot 4.5 \cdot 9.81 = 6.6\,\mathrm{N\,m\,rad^{-1}}$. Therefore, while the thrust may become smaller in forward flight, the parameters L_b and M_a are assumed constant in fitting the forward flight models.

$$M_a = \frac{k_\beta + hT}{I_{yy}} \tag{17}$$

The flight test used to fit the parameters is a forward flight test in level flight. The airspeed fluctuates between $17\,\mathrm{m\,s^{-1}}$ and $19.5\,\mathrm{m\,s^{-1}}$, while the RPM fluctuates between 1550 and 1720. This RPM range is quite broad compared to the hover experiments, especially considering the observed sensitivity of parameters to the RPM.

The parameters of the TPP and CD models are given in Table 5. Comparing these to the hover parameters as given in Table 4 shows that the hover and forward flight models have comparable parameters for the rotor dynamics in the TPP model case. It seems that the roll rate damping is very small, which is logical since the vertical stabilizer has a small moment arm to the center of mass.

TPP	Value	CD	Value
$\mathrm{A_{b_n}}$	-0.908	L_p	-10.690
$\mathrm{B_{a_n}}$	0.999	M_p	14.899
$\mathrm{L_b}$	147.550	L_q	-9.251
$\mathrm{M_a}$	713.380	M_q	1.050
τ_{f_n}	0.075	L_{lat}	6.605
$\mathrm{A_{lat}}$	-0.196	M_{lat}	-70.459
$\mathrm{A_{lon}}$	0.214	L_{lon}	-2.903
$\mathrm{B_{lat}}$	0.440	M_{lon}	11.532
$\mathrm{B_{lon}}$	-0.026	M_{elev}	10.263
$\mathrm{L_p}$	-0.930		
$\mathrm{M_q}$	4.691		
$\mathrm{M_{elev}}$	37.752		

Table 5: The fitted values for the TPP and CD models in forward flight. The variables for the TPP model have been made dependent on the RPM again by using the substitutions $\tau_f = \tau_{f_n}/\Omega$, $A_b = A_{b_n}/\Omega^2$ and $B_a = B_{a_n}/\Omega^2$. The $A_{TPP,FW}$ and $B_{TPP,FW}$ matrices of the forward TPP model are given in Equations (15) and (16). The CD model $A_{cyl,FW}$-matrix is the same as Equation (8), while the $B_{cyl,FW}$ matrix is as given in Equation (8), with the addition of a third input, elevator δ_{elev} linearly related to pitch acceleration $\dot{q}$ through parameter M_{elev}.

In Figures 8 to 10 the models are simulated on measurements of forward flight data, on roll, pitch and elevator chirps respectively. This chirp data was not used for fitting the parameters and can be used for validation. It is clear that the TPP model is better at predicting the high-frequency response than the CD model, but the fit is not as good as on the hover mode. This can be due to the RPM fluctuations or the TPP model not being applicable to the high rotor inflow experienced in forward flight. Another cause of model inaccuracy could be aerodynamic effects missing in the model. The angle of attack is not part of the model and was not measured, but could have an important influence. Surprisingly, the M_q parameter is positive, implying a positive feedback loop on the pitch rate. This could be due to the missing other influences in the model. The accuracies of the models can be seen

in Table 6.

	Axis	TPP model	CD model
Fitting	p	66.0	70.8
	q	54.7	21.7
Validation	p	49.7	53.1
	q	47.1	17.0

Table 6: Comparison of NRMSE percentage as given in Equation (10) for forward flight. Both fitting and validation percentages concern three chirps, one roll, one pitch and one elevator. Simulation of the models on the validation chirps can be found in Figures 8 to 10.

7 Conclusion

In order to design a new controller for the DelftaCopter, a new modeling approach was required that better captures the attitude dynamics. A system identification modeling approach was chosen and two models were compared: the previously used Cylinder Dynamics (CD) model which assumes a rigid rotor[1], and a Tip-Path Plane (TPP) model which was derived by Mettler[2]. Chirps were used as system identification maneuver and the models were compared. It is clear from Section 4 that the TPP model is much better at generating the high-frequency response than the CD model. This is validated using manually flown doublets, for which the TPP response also shows better accuracy. To show that this model is usable for control design, an attitude rate controller is designed using the standard LQR technique, with reasonable control response as shown. It can thus be concluded that the flapping dynamics have a significant influence on the attitude dynamics of the DelftaCopter.

The relationship between the identified parameters and rotor RPM was found to be different than predicted from theory. This may be due to the lumping together of unmodeled effects into the present parameters. Probably models at different RPMs are required for accurate control at these different RPMs.

For forward flight, the TPP model was extended to include roll rate and pitch rate damping, while both the TPP model and CD model include a constant for the elevator effectiveness. It is shown that the hover model with this extension is applicable to forward to some extent.

8 Recommendations

The following recommendations are made on what research could be conducted next:

- Measure the a and b states in flight to give more accurate models and validate the current model's prediction.
- Investigate the TPP model's parameters' dependence on RPM to broaden the accurate flight envelope of the model.
- Measure more aircraft states in forward flight, to allow the attitude dynamics model to depend on, in particular, angle of attack. Generalize the forward flight model for different airspeeds and RPMs.
- Use the forward flight model for attitude control.

Acknowledgements

The author would like to thank Kevin van Hecke, Freek van Tienen and Erik van der Horst from the DelftaCopter team for all help with doing flight tests and Bart Slinger and Willem Melching for the discussions on control theory.

References

[1] Christophe De Wagter and Ewoud J.J. Smeur. Control of a hybrid helicopter with wings. *International Journal of Micro Air Vehicles*, 9(3):209–217, sep 2017.

[2] Bernard Mettler. *Identification Modeling and Characteristics of Miniature Rotorcraft*. Springer US, Boston, MA, 2003.

[3] S Herbst, G Wortmann, and M Hornung. Conceptual design studies of vertical takeoff and landing remotely piloted aircraft systems for hybrid missions. *CEAS Aeronautical Journal*, 7:135–148, 2016.

[4] Menno Hochstenbach, Cyriel Notteboom, Bart Theys, and Joris De Schutter. Design and Control of an Unmanned Aerial Vehicle for Autonomous Parcel Delivery with Transition from Vertical Take-off to Forward Flight -VertiKUL, a Quadcopter Tailsitter. *International Journal of Micro Air Vehicles*, 7(4):395–405, 2015.

[5] Atsushi Oosedo, Satoko Abiko, Atsushi Konno, Takuya Koizumi, Tatuya Furui, and Masaru Uchiyama. Development of a quad rotor tail-sitter VTOL UAV without control surfaces and experimental verification. In *2013 IEEE International Conference on Robotics and Automation*, pages 317–322. IEEE, may 2013.

[6] B. Bataillé, J.-M. Moschetta, D. Poinsot, C. Bérard, and A. Piquereau. Development of a VTOL mini UAV for multi-tasking missions. *The Aeronautical Journal*, 113(1140):87–98, feb 2009.

[7] L.R. Lustosa, F. Defay, and J.M. Moschetta. Development of the flight model of a tilt-body MAV. In *IMAV*, jan 2014.

[8] M Bronz, EJ Smeur, and HG de Marina. Development of A Fixed-Wing mini UAV with Transitioning Flight Capability. *35th AIAA Applied*, 2017.

[9] Christophe De Wagter, Rick Ruijsink, Ewoud Smeur, Kevin van Hecke, Freek van Tienen, Erik van der Horst, and Bart Remes. Design, Control and Visual Navigation of the DelftaCopter. jan 2017.

[10] UAV Challenge. UAVC Medical Express 2018 Rules V2, 2017.

[11] Konstantin Kondak, Markus Bernard, Nikolas Losse, and Günter Hommel. Autonomously Flying VTOL-Robots: Modeling and Control. In *Proceedings 2007 IEEE International Conference on Robotics and Automation*, pages 736–741. IEEE, apr 2007.

[12] A.R.S. Bramwell, G. Done, and David. Balmford. *Bramwell's Helicopter Dynamics*. American Institute of Aeronautics and Astronautics, 2001.

[13] Bernard Mettler, Chris Dever, and Eric Feron. Scaling Effects and Dynamic Characteristics of Miniature Rotorcraft. *Journal of Guidance, Control, and Dynamics*, 27(3):466–478, may 2004.

[14] Konstantin Kondak, Markus Bernard, Nikolas Losse, and Günter Hommel. Elaborated modeling and control for autonomous small size helicopters. In *Proc. ISR/ Robotik*, 2006.

[15] Subodh Bhandari, Richard Colgren, Philipp Lederbogen, and Scott Kowalchuk. Six-DoF dynamic modeling and flight testing of a UAV helicopter. *AIAA Modeling and Simulation Technologies Conference and Exhibit*, (August):992–1008, 2005.

[16] Luis A Sandino, Manuel Bejar, Anibal Ollero, L A Sandino, A Ollero Grvc, M Bejar, and A Ollero. A Survey on Methods for Elaborated Modeling of the Mechanics of a Small-Size Helicopter. Analysis and Comparison. *Journal of Intelligent & Robotic Systems*, 72:219–238, 2013.

[17] Mark B Tischler and Robert K. Remple. *Aircraft and Rotorcraft System Identification: Engineering Methods with Flight Test Examples*. 2008.

APPENDIX A: CHIRP MEASUREMENTS

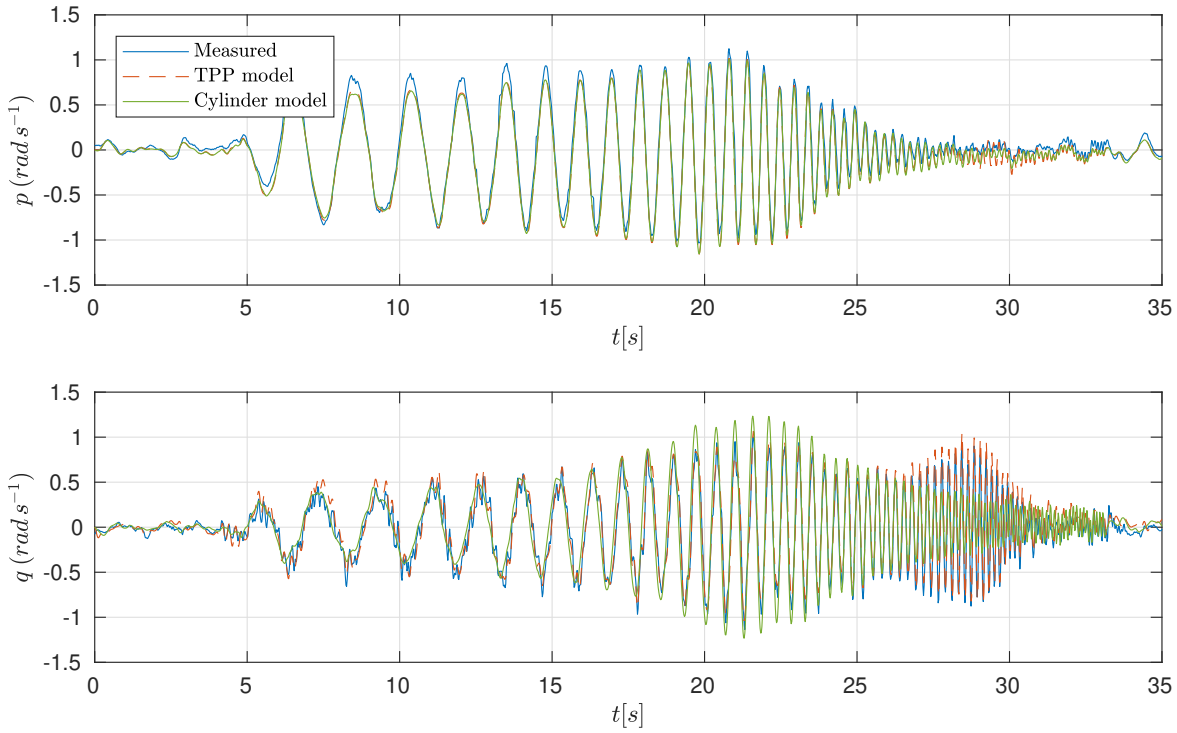

Figure 6: Chirp on the roll axis in hover. The pitch motions are mainly due to pitch-roll coupling. The TPP model is much better at producing the measured pitch signals in the higher frequency range.

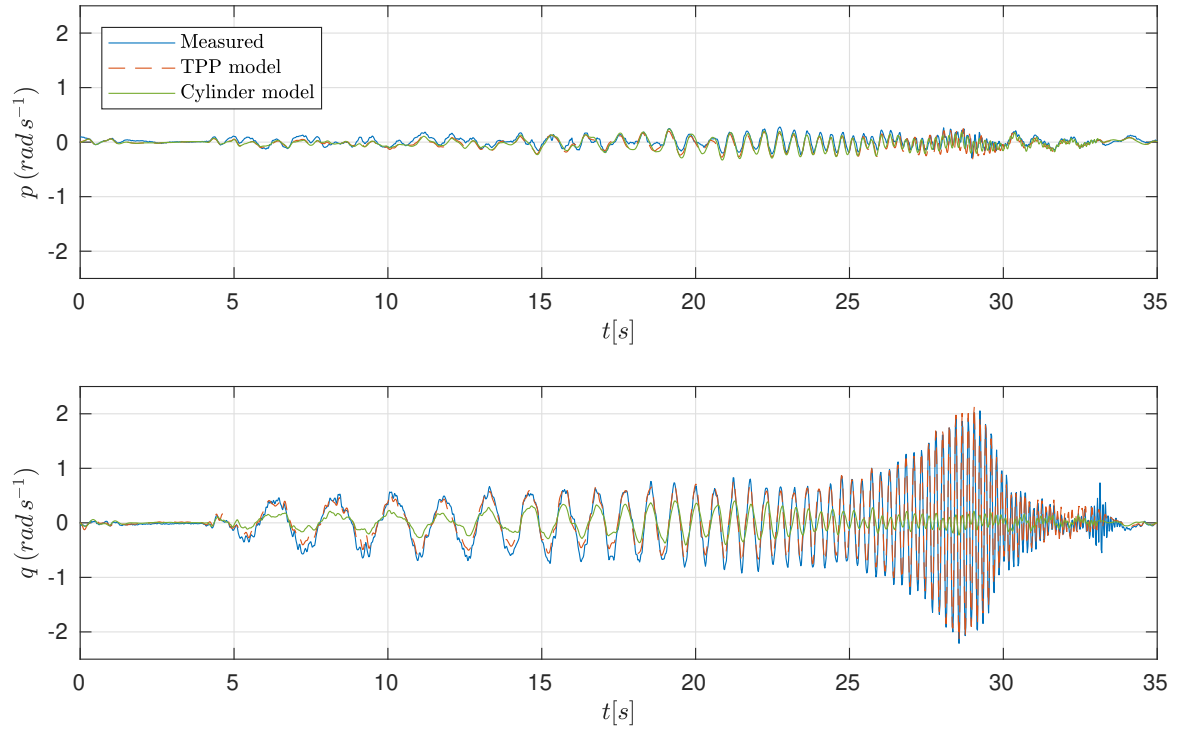

Figure 7: Chirp on the pitch axis in hover. The roll motion due to pitching is much less severe due to the high roll inertia compared to the pitch inertia. Now the CD model's accuracy at low frequencies is also worse than the TPP model.

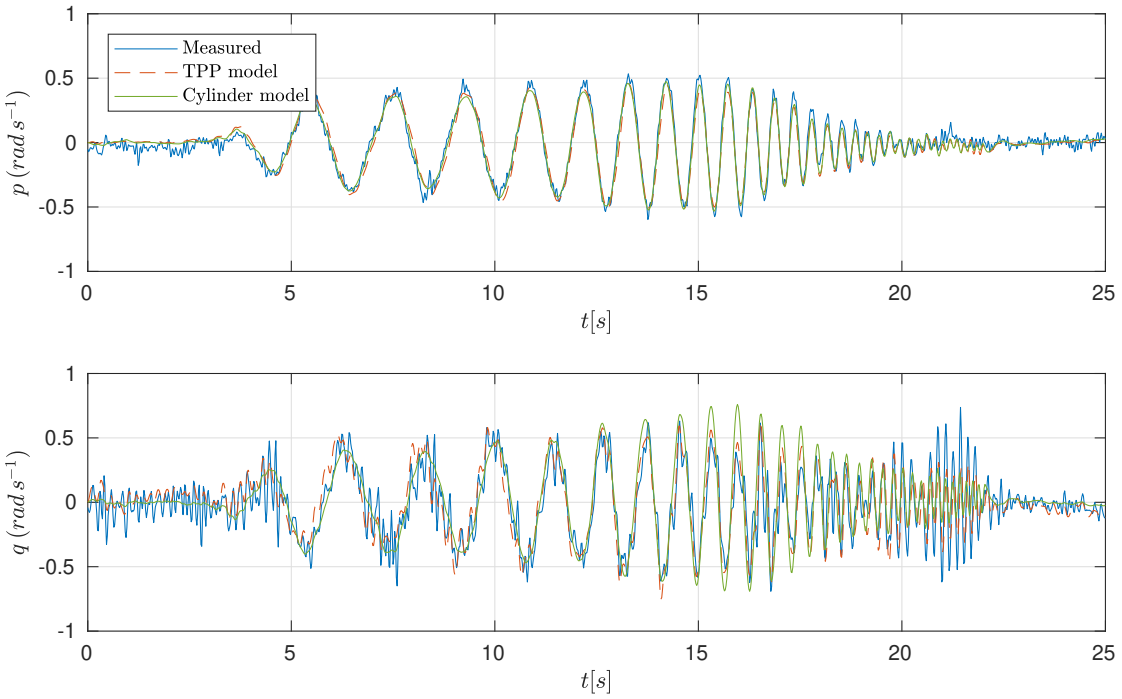

Figure 8: Validation chirp on the roll axis in forward flight. The pitch motions are probably mainly due to pitch-roll coupling. The TPP and CD model have a similar response. The high-frequency fluctuations in the pitch response are due to the attitude controller which is active during the chirp.

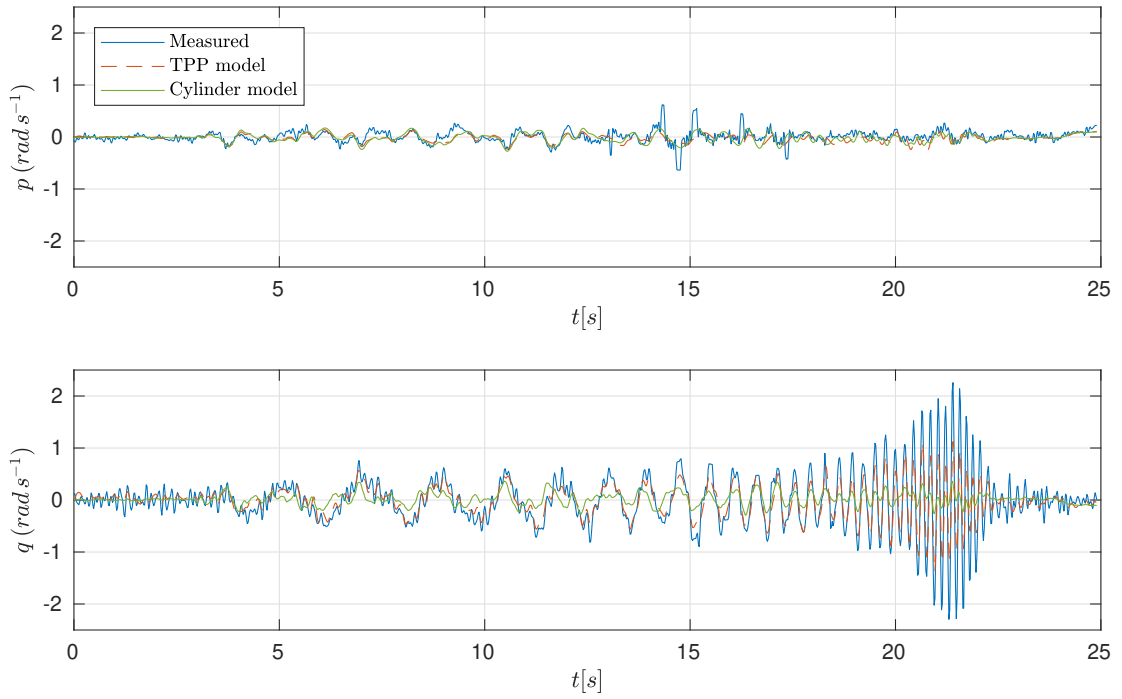

Figure 9: Validation chirp on the pitch axis in forward flight. The CD model's accuracy is much worse than the TPP model, while the latter is also unable to follow the measurement signal at higher frequencies. At around 15 s, the logging system shows some delays, leading to dropped measurements.

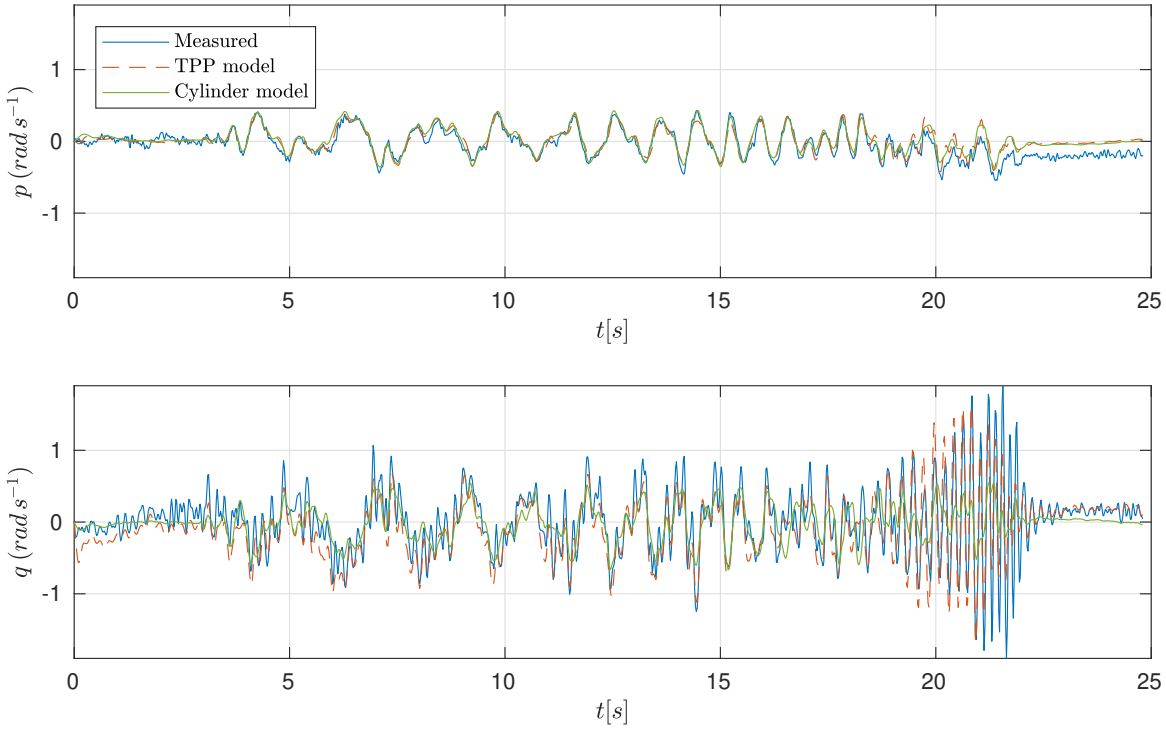

Figure 10: Validation chirp on the elevator axis in forward flight. The roll response q (yaw in standard aircraft reference frame) is fitted accurately by both TPP and CD models, while from around $15\,\mathrm{s}$ the CD model is unable to replicate the higher frequencies that the TPP model can still generate. The TPP model is still unable to replicate the highest frequencies of the chirp.

Chapter 5

Forward flight modeling

In forward flight, the rotorhead provides the propulsive force, and the wings provide the lift required to maintain altitude. Due to the airspeed (on the order of $20\,\mathrm{m\,s^{-1}}$), the attitude dynamics are altered by aerodynamic forces. This means that the hover model may not be applicable to the forward flight state and an extension is required. In literature, the combination of a helicopter rotorhead with cyclic pitch control tilted forward into the airflow with wings was not found. Therefore, an extension is proposed to the models already researched for the hover mode.

The research paper shown in the previous chapter gave some short results considering a forward flight model of the DC. The model displayed there only contains aerodynamic damping on the rotational rates, but more models were developed and tested against measurement data. In this chapter, these models are detailed and compared. Sections 5.1 to 5.4 discuss the development of the extensions to the hover models. These only use the pitch and roll directions, not the yaw. In section 5.5 it shown that the aileron effect on pitch and roll can be compensated fully by the elevator. This is why the yaw can be separated from the pitch and roll. Section 5.6 discusses the necessity of swashplate in forward flight and section 5.7 wraps up the chapter with a conclusion.

5.1 Differences with hover

In order to extend the hover model for forward flight, first the physical differences between the two flight states are summarized. These differences are specific to the attitude dynamics. Note that in the rest of the chapter, the same body-fixed reference frame is chosen as in the hover state. The reference frame remains attached to the DC during transition. This means that the z-axis points to the rear of the vehicle in forward flight while the x-axis points downwards. p and q are still the attitude rates around x and y axes respectively, with their direction defined using the right-hand rule. Angle of attack α and angle of sideslip β are the vertical and horizontal angles between aircraft body frame and the vector of the oncoming wind. Their directions and the other axes are shown in fig. 5.1.

The differences between forward flight and hover mode are given below.

1. Aerodynamic forces and moments: the wing and vertical stabilizer have a stabilizing effect[1]. This means that with non-trim attitude angles and non-zero attitude rates, an extra moment is applied to the fuselage, restoring the Unmanned Aerial Vehicle (UAV) to the trim position. These moments may be part of a new attitude dynamics model.
2. Four aerodynamic control surfaces are present in the wings that together supply the function of aileron and elevator. Each of the four surfaces' command signal is a linear combination of the elevator and aileron signal, depending on the location of the surface. The elevator and aileron signals themselves are an output of the attitude controller. The rotor gyroscopic effect does not influence the fuselage in the direction of rotation of the rotor. The aileron is therefore not included in the model. This assumption is elaborated on in section 5.5.
3. Increased axial flow to the rotor: due to the fact that the rotor axis is approximately aligned with the flow, the rotor axial air inflow is much larger than that in the hover state. This requires the blade collective pitch angle to be larger so as to maintain positive blade angle of attack.
4. Lower thrust from the rotor: the rotor does not have to carry the full weight ($\approx 44\,\mathrm{N}$) but has to balance the amount of drag ($\approx 5\,\mathrm{N}$[1]).

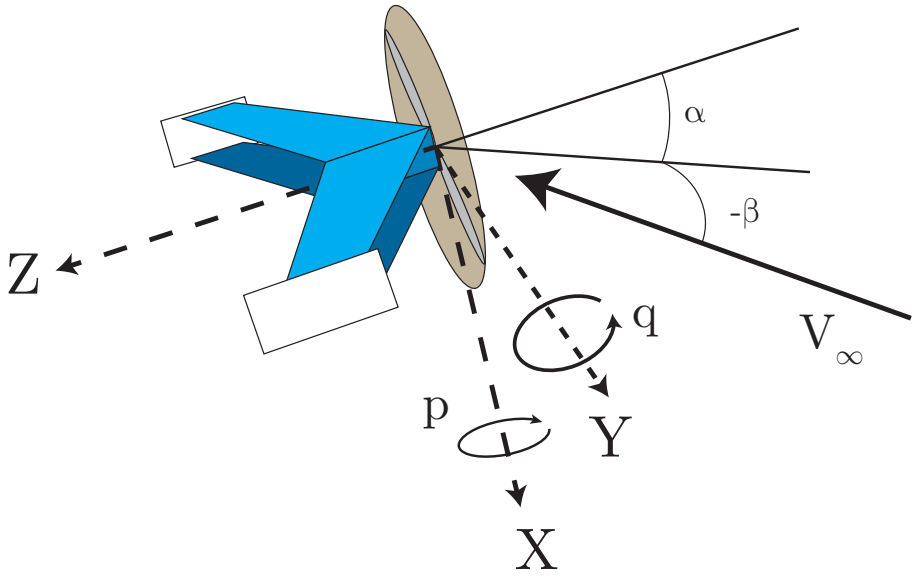

Figure 5.1: Forward flight reference frame and angle definitions. The angles α and β are defined such that their derivatives are related to the positive body angular rates q and p respectively, i.e. a positive p leads to an increasing α.

5.2 Model extensions

Multiple model extensions are implemented and tested against forward flight data to test for predictive quality. Below, they are ranked in terms of complexity. Every subsequent model includes the effects included in previous models. In later sections, the models will be referred to with the number that it has in this enumeration. Note that in the models, a constant airspeed is assumed.

1. Include the elevator. The elevator command is translated into servo signals which leads to an angular displacement of the surface. It is assumed that the aerodynamic moment induced by the elevator is linear with respect to the angular displacement, $M = M_{elev}\delta_{elev}$.

2. Include aerodynamic damping. The pitch and roll rate of the DC create a counter-acting moment: $L = L_p p$ and $M = M_q q$.

3. Include stability derivatives. The angle of attack α and angle of sideslip β naturally induce a restoring moment, which results in the aforementioned stability of the system. However, the DC is not fitted with angle of attack or angle of sideslip sensors. An estimate is required to include this state in the model. Euston et al. use a linearized equation for the angle of attack dynamics[28], which effectively constitutes a high-pass filter on the pitch angle, as shown in eqs. (5.1) and (5.2). The parameter τ_α is the time constant and will be fitted as a model parameter as well. For the angle of sideslip β a similar approach is taken, but using the roll rate in the dynamics, as shown in eq. (5.2). Finally the angle of attack and angle of sideslip are included in the dynamics by $L = L_\beta \beta$ and $M = M_\alpha \alpha$.

$$\dot{\alpha} = -\frac{1}{\tau_\alpha}\alpha + q \tag{5.1}$$

$$\dot{\beta} = -\frac{1}{\tau_\beta}\beta + p \tag{5.2}$$

Note that for a high-pass filter like this, the cut-off frequency in hertz is as given below.

$$f_{cutoff_{Hz}} = \frac{1}{2\pi\tau} \tag{5.3}$$

5.2.1 Implementation in Cylinder Dynamics model

The Cylinder Dynamics (CD) model in state-space form for hover is shown below:

$$\underline{x}_{cyl} = \left\{ \begin{array}{c} p \\ q \end{array} \right\}, \underline{u}_{cyl} = \left\{ \begin{array}{c} \delta_x \\ \delta_y \end{array} \right\} \tag{5.4}$$

$$A_{cyl} = \left[\begin{array}{cc} L_p & L_q \\ M_p & M_q \end{array} \right] \tag{5.5}$$

$$B_{cyl} = \left[\begin{array}{cc} L_x & L_y \\ M_x & M_y \end{array} \right] \tag{5.6}$$

$$C_{cyl} = \left[\begin{array}{cc} 1 & 0 \\ 0 & 1 \end{array} \right] \tag{5.7}$$

$$D_{cyl} = [\underline{0}] \tag{5.8}$$

For forward flight extension 1, the elevator is added to the input vector and B-matrix, as shown below. The rest of the matrices are the same as in hover.

$$\underline{u}_{cyl,FW1} = \left\{ \begin{array}{c} \delta_x \\ \delta_y \\ \delta_{elev} \end{array} \right\}, B_{cyl,FW1} = \left[\begin{array}{ccc} L_x & L_y & 0 \\ M_x & M_y & M_{elev} \end{array} \right] \tag{5.9}$$

For forward flight extension 2, no change is made to the model compared to extension 1. This is due to the fact that the extra parameters that should be included, L_p and M_q, are already part of the hover model. This means that the parameters already present in the model will increase or decrease based on the aerodynamic effects.

Forward flight extension 3 is included in the model, using the eqs. (5.1) and (5.2). This is then implemented in the state-space system as shown below.

$$\underline{x}_{cyl,FW3} = \left\{ \begin{array}{c} p \\ q \\ \alpha \\ \beta \end{array} \right\}, \underline{u}_{cyl,FW3} = \left\{ \begin{array}{c} \delta_x \\ \delta_y \\ \delta_{elev} \end{array} \right\} \tag{5.10}$$

$$A_{cyl,FW3} = \left[\begin{array}{cccc} L_p & L_q & 0 & L_\beta \\ M_p & M_q & M_\alpha & 0 \\ 0 & 1 & -\frac{1}{\tau_\alpha} & 0 \\ 1 & 0 & 0 & -\frac{1}{\tau_\beta} \end{array} \right] \tag{5.11}$$

$$B_{cyl,FW3} = \left[\begin{array}{ccc} L_x & L_y & 0 \\ M_x & M_y & M_{elev} \\ 0 & 0 & 0 \\ 0 & 0 & 0 \end{array} \right] \tag{5.12}$$

$$C_{cyl,FW3} = \left[\begin{array}{cccc} 1 & 0 & 0 & 0 \\ 0 & 1 & 0 & 0 \end{array} \right] \tag{5.13}$$

$$D_{cyl,FW3} = [\underline{0}] \tag{5.14}$$

5.2.2 Implementation in Tip-Path Plane model

The Tip-Path Plane (TPP) model is as shown in sec. 3.1 of the research paper, chapter 4. Again, only the changes of the matrices compared to the hover model are shown, the matrices that don't change are omitted. The first extension is the elevator, as shown below, where the other matrices remain the

same.

$$\underline{u}_{TPP,FW1} = \begin{Bmatrix} \delta_x \\ \delta_y \\ \delta_{elev} \end{Bmatrix} \tag{5.15}$$

$$B_{TPP,FW1} = \begin{bmatrix} 0 & 0 & 0 \\ 0 & 0 & \mathrm{M_{elev}} \\ \frac{\mathrm{A_{lat}}\,\Omega}{\tau_{f_n}} & \frac{\mathrm{A_{lon}}\,\Omega}{\tau_{f_n}} & 0 \\ \frac{\mathrm{B_{lat}}\,\Omega}{\tau_{f_n}} & \frac{\mathrm{B_{lon}}\,\Omega}{\tau_{f_n}} & 0 \end{bmatrix} \tag{5.16}$$

The second extension is the pitch and roll damping. Other than in the CD model, this does add new parameters to the model.

$$A_{TPP,FW2} = \begin{bmatrix} \mathrm{L_p} & 0 & 0 & \mathrm{L_b} \\ 0 & \mathrm{M_q} & \mathrm{M_a} & 0 \\ 0 & -1 & -\frac{\Omega}{\tau_{f_n}} & \frac{\mathrm{A_{b_n}}}{\Omega\,\tau_{f_n}} \\ -1 & 0 & \frac{\mathrm{B_{a_n}}}{\Omega\,\tau_{f_n}} & -\frac{\Omega}{\tau_{f_n}} \end{bmatrix} \tag{5.17}$$

$$\tag{5.18}$$

Finally, the angle of attack and angle of sideslip are added to the model. The implementation of these angles is not very different from the a and b angles: their derivative is equal to (minus) the pitch or roll rate and the derivative and the pitch and roll acceleration is a constant times the state's value. The difference is the cross-coupling between a and b which is not present between α and β and they are not directly influenced by the inputs.

$$\underline{x} = \begin{Bmatrix} p \\ q \\ a \\ b \\ \alpha \\ \beta \end{Bmatrix}, \underline{u} = \begin{Bmatrix} \delta_x \\ \delta_y \\ \delta_{elev} \end{Bmatrix} \tag{5.19}$$

$$A_{TPP,FW3} = \begin{bmatrix} \mathrm{L_p} & 0 & 0 & \mathrm{L_b} & 0 & \mathrm{L_\beta} \\ 0 & \mathrm{M_q} & \mathrm{M_a} & 0 & \mathrm{M_\alpha} & 0 \\ 0 & -1 & -\frac{\Omega}{\tau_{f_n}} & \frac{\mathrm{A_{b_n}}}{\Omega\,\tau_{f_n}} & 0 & 0 \\ -1 & 0 & \frac{\mathrm{B_{a_n}}}{\Omega\,\tau_{f_n}} & -\frac{\Omega}{\tau_{f_n}} & 0 & 0 \\ 0 & 1 & 0 & 0 & -\frac{1}{\tau_\alpha} & 0 \\ 1 & 0 & 0 & 0 & 0 & -\frac{1}{\tau_\beta} \end{bmatrix} \tag{5.20}$$

$$B_{TPP,FW3} = \begin{bmatrix} 0 & 0 & 0 \\ 0 & 0 & \mathrm{M_{elev}} \\ \frac{\mathrm{A_{lat}}\,\Omega}{\tau_{f_n}} & \frac{\mathrm{A_{lon}}\,\Omega}{\tau_{f_n}} & 0 \\ \frac{\mathrm{B_{lat}}\,\Omega}{\tau_{f_n}} & \frac{\mathrm{B_{lon}}\,\Omega}{\tau_{f_n}} & 0 \\ 0 & 0 & 0 \\ 0 & 0 & 0 \end{bmatrix} \tag{5.21}$$

$$C_{TPP,FW3} = \begin{bmatrix} 1 & 0 & 0 & 0 & 0 & 0 \\ 0 & 1 & 0 & 0 & 0 & 0 \end{bmatrix} \tag{5.22}$$

5.3 Fitting

For fitting these models in forward flight, the same chirp identification maneuvers were executed as in hover. Since the elevator is part of the model, chirps are also performed on the elevator axis. All flight tests were performed with an Rotations Per Minute (RPM) and airspeed V_∞ as constant as possible. This is done to allow the parameters in the model to remain constant during the flight and maintain a

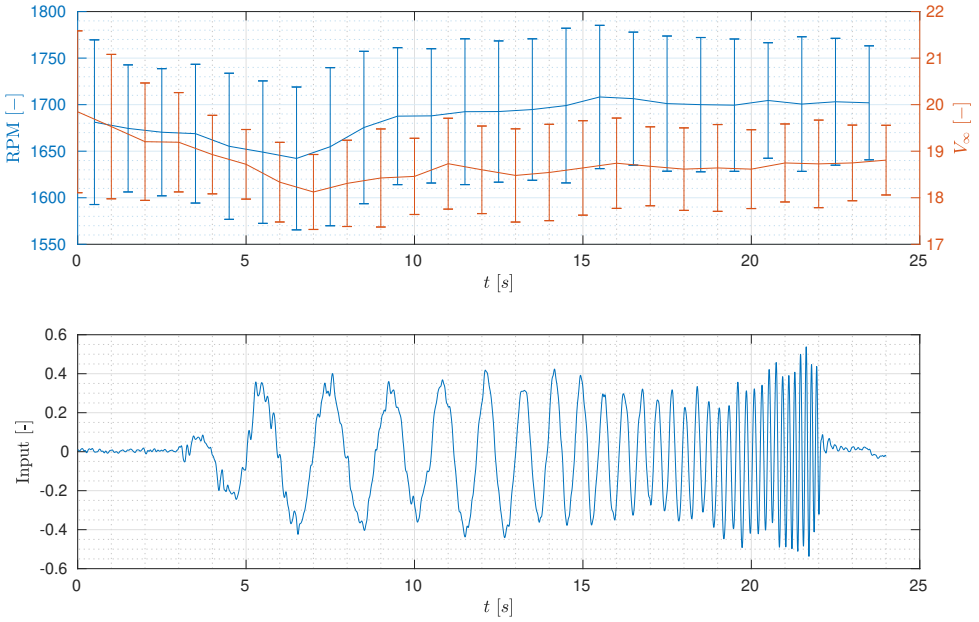

Figure 5.2: During forward, RPM and airspeed V_∞ and fluctuate more than in hover. The spread of 26 individual chirps is shown in this figure. The second plot shows the input of a single chirp for comparison: every chirp has the same length. The chirps are done at the straight sections of a figure 8. During the first seconds, the airspeed and RPM are dropping slightly. It could be that the steady-state after a turn is still te be reached. Both wind direction and the roll angle change from turning to flying straight.

linear system model. However, there still remains quite some spread, as shown in fig. 5.2. This is due to wind and altitude variations caused by a not so aggressively set controller.

The measured outputs of all the models are still just the pitch and roll rates of the DC (which would be pitch and yaw rates in a standard aircraft reference frame).

5.3.1 Tip-Path Plane fitting

It was found that fitting directly the models described before to the forward flight data did not yield consistent estimates of the parameters. The optimization was therefore run with multiple starting points, taking model with the lowest cost function of all the runs as best model fit. However, the spread within parameters was still quite large, and therefore the assumption described in the research paper was used: the L_b and M_a parameters are set equal to those and remain unchanged during the optimization. The physical meaning of these parameters is the apparent stiffness of the TPP deflection, i.e. the angular acceleration generated per unit TPP deflection. The equation, as derived in Mettler's book[18], is shown below.

$$L_b = \frac{k_\beta + hT}{I_{xx}} \tag{5.23}$$

$$M_a = \frac{k_\beta + hT}{I_{yy}} \tag{5.24}$$

As explained in the paper, these parameters do not change much from hover to forward flight. The thrust, approximately equal to the weight component, is much lower than the stiffness as reported by de Wagter et al.[3] Setting these parameters to a fixed value "ties down" the meaning of the a and b values. Without this setting of the parameters, the input-output dynamics can be quite similar for different values of a and b, if the A and B matrices are chosen appropriately. The setting also makes the rest of the parameters more comparable due to this tieing down of the a and b parameters.

Chirps that were not used for fitting are now used for validation. This is especially important since the fitting results are different between the multiple start-points of the fitting optimization. This could be a

result of overfitting, which can be detected if the validation accuracy is much worse than the accuracy on the dataset used for fitting.

5.4 Modeling results

The validation chirps are shown in fig. 5.4. During the flight, the attitude controller was active to maintain stability. The flight data shows high-frequency oscillations on the pitch rate, which may be caused by the attitude controller, possibly in conjunction with aerodynamic forces.

5.4.1 Cylinder Dynamics FW1,FW2

In table 5.2, the fit values of the hover and forward CD models. Between the F1,F2 and hover model, some parameters change much more than others. The L_p becomes five times as large, while M_q even changes sign. This is probably due to aerodynamic effects. It was not expected, however, that these changes would decrease the stabilizing effect of the the pitch rate damping. Furthermore, the inputs effectiveness on the pitch axis remains almost equal, while the input effectiveness on the roll channel changes drastically. In table 5.1, the fit Normalized Root Mean Squared Error (NRMSE) percentages are given for all models. From this table, it is clear that the pitch channel is, again, much less accurate for the CD models than the roll channel, which may explain the higher variability in the pitch parameters than the roll parameters. Another aspect is the fact that in forward flight, the pitch moment is highly influenced by the angle of attack, while the roll moment is less influenced by the angle of sideslip. This is due to a high roll inertia and less aerodynamic surface in the roll direction.

5.4.2 Cylinder Dynamics FW3

Incorporating the filtered values for angle of attack and angle of sideslip as in FW3 increases the NRMSE percentage for the pitch channel significantly, while slightly losing some accuracy on the roll. The angle of attack filter constant τ_α is, however, quite small, and the cutoff frequency of the high-pass filter as given in eq. (5.3) is then 15.9 Hz. This is quite high compared to the rotor-body coupled eigenfrequencies. From the NRMSE figures in table 5.1, it appears that the accuracy of the FW3 model is much higher than that of the the other forward models.

In figs. 5.3 and 5.4, the model simulations are shown for the fit and validation chirps respectively. In both plots, high-frequency oscillations are visible in the pitch channel. It is possible that they originate from aerodynamic effects. Due to the fact that no tail is present the airframe is marginally stable. This may lead to significant deviations from the trim position due to turbulence or possibly interactions with rotor vibrations or dynamics.

It is visible in the chirp simulations in figs. 5.3 and 5.4 that the CD FW3 model is much more accurate than the FW,FW2 models, where even in the validation chirps the FW3 model is much better at predicting the behavior of the DC. The identified model values are much different from both the FW1,FW2 models and the hover model. This may be evidence that aerodynamic moments play an important role in the dynamics of the DC in forward flight. It is interesting to note that the included parameters for aerodynamic damping add two states directly linked to the derivative of p and q. In this sense they may be compared to the a and b states of the TPP model, even though they are not influenced directly by the model inputs. This new model having a significantly higher accuracy than the model with two states, makes clear that the derivatives of the p and q states are important to include in the model.

5.4.3 Tip-Path Plane FW1 and FW2

The FW1 TPP model includes the elevator while the FW2 model also includes the aerodynamic damping. In table 5.3, the parameters for all TPP models (including the hover model) are shown. While for the CD models all forward model parameters are very different from the hover model, in the TPP case they remain more alike. The aerodynamic damping introduced in TPP FW2 increases the pitch accuracy of the model slightly, but as a whole the response of the models is very much alike as can be seen in figs. 5.5 and 5.5. The parameters A_b and B_a do seem to decrease quite a bit, leading to a lower cross-coupling between a and b states.

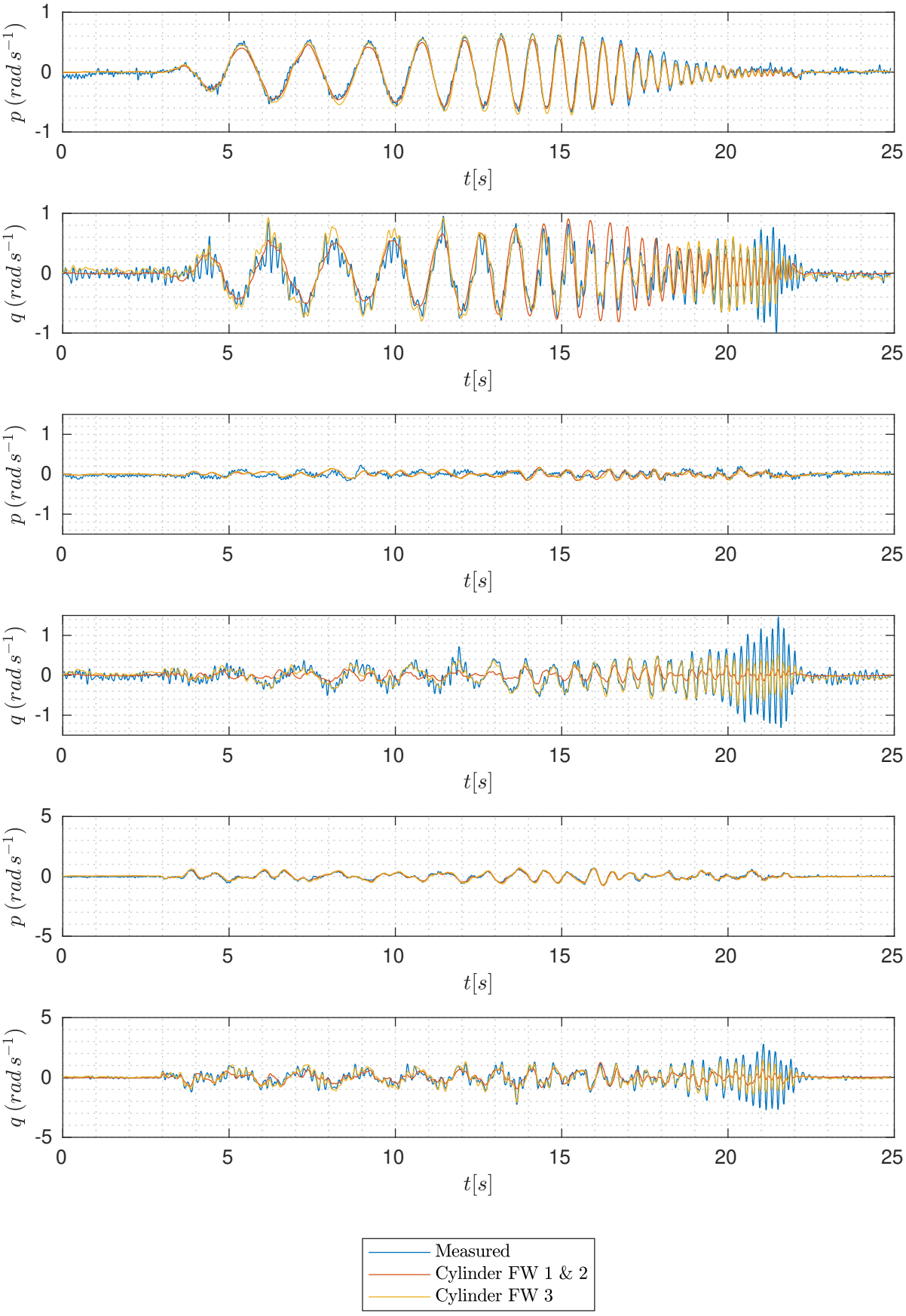

Figure 5.3: From top to bottom: roll and pitch rate during roll chirp, pitch chirp and δ_{elev} chirp. The forward flight CD models are simulated on the data that was used for fitting.

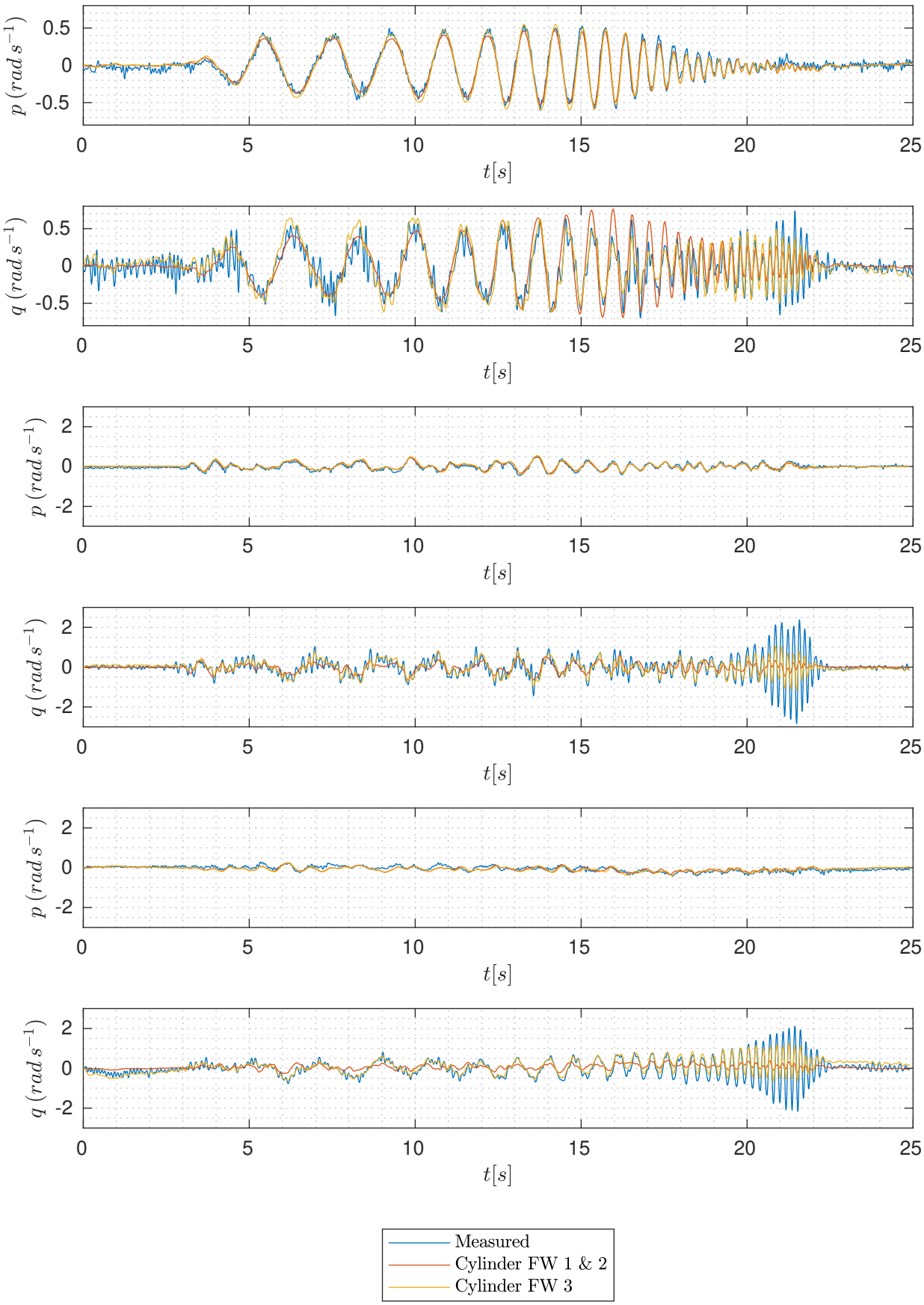

Figure 5.4: From top to bottom: roll and pitch rate during roll chirp, pitch chirp and δ_{elev} chirp. The forward flight data presented here was not used during fitting the models so it can be used as validation data. In the data high-frequency oscillations are visible in the pitch response during the chirp.

Table 5.1: Comparison of fitting and validation accuracy in forward flight

		CD		TPP		
		FW1,FW2	FW3	FW1	FW2	FW3
Fitting	p	70.7238	65.7507	67.8948	65.9181	68.6126
	q	21.7784	52.4019	51.3216	54.7566	71.4165
Validation	p	60.0718	55.2323	57.0935	55.4881	57.3338
	q	17.2319	48.5846	50.3391	51.6522	69.5777

Table 5.2: Comparison of parameters of fitted CD models in hover and forward flight. The hover column repeats the values for the model fitted on hover data. They are slightly different from the values mentioned in the paper due to reoptimization. The forward flight parameters are shown in the next two columns.

	CD hover	CD FW1,FW2	CD FW3
L_p	−2.083	−10.864	25.430
L_q	−7.926	−9.334	−1.240
M_p	10.498	14.987	2.252
M_q	−4.753	1.132	73.455
L_x	−5.330	6.592	6.473
L_y	9.857	−3.123	2.586
M_x	−67.356	−70.433	−50.844
M_y	11.053	11.683	24.979
M_{elev}	–	10.254	12.599
M_α	–	–	−7851.788
L_β	–	–	−922.136
τ_α	–	–	0.010
τ_β	–	–	0.030

5.4.4 Tip-Path Plane FW3

As opposed to the TPP FW1 and FW2 models, the FW3 model does change its parameters quite a lot compared to the hover models. The input matrix values considering a and b angles are much smaller, while the rotor time constant is also smaller. The graphs in figs. 5.3 and 5.4 show that the TPP FW3 model is the only model that is able to reproduce some of the higher-frequency motions. This may be due to aerodynamic motions, specifically the short-period.

5.4.5 Comparison of eigenfrequencies

Another way of viewing the differences between models, aside from the differences in parameters and model structure, is examining the eigenfrequencies and damping ratios. Table 5.4 shows these for all forward models of the DC2. Comparing the TPP FW1, TPP FW2 and CD FW1,FW2 models, the first pole is very similar in both frequency and damping ratio. This pole in the TPP model is related more to roll motion than pitch motion, and is clear from the discussions before that the roll response of both CD and TPP models are adequate. The faster pole related more to pitch motion is absent in the CD model, and this shows in the response. Looking at for example the elevator chirp in fig. 5.4, the model without α and β estimates is not able to reproduce the pitch behavior. This shows that the low-frequency behavior of the models is quite similar but at higher frequencies, also more related to pitch motion, the CD FW1,FW2 models are unable to generate the dynamic behavior.

It is also interesting to note that the TPP FW1 and FW2 frequencies are not very different from the frequencies of the model in hover. This suggests that the low-amplitude angular rate motions in forward flight are not all too different from those in hover. Of course, this may change when larger attitude angles are commanded, since aerodynamic moments then play an increasingly large role. Depending on the aerodynamic configuration, this will create a restoring moment to the trim state.

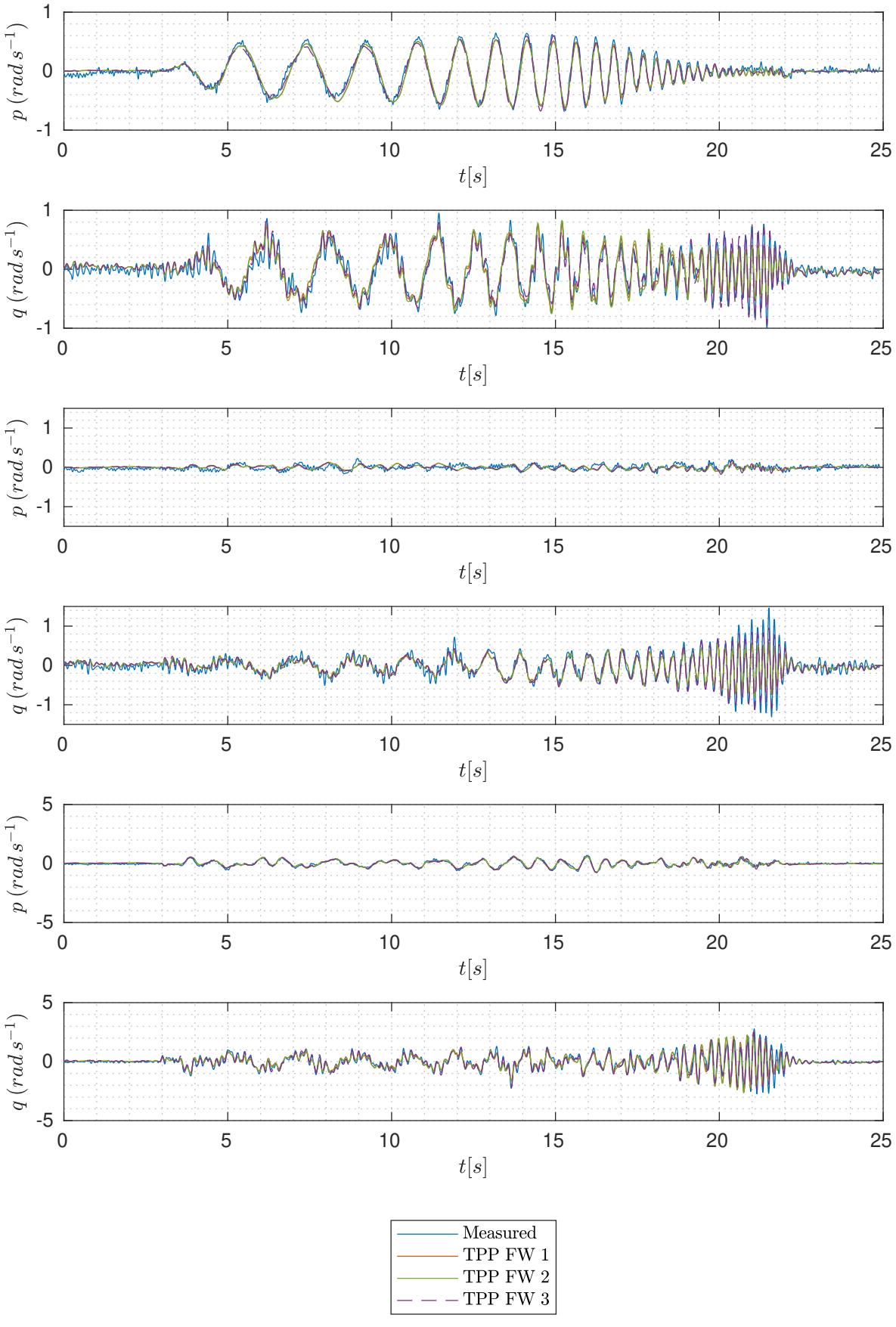

Figure 5.5: From top to bottom: roll and pitch rate during roll chirp, pitch chirp and δ_{elev} chirp. The forward flight TPP models are simulated on the data that was used for fitting.

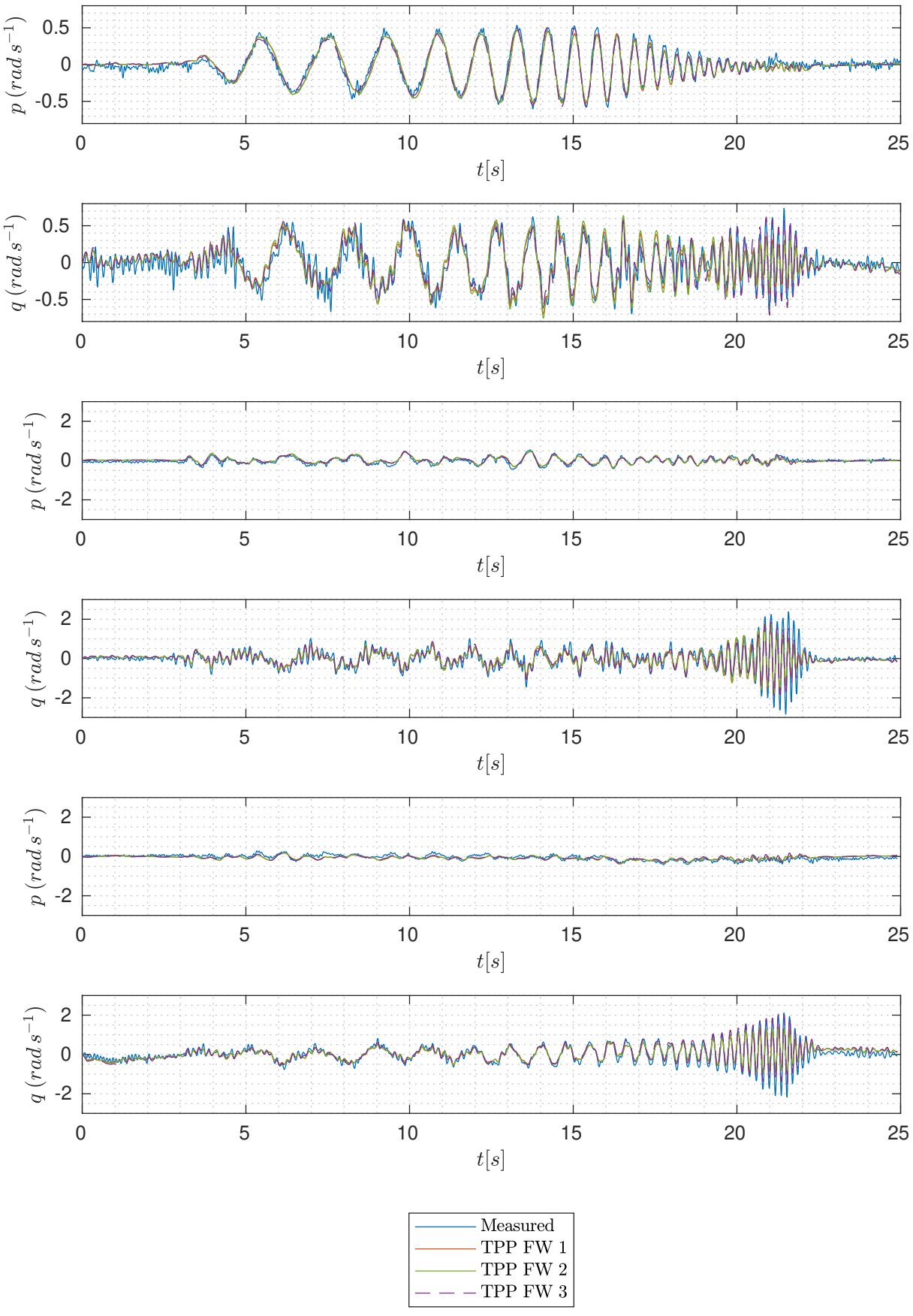

Figure 5.6: From top to bottom: roll and pitch rate during roll chirp, pitch chirp and δ_{elev} chirp. The forward flight data presented here was not used during fitting the models so it can be used as validation data. In the data high-frequency oscillations are visible in the pitch response during the chirp.

Table 5.3: Comparison of parameters of fitted TPP models in hover and forward flight. The hover column repeats the values for the model fitted on hover data. They are slightly different from the values mentioned in the paper due to reoptimization.

	TPP hover	TPP FW1	TPP FW2	TPP FW3
A_b	-1.358	-0.908	-0.924	-0.305
B_a	1.472	1.014	1.020	1.280
L_b	147.533	147.533	147.533	147.533
M_a	713.444	713.444	713.444	713.444
τ_f	0.092	0.087	0.076	0.018
A_{lat}	-0.282	-0.299	-0.195	-0.019
A_{lon}	0.296	0.266	0.214	0.038
B_{lat}	0.524	0.486	0.440	0.152
B_{lon}	-0.050	-0.052	-0.026	0.015
M_{elev}	–	42.441	37.725	7.908
L_p	–	–	-0.946	6.299
M_q	–	–	4.716	178.131
M_α	–	–	–	-36053.562
L_β	–	–	–	-104.670
τ_α	–	–	–	0.005
τ_β	–	–	–	0.092

Also note that the frequency added by the FW3 extension on the CD model is much more comparable to the second pole of the TPP FW1 and FW2 model than the third pole. As stated before, the α and β both affect the derivatives of the p and q states and as such are comparable to the a and b states from a mathematical point of view. It seems that more accuracy can be gained from including the higher eigenvalues tied to the a and b states than those of the α and β states in the TPP FW3 model.

In the TPP FW3 model, the added pole is of a higher frequency, which is then able to account for the high-frequency oscillations seen in fig. 5.6. It is difficult to judge whether this behavior is due to aerodynamic effects or some other coupling. Measuring the flight behavior with angle of attack and angle of sideslip sensors installed may allow more detailed analysis of these vibrations.

Finally, comparing the eigenfrequencies of the forward models, they seem quite comparable to them in hover. This indicates that the attitude rate dynamics do not change significantly. Of course, these results are applicable when the maneuvers are chirps around a certain trim point. It may well be the case that angle of attack and sideslip become more prominent when further away from this trim point.

Table 5.4: Comparison of the eigenfrequencies ω_n and damping ratios ζ of the forward flight models, sorted in ascending order of frequency. The hover eigenfrequencies were repeated from the hover modeling as shown in the research paper, chapter 4.

	CD			TPP			
	Hover	FW1,FW2	FW3	Hover	FW1	FW2	FW3
ω_n [Hz]	1.536	1.798	1.579	1.630	1.756	1.760	1.436
	-	-	3.962	5.041	4.679	4.630	5.180
	-	-	-	-	-	-	9.451
ζ [–]	0.354	0.431	0.391	0.386	0.433	0.447	0.397
	-	-	0.495	0.220	0.228	0.217	0.340
	-	-	-	-	-	-	0.981

5.5 Aileron modeling

Up until this point, all of the modeling has been performed using pitch and roll rate in the body frame. In hover, this is applicable since the tip rotors are capable of maintaining yaw orientation. Also, no coupling is present between the pitch and roll motion and yaw. Therefore, the yaw dynamics are separated from the pitch and roll dynamics. For forward flight, the aerodynamic surfaces function as both elevator and aileron. For the attitude dynamics it is important to verify that the aileron function does not have a significant effect on the pitch and roll motions.

In order to do this, chirps were also performed on the aileron. The same settings were used as for the elevator chirps. An additional model was devised, derived from the TPP FW3 model. The B-matrix was extended to include another input, namely the aileron. Two moment derivatives were added, L_{ail} and M_{ail} for roll and pitch respectively. The extended model was fitted using the same procedure as the other models, keeping L_b and M_a constant. It was found that the parameter $L_{ail} = 0.08$, which is insignificant compared to the other derivatives of L as can be seen in table 5.3. The parameter for pitch was found to be quite high, $M_{ail} = -1.66$, about a fifth of the elevator value M_{elev} shown in table 5.3. This indicates that the aileron and elevator may have mixed effects. The elevator and aileron functions are performed by the same aerodynamic surfaces. Therefore, a new mapping between aileron and elevator commands to actual surface deflections may remove this coupling.

5.6 Necessity of the swashplate in forward flight

One of the research questions is whether cyclic swashplate control is required to allow controlled forward flight. If the swashplate is not required, the aerodynamic surfaces, together with any inherent stability, will allow controllability of the DC. This may be more efficient than using the swashplate in forward flight. Furthermore, since the aerodynamic surfaces are unable to generate a p roll (aircraft yaw) moment, this would also imply that the aircraft has sideslip stability. The models developed in the preceding sections are stable, i.e. their poles have a positive damping ratio as shown in table 5.4. This means that the rates are stable and should converge to 0 without control input and disturbance.

Figure 5.7 shows a part of a flight with the swashplate and tip rotors set to inactive. Firstly, it can be seen that p, the aircraft yaw state, continuously returns to 0 after every disturbance. This means that the airframe does provide stability in this axis. Secondly, the flight is not unstable. While the elevator is clearly counteracting the pitch movements, it is able to maintain stability. The 10 s of flight shown in the graphs are during stable, steady forward flight. During further tests, it was shown that the DC is able to make turns by using the aileron and elevator alone. This indicates that the swashplate is not strictly necessary in the forward flight state.

5.7 Conclusion

In this chapter, the forward flight modeling approach as described in the research paper in chapter 4 was further detailed. The considered differences between hover and forward flight were given in section 5.1. The yaw (aircraft roll) motion does not couple with the gyroscopic effect, and the aileron's effect on pitch and roll (aircraft yaw) can be removed using the elevator. This is shown in section 5.5. Therefore, the aileron is not included in the rest of the forward flight models.

Three new extensions to the hover models were developed and fitted on forward flight data. In increasing order of complexity, they add the effects of the elevator, aerodynamic damping, and angle of attack/-sideslip to the model. The angle of attack and sideslip were included as states of the model as high-pass filtered versions of q and p respectively. The filter constant was an identification parameter.

The extended CD models all offer low accuracy in the high-frequency range. The extended TPP models offer higher accuracy, as evidenced by the graphs and fitting accuracy percentages. Between these extensions, the FW3 model provides the highest accuracy. The extra complex eigenvalue pair allows resolution of the high-frequency oscillations shown in the chirps. The parameters of the FW3 model change a lot compared to the FW1 and FW2 models, both for the CD and TPP case. It is unclear why. Testing with angle of attack and sideslip vanes allows measuring α and β directly. Then this modeling approach could be validated.

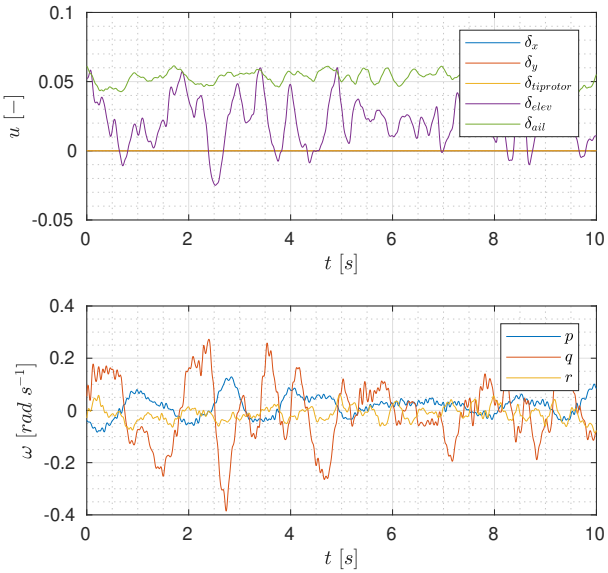

Figure 5.7: Forward flight measurements with the swashplate and tip rotors inactive. The inputs in the upper subplot show that only the aerodynamic control surfaces are active. In the lower subplot, it can be seen that the flight is quite steady. Note that p is what would normally constitute aircraft yaw rate and r is what would normally be considered aircraft roll. The steady-state offset visible in the input is due to imbalances in the airframe and the counter-moment needed due to the rotor.

Chapter 6

Modeling DelftaCopter 3 in hover

Up to this point, all modeling and system identification was performed for the DelftaCopter 2 (DC2). This resulted in quite accurate model fits for hover. The DC2 rotor blades and motor were described in the DelftaCopter (DC) paper[1]. After more research on the propulsion system by de Wagter et al.[29], it was found that with a different setup, flight efficiency could increase. Due to project timing, further hover control investigation after the control described in the research paper was to be performed on the new version of the system, called the DelftaCopter 3 (DC3).

The main difference between DC2 and DC3 setup is that the latter has rotor blades that rotate at a higher Rotations Per Minute (RPM). The new rotor is approximately 66 cm instead of the old 100 cm. To maintain lift with the smaller blades, in hover the rotor rotates at 2800RPM instead of 1650 RPM. In the theoretical derivation of the rigid rotor model, chapter 3, it is shown that the term describing the gyroscopic moment is ΩI_r. The fuselage itself remains the same, so any differences in system identification results are only due to the rotor size, higher rotational rate and rotor stiffness. In this chapter, it is shown that the models used before, offer less fitting accuracy on this new setup than on the DC2.

6.1 Fitting accuracy of DelftaCopter 3

Both the Cylinder Dynamics (CD) and Tip-Path Plane (TPP) models were fitted on pitch and roll chirps of the DC3. The fitting procedure was exactly the same, but yielded lower fitting percentages: for the TPP model, the Normalized Root Mean Squared Error (NRMSE) percentages were 50.65% and 63.07% for roll and pitch motion respectively. This is an obvious step back from 77.8% and 77.3% as shown in the research paper. Hand-flown validation doublets in fig. 6.1 show that the model response shows quite some large deviations. The TPP model has NRMSE percentages of 37.2% and 35.3%, significantly lower than those shown in the paper.

6.2 Advance angle

To try to improve the accuracy of the hover model on the DC3, a different strategy was used for adding the chirp to the control signal. The difference is whether the chirp is applied to a single actuator, or is applied to achieve a pure pitch or roll motion. The difference will be explained in this section and it is shown that while theoretically irrelevant, this has a large impact on fitting performance.

6.2.1 Advance angle in the DelftaCopter controller

The current controller works by independently controlling the pitch and roll axis, and multiplying the resulting command signal with a constant matrix. This matrix contains the advance angle, which is the angle between the actuator activation and the actual resulting body rotational rate. Due to linkage setup between servos and swashplate, there already is a -90° mechanical advance angle, i.e. an actuator pitch command leads to a cyclic pitch angle when the blade is aligned with the y-axis. This -90° angle is

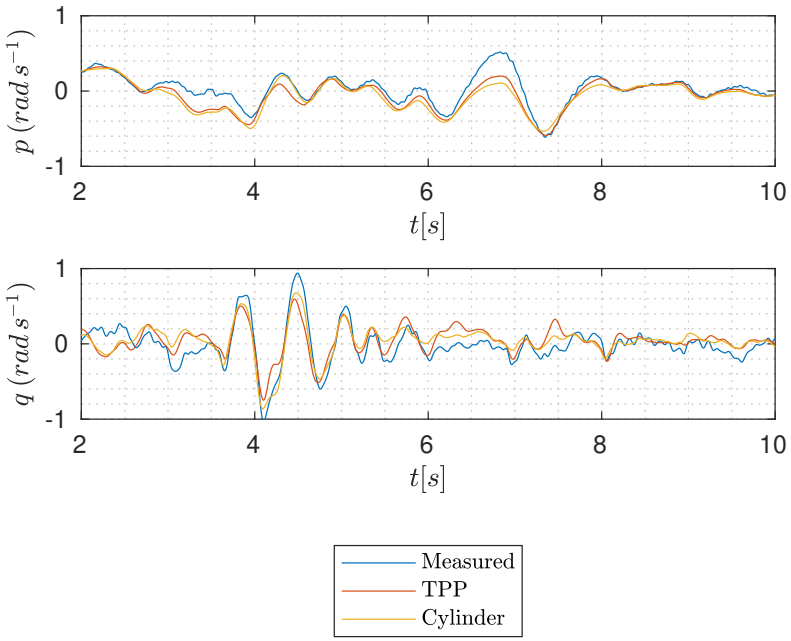

Figure 6.1: Simulation of hand-flown flight data on the DC3. The accuracy is clearly much worse compared to the doublet simulation shown in the research paper, chapter 4.

what would be required if the Unmanned Aerial Vehicle (UAV) behaves like a gyroscope without a non-rotating body attached. However, due to the heavy fuselage, the angle is between $-90°$ and $0°$. Instead of a diagonal actuator effectiveness matrix, the off-diagonal elements have a significant value. This effect is caught in the advance angle, i.e. the angle between actuator direction and rotational acceleration direction. It is different for the pitch and roll axis. To counteract this advancement, the control signal is multiplied by a matrix. The matrix used is given below, where $\angle_p$ is the roll advance angle and $\angle_q$ is the pitch advance angle.

$$adv = \begin{bmatrix} \cos\angle_p & \sin\angle_q \\ \sin\angle_p & \cos\angle_q \end{bmatrix} \tag{6.1}$$

This matrix is multiplied by the desired rotational accelerations to get the actuator values. The angle can be found from measurements by taking the inverse of the B matrix of the CD model and taking the appropriate inverse tangents. In practice, these two angles are a tuning parameter for the controller.

The currently used attitude rate controller works by passing the rotational rate error through a Proportional, Integral and Derivative Controller (PID) controller. This results in a desired attitude acceleration. The attitude acceleration is then multiplied by the advance angle matrix *adv* in eq. (6.1), which results in the actuator output of the controller. The *adv* matrix rotates attitude directions such that the actuator output will yield this direction of angular acceleration desired.

6.2.2 Chirps without advance angle

In all the preceding chirps, the chirp signal was inserted before the *adv* matrix. This means that in general, the chirps are not applied to a single actuator. Rather, the chirp is a linear combination of actuator values that should result in only a pitch or roll motion. In theory, this does not make a difference since the final actuator signal is logged. Thus, while fitting it is clear that in the case of the chirp including the *adv* matrix, both actuators are used during a single chirp, albeit in different magnitudes for different chirps. The model should be able to understand the differences in the direction.

In reality, the attitude controller is active during the chirps, which attempts to remove the "disturbance" created by the chirp.

Figure 6.2 shows the input and rotational rate of both a δ_x and δ_y chirp. During the low-frequency part of the chirp, 5 s to 15 s, the inputs are very alike, which is unexpected since the chirp should be applied

purely to one actuator. This is caused by the controller trying to counteract the chirp motions. The result is that the pitch rate is largely damped out in this first phase of the chirp. Interestingly, the roll rate p of both chirps in the low-frequency part seems very much aligned during both chirps, while the pitch rate q is almost exactly counterphase. During the high-frequency phase, the controller does not respond to the chirp disturbance, as is visible in the input plots. In this part, the roll motion is very small while the pitch motion of both chirps is now in phase instead of counterphase.

Having inputs that are so alike during the low-frequency part of the chirp means a model can not properly distinguish between the effects of the different actuators at these frequencies. The TPP and CD models are fitted on these chirps. The simulation performed with these models is compared to some hand-flown measurements in fig. 6.3. The quality of the fit is clearly much lower than the fits shown in section 6.1 which were simulated with a model obtained with chirps that did have the advance angle applied. Without applying the advance angle to the chirp, especially in the low frequencies, the pitch motion does not follow the trend of the measurements. During the roll chirp, the model's response seems even shifted in phase with respect to the measurements. This is particularly alarming since a controller based on such a model could then also steer based on the wrong phase.

In fig. 6.4, the model response of some manual inputs is shown. Comparing this to the doublet response of the DC2 as shown in fig. 6.1, it is clear that fitting models on chirp data with no advance angle applied yields significantly worse fits. This is probably due to the attitude controller removing important parts of the chirp.

6.3 Tip-Path Plane versus Cylinder Dynamics model

Besides the lower fitting accuracy of the models on the DC3, another change is also apparent. It seems that the TPP model does not outperform the CD model as much as it did for the DC2. The only difference with the results from the paper is the smaller rotor with higher rotational rate.

Table 6.1 shows a comparison between the eigenfrequencies of models fitted on DC2 and DC3 chirps, in terms of eigenfrequency. The eigenfrequencies become more spread out and more highly damped. In this case, the the time constant of the higher eigenfrequency becomes about three times faster after the rotor change. The lower eigenfrequency's time constant does not change significantly. With the old rotor the lower eigenfrequency's time constant was 1.75 times the time constant of the lower, while for the new rotor this ratio is 4.72. This lowers the importance of the higher eigenfrequency compared to the old rotor situation. It is this higher eigenfrequency that constitutes the behavior difference between TPP and CD model, which explains why with the new rotor the CD model does not seem worse than the TPP model.

Table 6.1: Comparison of eigenfrequencies and damping ratios of models fitted on the old (DC2) and new (DC3) rotor. For the TPP model, the lower eigenfrequency becomes slower while the faster eigenfrequency becomes faster. The spread thus becomes higher, while all eigenfrequencies become more damped.

	DC2		DC3	
	TPP	CD	TPP	CD
ω_n [Hz]	1.630	1.536	0.878	0.800
	5.041	-	5.939	-
ζ [−]	0.386	0.354	0.738	0.286
	0.220	-	0.515	-

6.4 Conclusion

In the research paper, chapter 4, it was shown that the TPP model is quite accurate at modeling the DC2 in hover mode. To increase the efficiency of the platform, the rotor was changed to a smaller variant with higher RPM. This new version of the platform is called the DelftaCopter 3. This chapter shows

that the new system has a worse fitting accuracy with exactly the same procedures as with the previous setup.

It was tried to perform the chirps on the actuators directly, instead of the direction that was expected to yield pure pitch or roll motion as was done on all preceding chirps. With the pure-actuator chirp, the chirp results in motion that is partially pitch and roll regardless of which axis it is applied on. Theoretically this should yield the same fitting results. However, the attitude controller is active during the chirps, and damps pitch motions during the low-frequency part of the chirps. This leads to the inputs to the system being very comparable for both chirps, and shows significantly worse fitting performance. With the chirps applied in the direction of pitch and roll moments respectively, the fitting yields better results. The percentages are still lower than for the DC2 setup.

With the DC3 system, the TPP model's eigenfrequencies are located further from each other: the lower eigenfrequency is lower than in the DC2 case while the higher eigenfrequency becomes even higher. This has the effect that the higher eigenfrequency is less present in the system response. The CD and TPP models are more comparable now that this is the case.

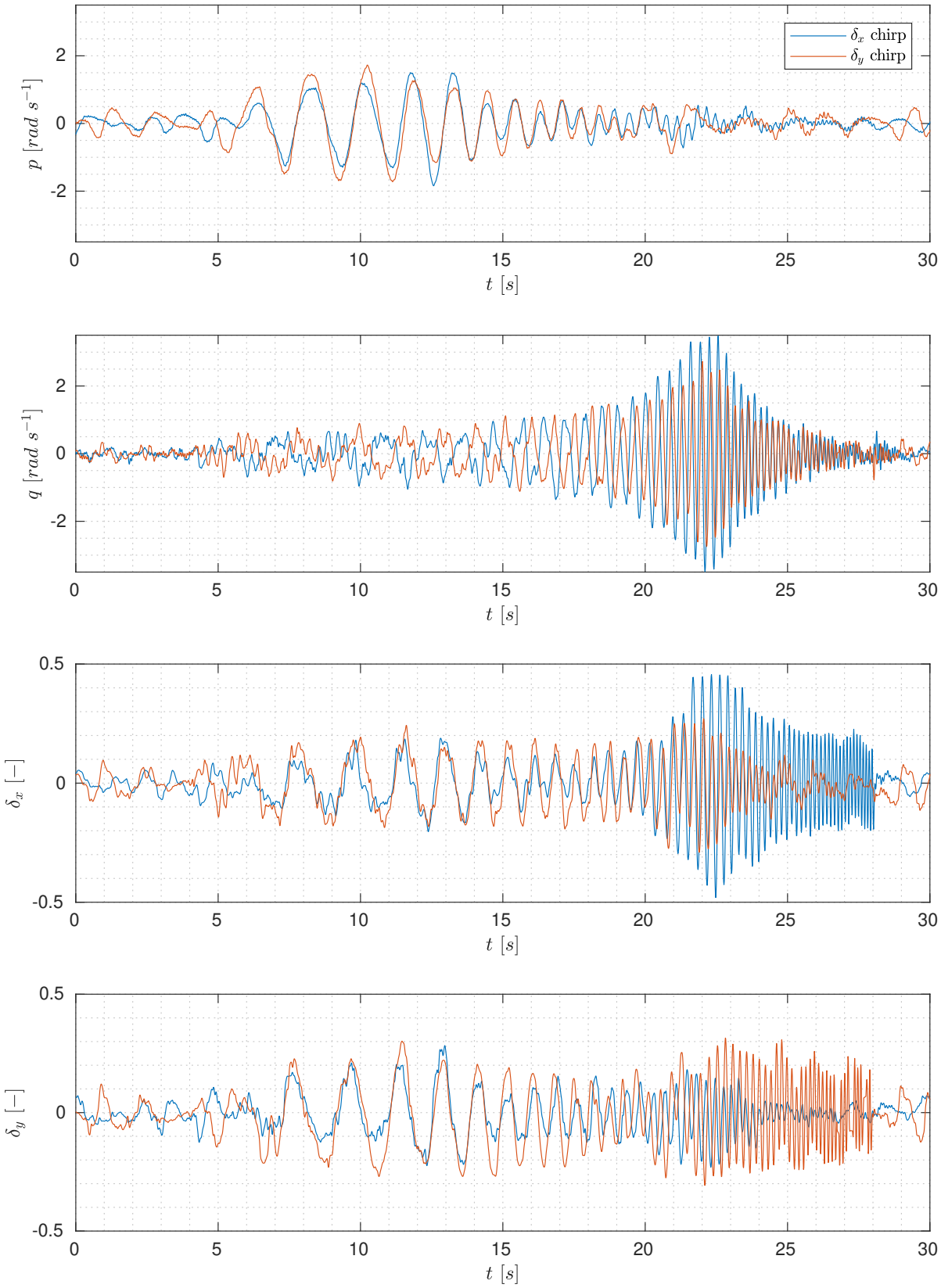

Figure 6.2: A chirp on the δ_x in blue and δ_y channel in red. The attitude controller makes the input of both chirps almost equal in the lower-frequency range. These chirps were applied to the actuator without multiplying the *adv* matrix from eq. (6.1).

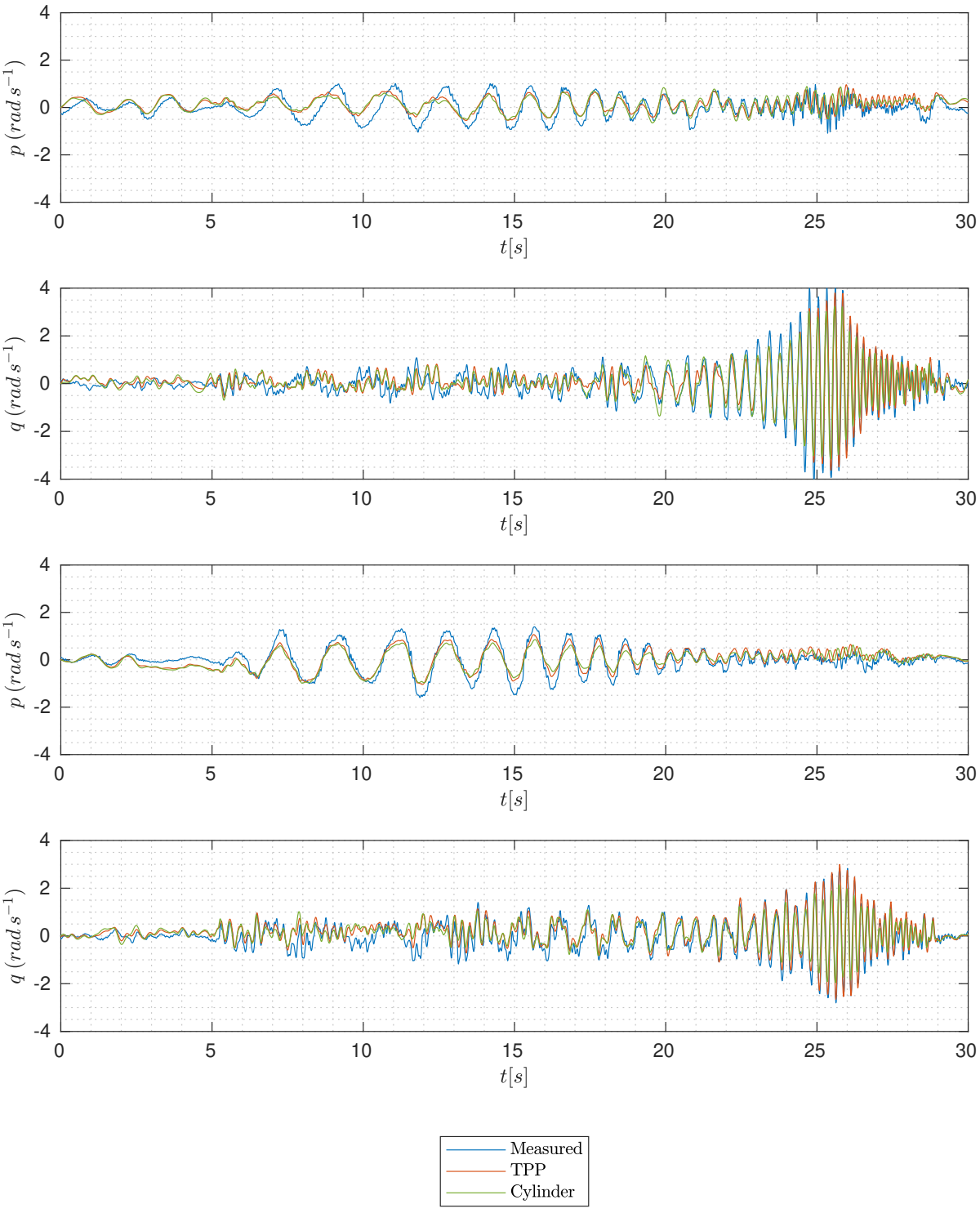

Figure 6.3: A pitch and roll chirp are both fitted and the resulting model simulation is shown. Comparing this figure to the figures in the research papers, the quality of the fit is clearly lower in this instance. At the lower frequencies a phase shift is visible between measurement and model output.

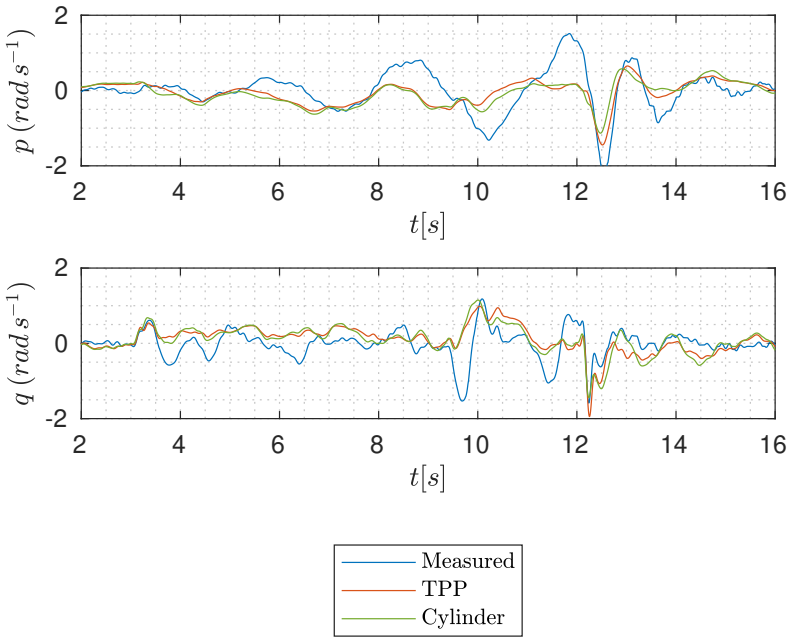

Figure 6.4: The model fitted on the chirps with no advance angle applied leads to this simulation on validation data. It is clear that both TPP and CD models are unable to follow both low and high frequency motions.

Chapter 7

Hover control of DelftaCopter 3

In the research paper, chapter 4, the controller design was concisely reported. Section 7.1 goes into more depth of the control and state estimation design. Afterwards, the model developed for the DC3 as shown in chapter 6 is used as basis for a controller for that same UAV. Section 7.2 shows systematic tests for this attempt and compares it to the control performance as shown in the research paper.

7.1 Control framework

From the hover modeling identification results, it is clear that the pitch and roll axes are coupled heavily, and that the four eigenfrequencies are close enough together to influence eachother. This is also exemplified by the fact that a step response to the hover model leads to an initial acceleration that is in a very different direction than the final rotational rates. This can be seen in fig. 7.1. While the final rotational rates of the model converge to certain values, the initial acceleration yields a large peak in roll rate. These effects are purely due to a coupling between pitch and roll, since the input is constant. In order to steer the UAV exactly where it needs to go, these coupling should be minimized. Feedback control is used to try to minimize these couplings.

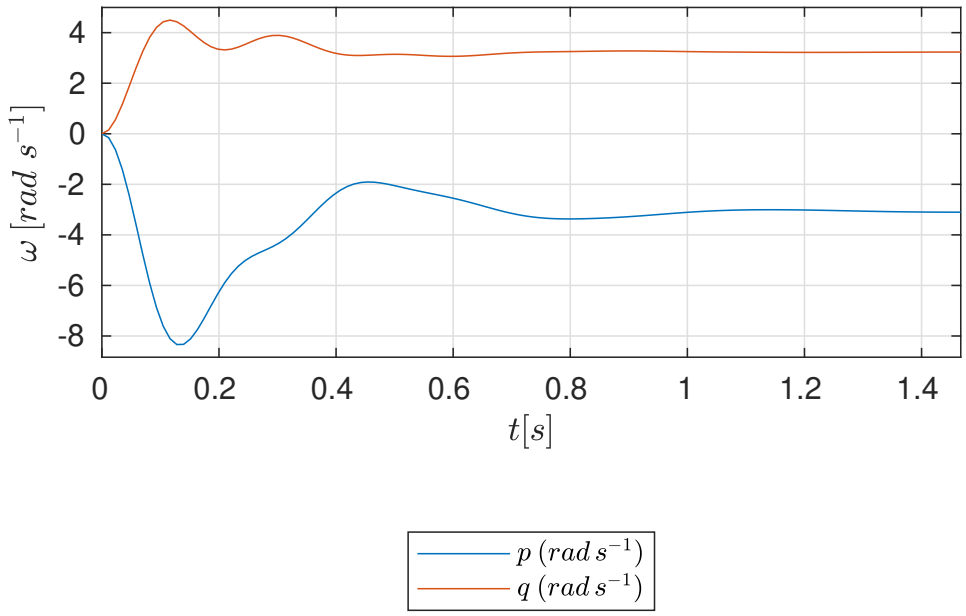

Figure 7.1: Simulated step response on the y-input of the TPP model. Over time the pitch and roll rates converge to a certain value, but the initial acceleration is in a different direction.

State feedback control was chosen using the identified hover TPP model. An observer was constructed to estimate the full state of the system since the a and b angles are not measurable. The state estimation

equations are given below.

$$\dot{\hat{x}} = A\hat{x} + B\bar{u} + L(\bar{y}_{measured} - \hat{y}) \tag{7.1}$$

$$\hat{y} = C\hat{x} \tag{7.2}$$

In this equation, A, B and C are the TPP state-space matrices, $\hat{x}$ is the current estimate of the state vector, $\hat{y}$ the expected measurement vector (consisting of roll and pitch rate). This differential equation is discretized using the rate of the autopilot (512 Hz), and updated on-line at this frequency using the filtered state estimate and autopilot actuator inputs. The state estimate is then used for state feedback, using the equations below.

$$\bar{u} = -K\hat{x} + g\bar{y}_{ref} \tag{7.3}$$

$$g = (C(-A + BK)^{-1}B)^{-1} \tag{7.4}$$

g is the inverse of the stead-state gain of the controlled system. The steady-state gain of the system transforms a constant input into the output the system will have when time approaches infinity with this constant input, and is calculated using the matrix transfer function with s set at 0. The inverse of this matrix is the input required for a certain steady-state reference output $\bar{y}_{ref}$. This is added to the state feedback control output. The controller tries to stabilize the state to 0, but since g incorporates the controller's effect, the steady-state value of the system will be $\bar{y}_{ref}$, if the model is accurate. The controller should minimize the coupling between pitch and roll. Figure 7.2 shows a block diagram of the controller and observer. The DC block in this figure is the actual physical UAV. The vibrations in the upper block are mainly due to the rotor. On-board, the gyroscope readings are filtered through a filter. It was found that the filter can be accurately modeled with a first-order lag, with a pole at -25. The online observer in the block diagram is the discretized version of the observer as given in eqs. (7.1) and (7.2).

Both L and K have to be chosen for the controller. This can be done in several ways, which are described in further in the next section.

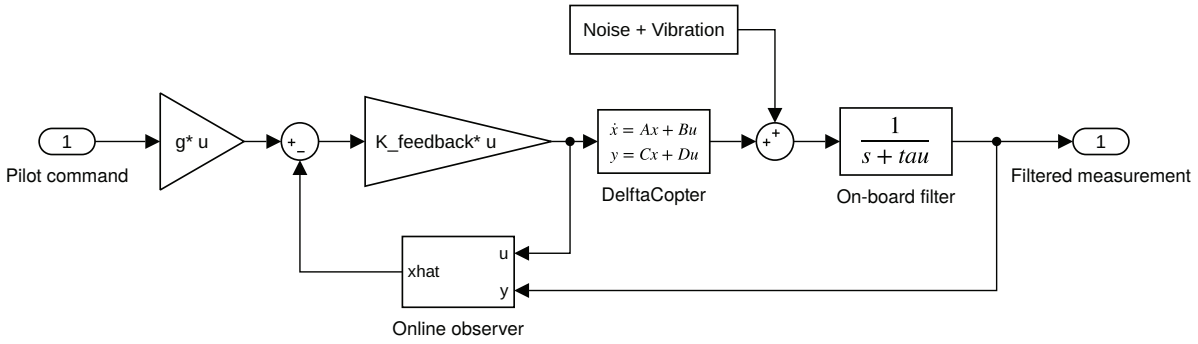

Figure 7.2: Block diagram of the linear controller and observer. g is the matrix given in eq. (7.4), the observer is ran according to a discretized version of eqs. (7.1) and (7.2). The vibrations are mainly due to the rotor.

The currently implemented controller design is shown in fig. 7.3. The difference between the filtered rotational rate and the commanded rate is fed through a proportional gain. The resulting wanted acceleration is then multiplied by the *adv* matrix, as given in eq. (6.1). Tuning the two advance angles in *adv* and the two proportional gains for pitch and roll allows easy tuning of coupling between pitch and roll and how aggressive the controller reacts.

7.1.1 Controller design

For linear systems, pole placement and Linear Quadratic Regulator (LQR) are standard methods of designing the controller, i.e. choosing the K matrix. With pole placement the exact location of the controlled system's poles are chosen, allowing complete freedom in choosing the controlled system's response. For a stable controlled system, there are still bounds on the poles that can be chosen due to instabilities created by input and output lag and delays.

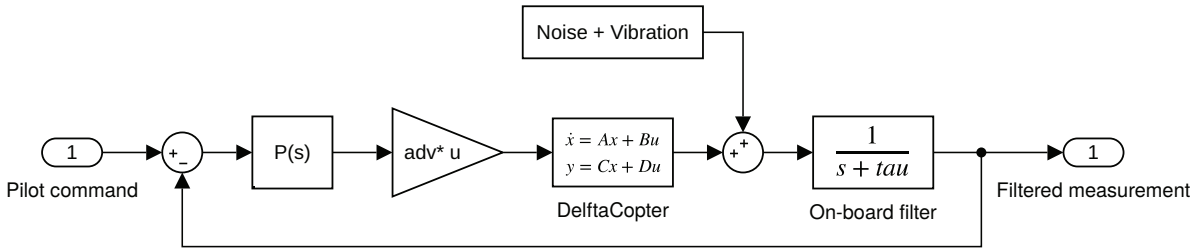

Figure 7.3: Block diagram of the current rotational rate controller, which is a proportional controller with the *adv* block for using the correct steering direction. The *adv* block contains the matrix given in eq. (6.1).

For pole placement, all poles of the system are set at the same time. This requires a specification of all the poles of the controlled system, four in the case of the hover TPP model. Since oscillations in the system, including the wobble described in the literature review, are unwanted, poles are placed on the negative real axis. This should remove oscillations if the model is completely accurate. With poles close to the origin, it was expected that the controller output would be small, leading to a slightly stable system. It was found, however, that this resulted in very unstable behavior of the controlled system. It is hypothesized that this is due to the controller trying to remove the naturally oscillatory coupling between the a and b states. It takes a lot of control effort to completely remove these oscillations, even though the poles are close to the origin and the controlled system's response should be slow. An example measurement of the unstable feedback loop is shown in fig. 7.4.

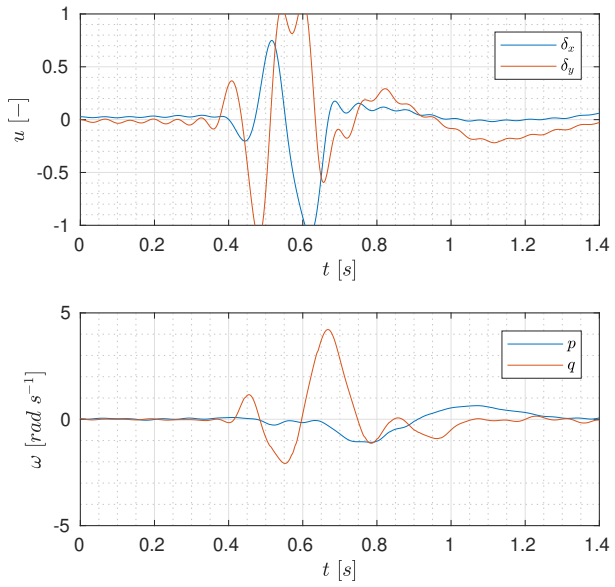

Figure 7.4: Naive pole placement with poles close to the origin on the real axis (around -5) based on the model leads to a positive feedback loop. The pilot was allowed to change the controller using a switch on the remote. At 0.35 sec the controller is switched from the current attitude controller to the controller using pole placement based on the model. Already during the first oscillation the maximum controller output of 1 is reached. Note the high rotational rates until at around 0.65 s the controller is switched back to the current attitude controller.

LQR is a controller design method with which not the exact system response, but the cost of inputs and output errors are chosen. This is done by choosing the matrices Q and R as shown in the LQR equation below. J is the cost function which is minimized by solving the Riccati equation, in MATLAB with function lqr. This yields a feedback gain matrix K since the feedback law $\bar{u} = -K\bar{x}$ is chosen.

$$J(u) = \int_0^\infty (x^T Q x + u^T R u) dt \tag{7.5}$$

With this specification, the a and b states can be given very low weight such that only the body rates and inputs are optimized for. Both Q and R cost matrices are chosen as diagonal matrices, with the structure as given below. Note that the TPP state is $x_{TPP} = (p, q, a, b)^T$, such that the third and fourth element on the diagonal relate to the a and b states. In the Q and R matrices, there remains only one parameter, namely c. Using this parameter, the aggressiveness of the controller can be chosen: using a higher value of c increases the cost of the input and leads to a slower control response. Note that only the relative values of the cost matrices are relevant, the absolute size does not matter.

$$Q = \begin{bmatrix} 1 & 0 & 0 & 0 \\ 0 & 1 & 0 & 0 \\ 0 & 0 & 0.0001 & 0 \\ 0 & 0 & 0 & 0.0001 \end{bmatrix} \tag{7.6}$$

$$R = \begin{bmatrix} c & 0 \\ 0 & c \end{bmatrix} \tag{7.7}$$

7.1.2 State estimation

For the state estimation, a steady-state Kalman filter is used. A Kalman filter is an observer where the gain matrix L is the optimal matrix given noise characteristics of the process, measurements and current state estimate uncertainty. Over time the gain matrix L converges to a constant matrix which can be found with the Riccati equation, in MATLAB using command kalman. Using this constant gain matrix reduces the Kalman filter to a normal observer with optimal gains for the specified noise characteristics. The gyroscope sensor noise characteristics were found by looking at steady flight conditions. The process noise, however, is much harder to find and in practice was used as a tuning parameter. A higher process noise parameter means the filter will put more importance on incoming measurements while a lower parameter makes the internal model more important. Model errors can also be seen as form of process noise. Using a higher process noise parameter thus allows a lower model accuracy since the measurements are trusted more. On the other hand, a too high process noise parameter will put too much emphasis on measurements. This will let more noise, measurement errors and vibrations picked up by the gyroscopes through the filter. A noisy state estimate is the result, which will lead to the state feedback controller to output high-frequency noise to the actuators.

An important aspect of state estimation to consider is what input signals the estimator will get to process. During fitting of the models presented before, the gyroscope signals are filtered using an ideal low-pass filter. This removes noise such that the signal approximates the true motions as closely as possible. Onboard, however, an ideal filter is not possible since any low-pass filter implementation will add lag to the signal. This is also the case for the onboard filter implemented in the autopilot.

The control code uses this onboard filtered gyroscope signal as input to the Kalman filter, at the cost of some lag. This is done since the amount of noise present in the gyroscope signal is very high. However, this does mean that the input signal to the Kalman filter is delayed with respect to what it would expect based on the model fitted on the ideally filtered data. This would reduce the accuracy of the filter.

Two methods were attempted to remedy this problem. The first method was a change in how the model. Instead of fitting the model on the ideally filtered gyroscope readings, the online filtered version of the signal was used for fitting. This means the lag introduced by the filter is lumped into the other fitting parameters of the model. The Kalman filter and controller matrices were then derived using this other version of the fitted model. The second method was to add two states, representing the filtered version of the true body rates. As described before, a first-order lag with $\tau = 25$ was found to accurately model the relationship between ideal filtered and onboard filtered body rates. This relationship can be used to include the onboard filtered rates as states in the A matrix of the state-space system. The output matrix C is then chosen such that not the true body rates, but the filtered version is measured. The Kalman filter is then used to update the states, knowing that what it measures is the onboard filtered states instead. In this sense, the Kalman filter works as a lead-generating filter for the filtered signal. It also relies more on the fitted model since the link between measurements and true body rotational rate states is more indirect.

Between these two approaches, it was found that the first has a more accurate estimate of the body rotational rates. This is shown in fig. 7.5. In this figure, the ideally filtered ("Truth") rates are shown

versus the onboard filtered gyroscopes. The first approach ("Normal observer") and second approach ("Lead filter") are also shown. Large deviations between the ideally filtered gyro and the second approach are visible. It was found that the second approach also does not yield a better control performance.

Other than the two used approaches, it would probably have been better to use the unfiltered gyroscope altogether. The measurement noise parameter of the Kalman filter can then be set to an appropriate level. This removes lag in the measurements used by the Kalman filter.

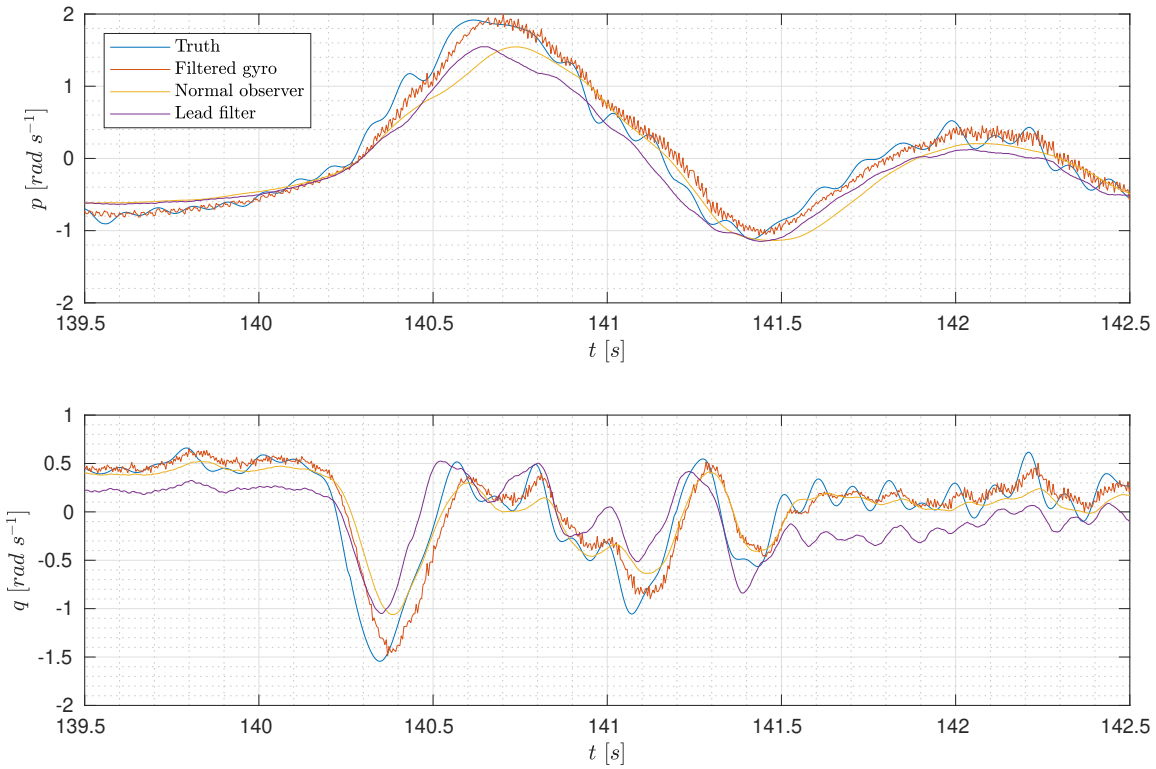

Figure 7.5: Comparison of two observers' output with the true rotational rate (from ideal filtered gyroscope readings) and the on-board filtered rates. While the lead filter is sometimes better at following fast motions, the normal observer has a higher accuracy overall.

7.2 Control tests DelftaCopter 3

The controller and observer tuning parameters are chosen by alternately updating the parameters and letting the pilot assess how well the system responds to its inputs. For both the controller and observer certain bounds were found. A higher process noise parameter leads to better performance, until an upper bound is reached after which it starts to oscillate. The oscillation then happens for all choices of controller parameter.

The same holds true for the selection of the controller parameter. The more aggressive the parameter, the better the performance according to the pilot. Past a certain point, instability is introduced in the system in the form of oscillations increasing in magnitude.

The controller performance shown in the research paper, chapter 4, shows great promise. The measured signal is lagged with respect to the commanded signal and the pitch rate still shows response coupled to the roll rate. However, the response was found to be adequate by the pilot. Unfortunately, due to project timing and the converting of the DC2 to the DC3, no systematic automated doublets were performed to reliably establish control performance.

The model developed for the DC3 in chapter 6, was used to synthesize a controller in the same was as had been done for the DC2, detailed in the preceding sections. The controller and state estimation parameters were tuned based on the human pilot's feedback. The controller response was tested and

compared to the old (currently implemented) controller as described above. The comparison is made by performing automated doublets on the rate command of the controller. Since they are automated, the response characteristics are comparable between multiple controllers.

Figure 7.6 shows these responses for pitch and roll doublets. Per axis and controller combination, multiple doublets are performed to show the spread in response. It is clear that the new controller is able to stabilize the DC. However, its performance is worse than controller as it was implemented on the DC2. For example, in the case of a pitch doublet, the roll response is considerable while this should be 0. This is not the case for the controller shown in the research paper.

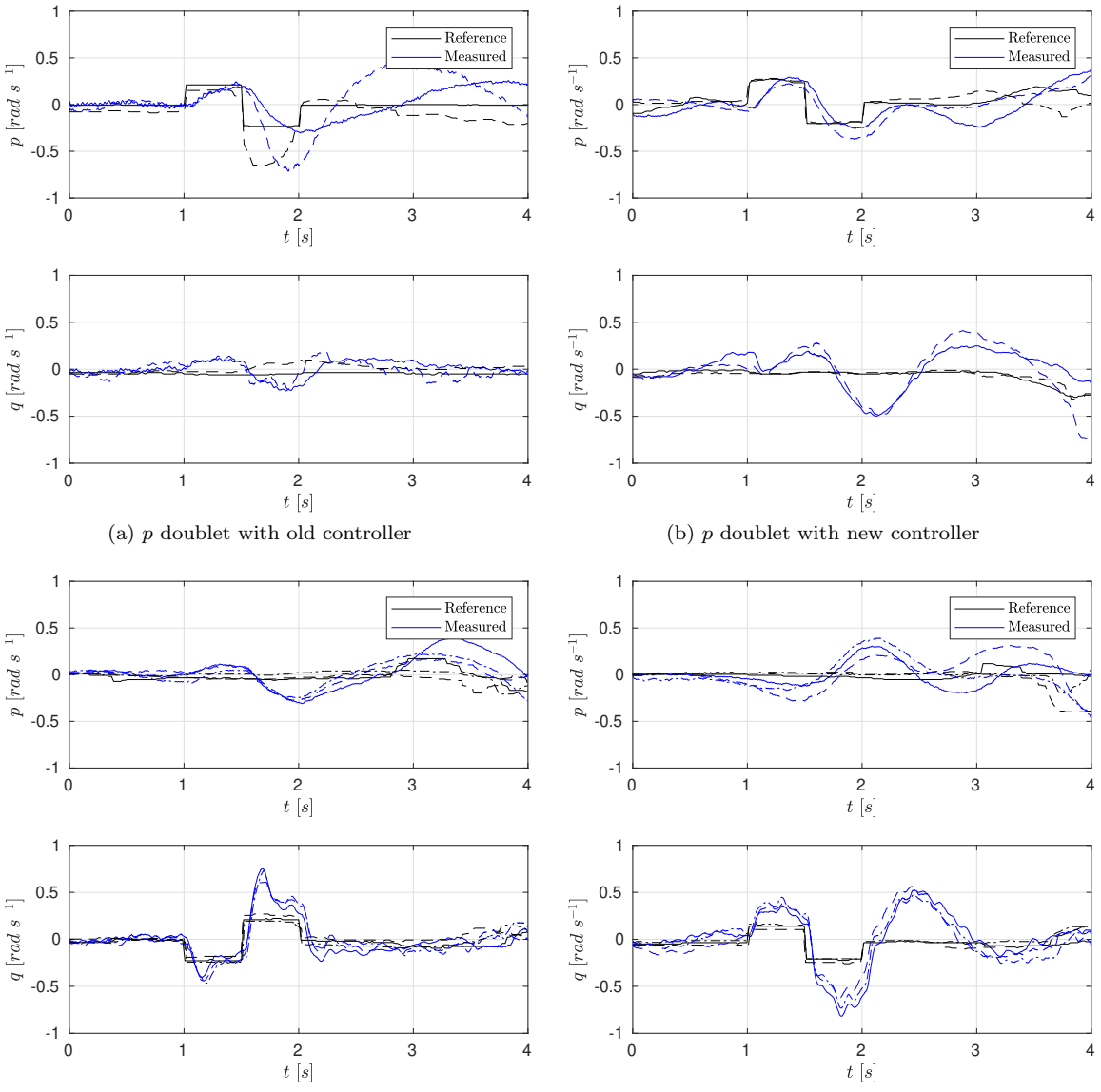

(a) p doublet with old controller

(b) p doublet with new controller

(c) q doublet with old controller

(d) q doublet with new controller

Figure 7.6: Commanded doublets on pitch and roll rates for the new and old controllers. While the doublets themselves are progammatically performed, they are added to the pilot's RC signal to maintain controllability. This results in reference with disturbances, sometimes required to maintain the UAV within the confines of the testing area. Same line strokes within one subplot correspond to same tests. The measured rates are the output of the on-board state estimator built in the autopilot. It has been smoothed to remove vibrations from the rotor.

7.3 Conclusion

From the simulated model step response, it is clear that the initial direction of rotation of the DC is not the same as the final rotational rate direction. A high performance controller should therefore include this transient response.

A controller was implemented on the DC using an LQR controller paired with a Kalman filter. For the LQR cost matrix, the gains of the a and b states were set very low and the input cost was used as a single tuning parameter for the controller.

It was shown that using real poles in a pole placement approach for control design yielded a highly unstable controller. It is hypothesized that this is due to the fact that the controller attempts to remove oscillations from the naturally fast oscillatory coupling between TPP angles and fuselage. This removal of oscillations is not in line with the actual steering of the fuselage.

The controller implemented on the DC3 shows much higher coupling between pitch and roll than the one implemented on the DC2. As described in chapter 6, the model accuracy attained on the DC3 is lower than the DC2. That may explain why the control performance is also worse on the DC3: there are significant unmodeled effects, which then cannot be counteracted by a controller based on that model.

Chapter 8

Conclusion

The DelftaCopter (DC) is a hybrid tailsitter Unmanned Aerial Vehicle (UAV) combining a single-rotor helicopter system for hover and a fixed wing for forward flight. This combination allows it to fly far and fast but land without a smooth landing patch, enabling a broad scope of missions. The single rotor makes hover and forward flight more efficient compared to multiple rotors. The cost of this is added complexity, from a modeling, control and system's perspective.

Previous research on the DC has been dedicated to finding the correct modeling approach for hover mode, as explained in the literature review, chapter 2. It was found that the particular model used was still unable to explain all dynamics observed: the controller based on the model was unable to remove all pitch and roll coupling due to the rotor[3] The main goals of this thesis were to explain these shortcomings, and to extend the modeling effort to the forward flight state for which no model has been developed before.

The first part of this goal concerns what physical phenomena dictate the attitude behavior of the DC in hover mode. In the previous DC research and many other papers it is assumed that the rotor is rigid. In this thesis this kind of model is named the Cylinder Dynamics (CD) model, due to the rotor being modeled as a rotating cylinder. Since the rotor rotates with respect to the fuselage, gyroscopic moments are generated. If the rotor is indeed modeled as a rigid body, the theoretical investigation in chapter 3 shows the large effect of the rotor on the attitude dynamics: to achieve a pitch rate, a roll moment should be applied and vice versa. Chapter 3 also shows that the DC is different from normal helicopters since the fuselage has high inertia compared to the momentum of the rotor. This makes the behavior less like an ideal gyroscope.

Most literature on attitude modeling of small helicopter uses the CD model. The rigid rotor assumption implies the up and down flapping of the blades is not relevant to the dynamics. To test this assumption, a model by Mettler[18] dubbed the Tip-Path Plane (TPP) model is compared with the CD model. The TPP model does include the flapping dynamics. By fitting both models on hover flight data, it was shown that the TPP model is much more accurate in the high frequency range. This can be seen in the research paper, chapter 4 figures 6 and 7. Both the CD and TPP model have an eigenfrequency at around 1.6 Hz, while only the TPP model has the higher eigenfrequency around 5.0 Hz. This eigenfrequency is visible in the later parts of the chirps, for example in the paper figures 6 and 7.

An attitude rate controller for hover was synthesized using Linear Quadratic Regulator (LQR) based directly on the TPP model. This controller was able to stabilize the UAV, as shown in the paper, chapter 4 section 4. This validates that the hover model captures key dynamics of the DC.

The second research goal concerns the horizontal, forward flight regime. During the forward flight regime, the wing and elevator aerodynamics play a role in the attitude dynamics. In this thesis three extensions to the attitude models are proposed, each adding incrementally another aspect of the aerodynamics: the elevator generating a pitch moment (FW1), the pitch and roll rate having a damping effect (FW2) and an estimate of angle of attack and sideslip producing moments on pitch and roll axes (FW3), as detailed in section 5.2. Fits on flight data show that FW1 and FW2 yield comparable performance, and are both able to predict some part of the lower-frequency dynamic but are lacking in the higher frequency range. The FW3 is quite accurate at producing the high-frequency fluctuations seen in the measurement data, figs. 5.4 and 5.6. Comparing the CD and TPP models, it is clear that again the latter one is

more accurate. Some new parameters are introduced into both models for the different extensions. The parameters present in both the hover and forward flight models don't change significantly between hover, FW1 and FW2 for the TPP model. For FW3 they do change significantly, as shown in table 5.3. It is clear that the parameters concerning the angle of attack estimate play a large role in this model. In future research, measurements in which angle of attack and angle of sideslip are measured instead of estimated may shed light on this.

It was also found that the DC can be flown without using the swashplate and tip rotors in forward flight. The aerodynamic stability in combination with aerodynamic control surfaces was sufficient to allow steady horizontal and turning flight.

The DC was partially rebuilt to have a smaller rotor (61 cm versus 100 cm diameter) rotating at a much faster rate (2800 RPM versus 1650 RPM). Unfortunately, quite some results described above change with this setup. Chapter 6 shows that the fitting results are worse for this new setup. An attempt to improve this was to change the input direction on which the chirp is applied. It is shown that although theoretically irrelevant, chirps result in better fits when they result in pitch or roll motion. This is in contrast with chirps performed purely on the actuator axes that lead to combined pitch and roll motion, as described in section 6.2. These result is significantly worse fits. It appears that for the DelftaCopter 3 (DC3) setup, the TPP and CD model are on the same level op accuracy.

In chapter 7, the same control approach is tried as in the paper, but on the DC3. From the doublets shown in fig. 7.6, it is clear that the state feedback controller is now worse than the currently implemented controller. An attempt was made to improve the on-board state estimation by using a model to estimate true roll and pitch rate from the onboard filtered signals. This proved unsuccessful, as explained in section 7.1.2 It seems that the rotor in the DC3 yields new modeling challenges that also lead to a worse performing controller. These unmodeled effects are a starting point for further research.

It can thus be concluded that with the TPP model, the high-frequency attitude dynamics of the DC can be modeled much more accurately than with the CD model. It is also shown that with the new model extensions introduced in this thesis, forward flight dynamics can be modeled. Still, the modified DC3 posed new challenges to the models and more research will be required to understand why.

Bibliography

[1] C. De Wagter, R. Ruijsink, E. Smeur, K. van Hecke, F. van Tienen, E. van der Horst, and B. Remes, "Design, Control and Visual Navigation of the DelftaCopter," jan 2017.

[2] UAV Challenge, "UAVC Medical Express 2018 Rules V2," 2017.

[3] C. De Wagter and E. J. Smeur, "Control of a hybrid helicopter with wings," *International Journal of Micro Air Vehicles*, vol. 9, pp. 209–217, sep 2017.

[4] M. Hassanalian and A. Abdelkefi, "Classifications, applications, and design challenges of drones: A review," *Progress in Aerospace Sciences*, vol. 91, pp. 99–131, may 2017.

[5] S. Herbst, G. Wortmann, and M. Hornung, "Conceptual design studies of vertical takeoff and landing remotely piloted aircraft systems for hybrid missions," *CEAS Aeronautical Journal*, vol. 7, pp. 135–148, 2016.

[6] R. D. Salazar, M. Hassanalian, and A. Abdelkefi, "Defining a conceptual design for a tilt-rotor micro air vehicle for a well-defined mission," in *55th AIAA Aerospace Sciences Meeting*, (Reston, Virginia), American Institute of Aeronautics and Astronautics, jan 2017.

[7] J. T. VanderMey, *A tilt rotor UAV for long endurance operations in remote environments*. PhD thesis, 2011.

[8] G. Ducard and M.-D. Hua, "Modeling of an unmanned hybrid aerial vehicle," in *2014 IEEE Conference on Control Applications (CCA)*, pp. 1011–1016, IEEE, oct 2014.

[9] K. Muraoka, N. Okada, and D. Kubo, "Quad Tilt Wing VTOL UAV: Aerodynamic Characteristics and Prototype Flight," in *AIAA Infotech@Aerospace Conference*, (Reston, Virigina), American Institute of Aeronautics and Astronautics, apr 2009.

[10] E. Çetinsoy, E. Sirimolu, K. T. Öner, C. Hancer, M. Ünel, M. F. Akit, I. KANDEMIR, and K. Gülez, "Design and development of a tilt-wing UAV," *Turk J Elec Eng & Comp Sci*, vol. 19, no. 5, 2011.

[11] M. Bronz, E. Smeur, and H. de Marina, "Development of A Fixed-Wing mini UAV with Transitioning Flight Capability," *35th AIAA Applied*, 2017.

[12] A. Oosedo, S. Abiko, A. Konno, T. Koizumi, T. Furui, and M. Uchiyama, "Development of a quad rotor tail-sitter VTOL UAV without control surfaces and experimental verification," in *2013 IEEE International Conference on Robotics and Automation*, pp. 317–322, IEEE, may 2013.

[13] M. Hochstenbach, C. Notteboom, B. Theys, and J. De Schutter, "Design and Control of an Unmanned Aerial Vehicle for Autonomous Parcel Delivery with Transition from Vertical Take-off to Forward Flight -VertiKUL, a Quadcopter Tailsitter," *International Journal of Micro Air Vehicles*, vol. 7, no. 4, pp. 395–405, 2015.

[14] L. Lustosa, F. Defay, and J. Moschetta, "Development of the flight model of a tilt-body MAV," in *IMAV*, jan 2014.

[15] B. Bataillé, J.-M. Moschetta, D. Poinsot, C. Bérard, and A. Piquereau, "Development of a VTOL mini UAV for multi-tasking missions," *The Aeronautical Journal*, vol. 113, pp. 87–98, feb 2009.

[16] A. Bramwell, G. Done, and D. Balmford, *Bramwell's Helicopter Dynamics*. American Institute of Aeronautics and Astronautics, 2001.

[17] V. Gavrilets, B. Mettler, and E. Feron, "Nonlinear Model for a Small-Size Acrobatic Helicopter," *AIAA Guidance, Navigation and Control Conference and Exhibit*, 2001.

[18] B. Mettler, *Identification Modeling and Characteristics of Miniature Rotorcraft.* Boston, MA: Springer US, 2003.

[19] K. Kondak, M. Bernard, N. Losse, and G. Hommel, "Elaborated modeling and control for autonomous small size helicopters," in *Proc. ISR/ Robotik*, 2006.

[20] L. A. Sandino, M. Bejar, A. Ollero, L. A. Sandino, A. Ollero Grvc, M. Bejar, and A. Ollero, "A Survey on Methods for Elaborated Modeling of the Mechanics of a Small-Size Helicopter. Analysis and Comparison," *Journal of Intelligent & Robotic Systems*, vol. 72, pp. 219–238, 2013.

[21] Y. Al-Younes and M. Jarrah, "Attitude stabilization of quadrotor UAV using Backstepping Fuzzy Logic & Backstepping Least-Mean-Square controllers," in *2008 5th International Symposium on Mechatronics and Its Applications*, pp. 1–11, IEEE, may 2008.

[22] A. M. Girfanov and V. V. Pavlov, "Effect of Gyroscopic Couples on Disk-Wing Aircraft Stability," *Izvestiya VUZ. Aviatsionnaya Tekhnika*, vol. 56, no. 1, pp. 1–6, 2013.

[23] A. Dorobantu, A. Murch, B. Mettler, and G. Balas, "System Identification for Small, Low-Cost, Fixed-Wing Unmanned Aircraft," *Journal of Aircraft*, vol. 50, pp. 1117–1130, jul 2013.

[24] K. K. Valavanis, *Advances in unmanned aerial vehicles: state of the art and the road to autonomy.* Springer, 2012.

[25] K. Kita, A. Konno, and M. Uchiyama, "Transition between Level Flight and Hovering of a Tail-Sitter Vertical Takeoff and Landing Aerial Robot," *Advanced Robotics*, vol. 24, pp. 763–781, 2010.

[26] R. Bapst, R. Ritz, L. Meier, and M. Pollefeys, "Design and Implementation of an Unmanned Tail-sitter," in *IEEE/RSJ International Conference on Intelligent Robots and Systems (IROS)*, (Hamburg), pp. 1885–1890, 2015.

[27] J. Meulenbeld, C. De Wagter, and B. Remes, "Modeling DelftaCopter from Flight Test Data," in *10th International Micro Air Vehicle Competition and Conference,* (S. Watkins, ed.), (Melbourne, Australia), pp. 18–29, 2018.

[28] M. Euston, P. Coote, R. Mahony, J. Kim, and T. Hamel, "A complementary filter for attitude estimation of a fixed-wing UAV," in *2008 IEEE/RSJ International Conference on Intelligent Robots and Systems, IROS*, 2008.

[29] C. de Wagter, B. Remes, R. Ruijsink, E. van der Horst, F. van Tienen, D. van Wijngaarden, J. Meulenbeld, and K. van Hecke, "DelftaCopter Propulsion Optimization from Hover to Fast Forward Flight using Windtunnel Measurements," in *10th International Micro Air Vehicle Competition and Conference,* (S. Watkins, ed.), (Melbourne, Australia), pp. 30–38, 2018.